EVALUATING ECOLOGICAL INFLUENCES OF ALTERED FLOW REGIMES USING TWO- AND THREE-DIMENSIONAL HYDRODYNAMIC MODELS

Yi Shen

Dissertation submitted to the faculty of the Virginia Polytechnic Institute and State University in partial fulfillment of the requirements for the degree of

Doctor of Philosophy
In
Civil Engineering

Panayiotis Diplas Chair
Clint L. Dancey
Marte S. Gutierrez
Donald J. Orth
Joseph A. Schetz

September 9 2009
Blacksburg, Virginia

Keywords: Two-Dimensional Models, Three-Dimensional Models, Aquatic Habitat, Unsteady Flows, Fluctuating Flow Regimes, Reservoir Releases, Spatial Flow Patterns

EVALUATING ECOLOGICAL INFLUENCES OF ALTERED FLOW REGIMES USING TWO- AND THREE-DIMENSIONAL HYDRODYNAMIC MODELS

Yi Shen

ABSTRACT

Reservoir releases for generating power need to be reconciled with efforts to maintain healthy ecosystems in regulated rivers having irregular channel topography. Fluctuating, complex flow patterns near river obstructions such as boulders and large woody debris provide unique habitat for many aquatic organisms. Numerical modeling of the flow structures surrounding these obstructions is challenging, yet it represents an important tool for aquatic habitat assessment. Moreover, efforts for modeling the morphologically and biologically important transient flows, as well as quantifying their impacts on physical fish habitat during the unsteady-flow period remain rare.

In this dissertation, the ability of two- (2-D) and three-dimensional (3-D) hydraulic models to reproduce the localized complex flow features at steady base and peak flows is examined first. The performance of the two hydraulic models is evaluated by comparing the numerical results with measurements of flow around a laboratory hemisphere and boulders located at a reach of the Smith River in Virginia. Close agreement between measured values and the velocity profiles predicted by the two models is obtained outside the wakes behind these obstructions. However, results suggest that in the vicinity of theses obstructions the 3-D model is better suited for reproducing the circulation flow behavior favored by many aquatic species over a broad range of flows.

Further, time-dependent flow features affecting channel morphology and aquatic physical habitat are investigated using the numerical models for the same reach in the Smith River. Temporal variation measurements of water surface elevation and velocity profile obtained in the field during a reservoir release are in good agreement with the numerical results. A hypothetical “staggering” flow release scenario simulated by the 3-D model leads to reduced erosional area and longer refugia availability for juvenile brown trout during hydropeaking. Finally, an unsteadiness parameter β is proposed for determining whether an unsteady flow regime can be either modeled using a truly dynamic flow approach or a quasi-steady flow method.

ACKNOWLEDGEMENTS

I have been assisted by many people throughout my graduate career at Virginia Tech and the development of my dissertation research.

First, I would like to express all my gratitude to my advisor, Dr. Panos Diplas, for his encouragement and support throughout my study at Virginia Tech.

Second, I would also like to acknowledge my committee members (Dr. Donald Orth, Dr. Clint Dancey, Dr. Joseph Schetz, and Dr. Marte Gutierrez) for their help and guidance throughout my project.

Finally, I am thankful to all my fellow graduate students and research associates who aided in the production of data and idea contained in this work. The names of these people include Colin Krause, David Crowder and Douglas Novinger.

TABLE OF CONTENTS

List of Figures

FIGURES IN CHAPTER II

FIGURES IN CHAPTER III

FIGURES IN CHAPTER IV

List of Tables

TABLES IN CHAPTER III

TABLES IN CHAPTER IV

Chapter I: INTRODUCTION

OVERVIEW

Localized, complex, small- and meso-scale flow patterns including velocity shelters, turbulent wakes, and overhead cover are of biological importance and provide favorable environment for many aquatic species. These flow patterns are not only created by various river obstructions, but also impacted by multiple hydraulic/hydrologic factors such as different discharge magnitudes and degree of flow fluctuation.

The purpose of this dissertation is to investigate a means of using two- and three-dimensional hydraulic models to better reproduce and quantify the flow complexity around natural irregular boulders at various flow conditions. Results of this study will assist the efforts of properly accounting for the role of flow obstructions on aquatic habitat enhancement in the design of stream restoration projects. Two- and three-dimensional flow structures of biological importance near fish habitat are examined at base and peak flows in a regulated river. Case studies regarding the links between dynamic hydraulic characteristics under hydropeaking and certain types of physical fish habitat are also presented. However, a detailed description of the temporal variations of natural turbulence structures is beyond the scope of this thesis. Instead, the main purpose of this thesis is to explore a way using the best available science to reproduce flow complexity at certain levels and its potential impact upon physical fish habitat under various flow conditions. A good understanding of the interaction between hydrodynamic characteristics and aquatic habitat will provide insights into the development of better habitat suitability criteria for complex ecological stream flows.

ORGANIZATION

This thesis is organized into three major chapters (Chapters 2-4). Each of these chapters is a self-contained manuscript that either has been submitted to or published in referred journals and proceedings. These manuscripts have been edited substantially to meet the uniform format requirements for use in preparation of the thesis.

Chapter 2 presents a simple numerical modeling study aimed at assessing the impact of river flow obstructions on local flow heterogeneity and microhabitat selection by aquatic species. Specifically, a reach of the Smith River in Southern Virginia, is modeled with and without topographic data on selected boulders using a steady two-dimensional (2-D) hydraulic model. The different impacts the boulders have on local flow patterns and fish drift-feeding habitat at base and peak flows are then examined and compared.

In Chapter 3, the study conducted in Chapter 2 is extended by using a steady three-dimensional (3-D) hydraulic model. To better account for the local complex flow patterns near the boulders, Reynolds Stress Model (RSM) is employed as turbulent stress closure scheme in the 3-D model. The performance of the 2-D and 3-D models is then evaluated by comparing the numerical results with field measurements obtained at base and peak flows. The complex flow patterns behind the boulders are explored by using concepts of vorticity and circulation.

The focus of Chapter 4 turns from the modeling of steady flows to unsteady fluctuating flows encountered in the Smith River downstream of the Philpott Dam. Here reservoir released time-dependent flow features affecting channel morphology and aquatic physical habitat are investigated using one-, two- and three-dimensional hydraulic models. The impacts of different reservoir release scenarios upon potential bed erosion and fish refugia availability are explored using the 3-D modeling approach. An

unsteadiness parameter β is proposed to determine whether an unsteady flow should be modeled using a truly dynamic flow approach or a quasi-steady flow method.

Finally, Chapter 5 summarizes the major findings of this dissertation and discusses some ideas about future work.

Chapter II: Two-dimensional hydraulic modeling: a tool for stream restoration studies

Y. Shen P. Diplas and D.W. Crowder
This chapter is a modified version of a published article. It is reprinted from Proceedings of 5th International Symposium on Ecohydraulics, IAHR, Madrid, Spain.
Department of Civil & Environmental Engineering, Virginia Tech, Blacksburg, VA, U.S.A.

ABSTRACT: Hydraulic modeling of complex flow patterns plays an important role in fish habitat assessment studies. Two-dimensional (2-D) models have been proposed recently as suitable tools for reproducing the major features of such flows. In this paper, a study reach in Smith River, Virginia, where abundance of trout was found, is modeled using a 2-D hydrodynamic model (RMA2) at two different conditions: in one case, selected boulders are included as part of the stream topography, while in the other, they are purposely omitted. Both approaches are calibrated and validated at multiple flows. Local flow patterns in the vicinity of the obstructions are compared between the two cases. Results show that the first approach, which incorporates the boulders, can capture substantial flow complexity, while the second method, unavoidably, masks such crucial flow features. Furthermore, the results are coupled with an existing bioenergetic model to predict favored drift-feeding habitat in the study site. Finally, a stream restoration approach is proposed under the guidance of the 2-D hydraulic modeling.

INTRODUCTION

Regulated rivers and their attendant multiple flow regimes often have detrimental effects on fish habitat. For example, an initially suitable habitat can be changed to a

harmful environment within minutes by releasing highly fluctuating flows from a reservoir (Ghanem et al. 1996). Velocities can become too high within a short time and cause downstream fish displacement (Orth 1999). Furthermore, the simplicity of channel geometry, usually present in regulated rivers, results in relatively uniform flows, compared to natural streams. To avoid these problems, measures need to be taken to minimize their impact on fish habitat, in terms of both diversity and biomass. For the past few decades, investigations on this topic have been mostly accomplished by field measurements and laboratory experiments. However, these traditional methods are often labor intensive while the results are usually limited to specific sets of conditions. Furthermore, it is difficult to examine what is going on during high flows, such as floods. Understanding the capabilities of numerical modeling and developing a protocol suitable for analyzing the ecology of a stream might provide an improved way for examining available aquatic habitat and developing rational and cost effective stream restoration practices.

A widely used mathematical tool to analyze stream restoration is PHABSIM (Physical Habitat Simulation), which incorporates a one-dimensional (1-D) hydraulic model for the study of instream flow requirements. Because the prediction of PHABSIM is based on the assumption of uniform velocities in the downstream channel direction, the model results are not always consistent with field observations, particularly near complex river geometries. To partially rectify this shortcoming, more attention has been paid recently to two-dimensional (2-D) models. Compared with the 1-D models, the 2-D models are more accurate and hold the promise of providing spatially explicit solution of the flow field (Crowder and Diplas 2000). A typical 2-D model (e.g. RMA2 1996) solves the 2-D steady/unsteady shallow water (Saint-Venant) equations and can obtain local water depths and depth-averaged streamwise and lateral velocities over the entire

modeled site. Consequently, transverse flows and vortices around complex river structures of biological importance (i.e. fish rocks, large woody debris) may be adequately quantified.

Currently, most stream applications of 2-D models are focused on reproducing channel-scale flow processes. For example, Ludlow and Hardy (1996) employed the 2-D numerical model RMA2 to explore the potential fish habitat in a 0.5-km natural channel. Similarly, Guay et al. (2000) developed and used an in-house 2-D model to predict the distribution of juvenile salmon in a 1.5-km river reach. These studies constitute significant improvements in hydraulic simulation and habitat assessment. However, the modeling of flow features created by small to medium river flow obstructions, such as boulders and woody debris, have been largely ignored, although their importance for stream habitat quality and abundance has become increasingly evident from extensive field studies during the last 25 years. This issue becomes particularly crucial in mountain streams, like the Smith River, Virginia, USA, where fish habitat is influenced by the presence of numerous boulders.

To investigate the role played by local mesoscale river flow obstructions in creating habitat heterogeneity, it is necessary to determine how the presence of these obstacles affects small-scale velocity distribution and microhabitat selection by aquatic species. In this paper, a reach in the Smith River, where abundance of trout species has been documented, is modeled using RMA2, a 2-D hydrodynamic model for two different scenarios: in the first case, a small number of selected boulders are included in the stream topography; in the second case, they are purposely omitted. The results from the first case show that complicated flow patterns exist near the boulders; while in the second case, flow complexity is significantly suppressed. The comparison between the two cases is

further elaborated in light of habitat prediction from a bioenergetic model for drift-feeding fish.

MATERIALS AND METHODS

Study site and data collection

The study reach is 160 m long and is located 4.2 km downstream of the Philpott Dam, which is the upstream end of the Smith River, VA. This short reach includes an island in the middle of the channel, several pool-riffle sequences, as well as numerous boulders at various locations, features that typically enhance fish habitat. The study site has a flow rate of approximately 42 m^3/s at peak flow and 1.79 m^3/s at base flow. The average channel width is 30 m, with an average slope of 0.08%.

Detailed river topography was obtained in the form of XYZ coordinates, using a Leica TC 600 total station. More than 2000 spot elevations were collected over the entire study site, with an average spacing of approximately two sampling points per square meter. In addition, the dimensions of selected boulder obstructions located near the fish habitat were measured. In an effort to accurately represent the geometry of the flow obstructions, in terms of both size and shape, nine measurements were taken for each boulder. Four of them were taken at the base, another four obtained in the middle of the boulder, and one point was located on the top of the boulder.

At this site, depth and velocity data were collected at a peak flow of 42 m^3/s, a moderate flow of 19 m^3/s, and a base flow of 1.79 m^3/s. These three discharges represent the range of flow conditions commonly encountered in the Smith River and their magnitudes were determined from the readings obtained at a USGS gage station located immediately downstream of the Philpott dam. Measurements of water depth and velocity

were taken along several selected transects (Figure 1). At the base flow, water depths were obtained using a wading rod, and mean column velocities were measured with a Marsh McBirney Model 2000 flow meter. At the higher flows, when the river became unwadable, an ADCP (Acoustic Doppler Current Profiler) was deployed to record the transect water depths and velocity profiles. Aside from that, the substrate was inspected visually and the particles were classified into different size groups. This, in turn, was used to estimate the local channel bottom roughness. In addition, horizontal surveying was employed to determine the fish locations within the reach. Most trout fish were observed in slower water, but close to a fast current augmented by the boulders.

Two-dimensional hydraulic modeling

RMA2 (RMA2 1996), a 2-D numerical program developed by U.S. Army Corps of Engineers, was employed for simulating the flow within the Smith River reach. The model solves the depth-averaged shallow water (Saint-Venant) equations with the finite element method. The outputs of the model include horizontal depth-averaged velocities in the streamwise and transverse directions, water depths, as well as water surface elevations.

Two identical meshes, each having 46,191 elements, were created to investigate the effects of the presence and absence of mesoscale (compared to channel-scale) features, like boulders, on local flow patterns and habitat environments (Figure 1). In the first case (CASE 1), the data set used to generate the mesh is comprised of all the bathymetry information, including the boulders. For the second case (CASE 2), the data set consists of the same topography as the first case, except for selected boulders found near identified fish locations, which are purposely excluded. This modeling strategy has

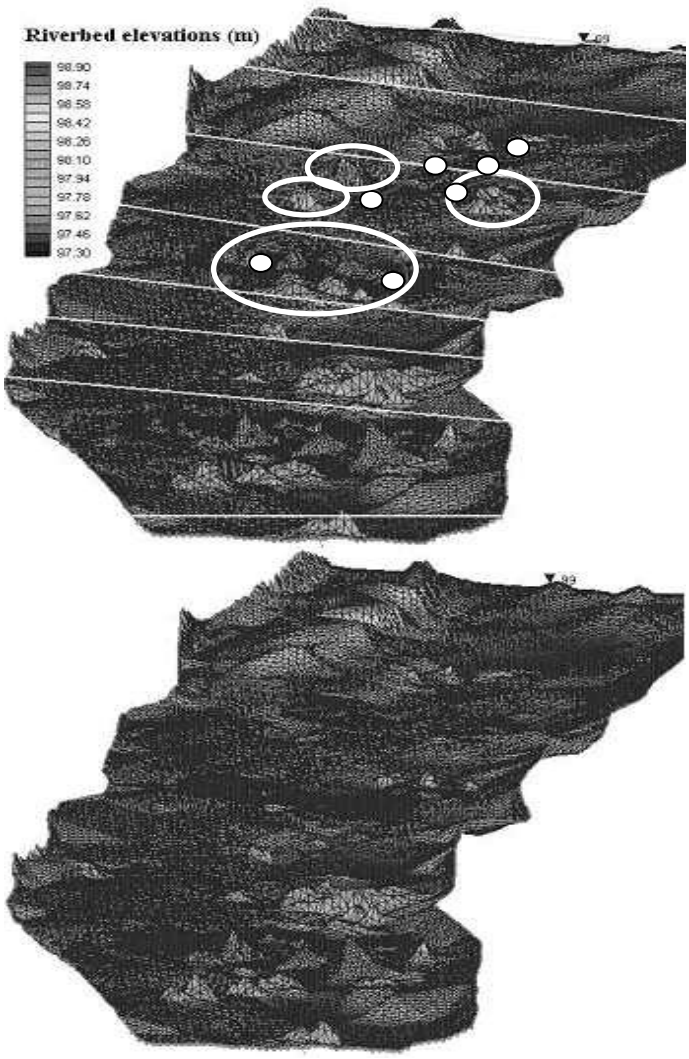

Figure 1. Top view of the riverbed geometry of the modeled site. Both meshes have the same resolution. The upper mesh includes a number of selected boulders (shown inside the white circles) near identified fish locations (shown with white solid ovals); the lower mesh does not consider those boulders. The straight lines represent the cross sections where the water depths and velocities were measured. Flow is from bottom to top of each graph.

been adopted for the following three reasons. First, by keeping the same mesh resolution over the entire modeled site, any difference between the two cases can be attributed to the removal of the selected boulders. Second, since only a small number of boulders are excluded from the second mesh construction, the overall change in riverbed topography

is small and localized in nature. Third, since all the selected boulders are close to observed fish habitat, the simulation results can help determine the biological influence of the inclusion or exclusion of river obstructions on local fish environments.

To explore the extent to which the river obstructions impact local flow patterns at different flows, the three discharges at which velocity and depth data were collected were simulated. Among them, the moderate flow (19 m^3/s) was used for model calibration, while the base (1.79 m^3/s) and peak (42 m^3/s) flows were used for validation for both study cases (i.e. with and without boulders). During the calibration procedure, the roughness coefficient and the isotropic eddy viscosity were adjusted in the hydraulic model until the predicted velocities and depths provided a good match for the corresponding measured values based on visual inspection as well as statistical analysis.

Bioenergetic modeling

In a lotic system of a mountain river, some fish species (e.g. trout) often take up feeding stations where they remain relatively stationary and feed on food that drifts by them. Presumably, these fish occupy locations having "optimal" velocity conditions, conditions where a fish's energy expenditure (e.g. swimming cost) are minimized, while energy intake is maximized. In other words, the drift-feeding fish will try to occupy a focal point velocity to maximize its net energy intake (i.e. energy gain from the food minus energy cost for swimming). The relationship between the flow velocity (V) and fish's net energy intake has led to the establishment of the following equation proposed by Grossman et al. (2002):

$$e^{(b+cV)} = 1/(cV - 1) \quad (1)$$

where *b* and *c* are fitting constants. These two empirical parameters can be obtained from the prey capture success curve (i.e. prey capture success P versus velocity V), which can be expressed as:

$$P = 1/(1 + e^{(b+cV)}) \quad (2)$$

In this paper, a prey capture success curve for medium size trout (71 ~ 125 mm in length) (Hill and Grossman 1993) was fit using Equation 2 (Figure 2). The obtained curve parameters *b* and *c* were then substituted into Equation 1 to calculate the optimal fish velocity, which is 23 cm/s in our study. Given that the RMS (root-mean-square) error of our hydraulic model simulation at base flow is 4 cm/s, any location having velocity between 19 to 27 cm/s is deemed as a potential feeding station at that flow rate. Consequently, by providing a contour map of the velocities in the vicinity of boulders from the 2-D model, potential drift-feeding fish habitat having optimal velocities is predicted. The results are then compared between the two study cases to evaluate the influence of boulders on local aquatic environments.

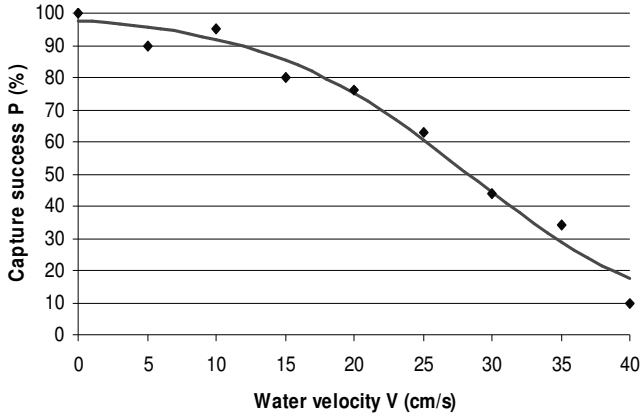

Figure 2. A prey capture success curve for medium trout, $P=1/(1+e^{(-3.76311+0.133102*V)})$, where b = -3.76311 and c = 0.133102.

RESULTS AND DISCUSSION

2-D model calibration and validation

Calibration and validation procedures were applied at locations where corresponding field measurements of water surfaces elevations and velocities are available.

The relative errors between measured and simulated water surface elevations were computed at 186 random locations for each modeling scenario (i.e. with and without boulders) under each of the three modeled discharges. All relative errors were within 10%. The mean absolute error of the water depth prediction throughout the site is 0.03 m for both cases at the base flow with a mean water depth of 0.6 m, increasing to 0.04 m at the peak flow with a mean water depth of 1.6 m. Overall, the agreement between the predicted and observed water surface elevations is fairly good.

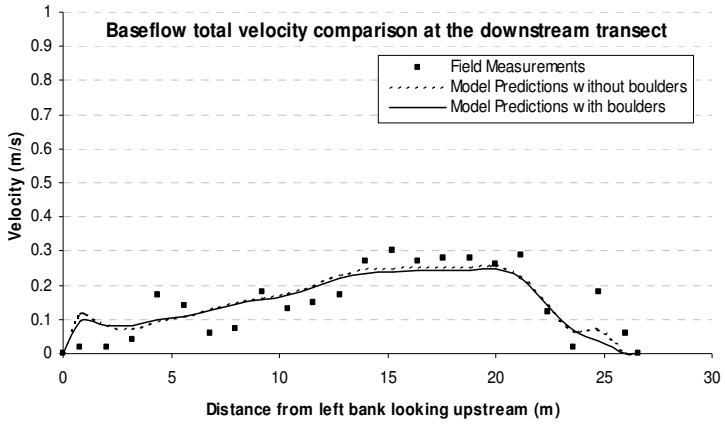

(a)The base flow

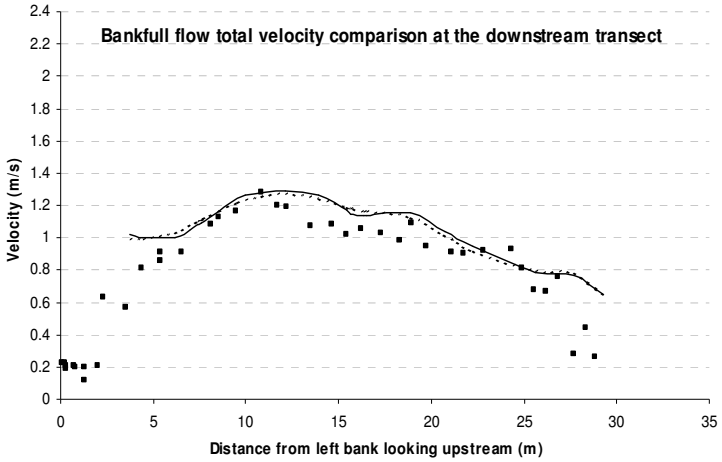

(b) The peak flow

Figure 3. Comparison of the total velocity profiles between two study cases (with and without boulders) at the base and peak flows. The velocities are in the directions having maximum magnitudes. RMS (root-mean-square) value for base and peak flow simulations is 0.04 m/s and 0.09 m/s, respectively.

Individual values of water velocity predicted by the 2-D model are well correlated with measured velocities for both study cases at the three different flows. Figure 3 shows the comparison of velocity profiles at a selected transect between the model calculated values for the two cases and the corresponding measured values at base and peak flows. At base flow, a close examination of the error distribution between the predicted and measured values illustrates that larger errors exist near the banks (Figure 3a). The error in the calculated velocity values near the channel sides may be attributed to the lack of information on riverbank friction (vegetative cover) and possibly insufficient mesh refinement in the near bank regions. Similar error trends were exhibited for the peak flow scenario, though it was not possible to collect data very close to the banks because of equipment limitations (ADCP requires at least 0.5 m water depth for correct deployment).

Comparison of small scale flow patterns

Although the channel-scale hydraulic outputs from the two study cases are similar as illustrated in Figure 3, significant deviations of velocity predictions are found in the vicinity of boulders, where pronounced spatial variability in velocity exists, an environment exploited by drift-feeding fish. An evaluation of how the incorporation of obstructions into hydraulic modeling affects local complex flow patterns is provided here.

Figures 4 and 5 depict the computed velocity results with and without the boulders for a downstream portion of the study reach at base and peak flows. At base flow, when the boulders are excluded for the stream topography, the flow pattern appears quite uniform and remains mainly parallel to the banks (Figure 4b). In contrast, when the boulder clusters are included, at the same flow rate, the current becomes swifter around the boulders and produces heterogeneous velocity patterns (Figure 4a). Due to the existence of the boulders, the channel width upstream of the island is now effectively reduced by nearly one third. Consequently, a large portion of water is shifted to the middle between two separate boulder clusters. Compared to the simulation without the boulders, a high velocity region occupying an area of 35 m^2 is generated between the two boulder clusters, with its local maximum velocity increasing by 30%. Besides this area, wakes having low velocities appear behind the two boulder clusters. From our field observations, the high and low velocity areas are connected by steep velocity gradients and are often occupied by a number of young trout. For the peak flow, however, when the boulders well submerged under the water, the river obstructions behave like roughness elements and the flows return to uniform patterns for both cases (Figure 5).

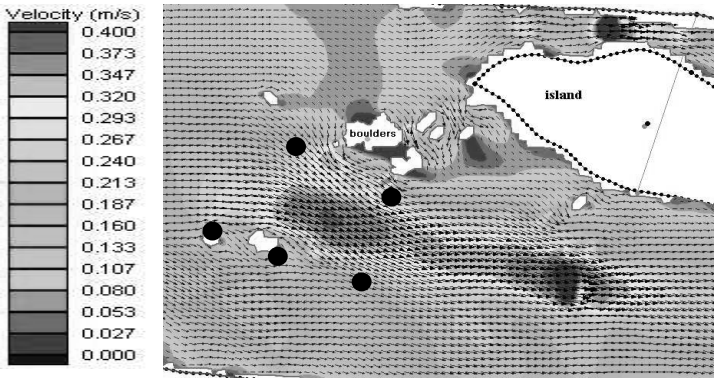

(a) With boulders at the base flow

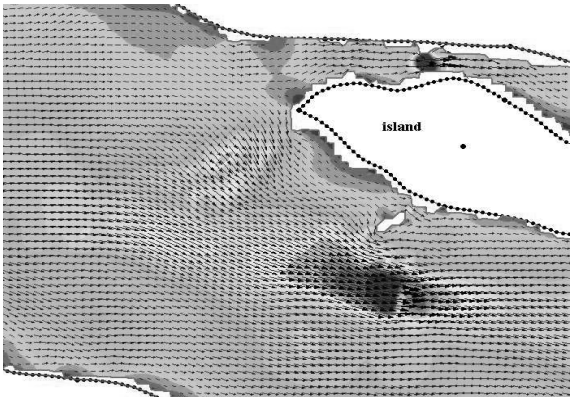

(b) Without boulders at the base flow

Figure 4. Model base flow velocity output in the downstream portion of the study reach, when boulders are present or not present. Arrows represent flow direction and are scaled to velocity magnitude. White polygons denote river boulders and black solid ovals are the observed trout locations.

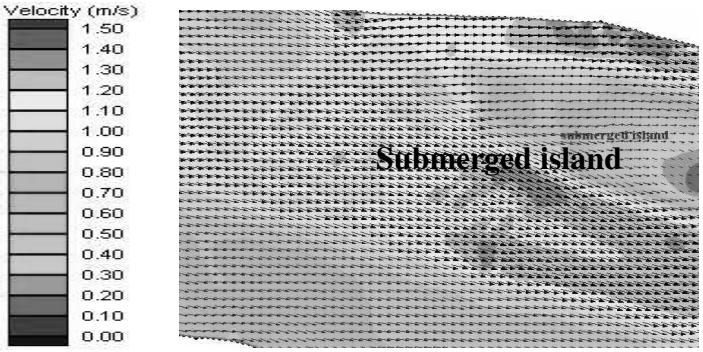

(a) With boulders at the peak flow

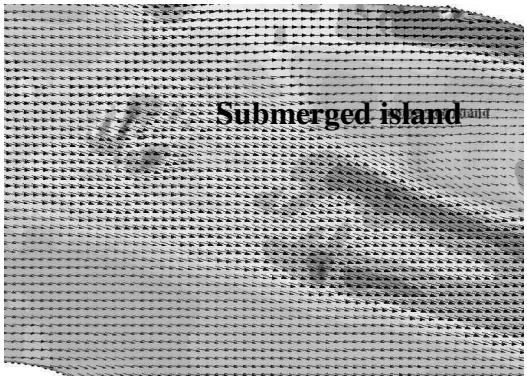

(b) Without boulders at the peak flow

Figure 5. Model peak flow velocity output in the downstream portion of the study reach, when boulders are present or not present. Arrows represent flow direction and are scaled to velocity magnitude.

Recently, vorticity, a vector quantity that describes the rotation rate of a fluid element about its axis (e.g. Munson et al. 1990), has been proposed as a metric property characterizing fish habitat (Crowder and Diplas 2002). Its suitability for use as a metric stems from its capability to quantify the complexity of small-scale flow structures, such as those found in the vicinity of boulders. The biological implications of vorticity are well documented. Researchers have reported that fish rocks, spur-dykes, and other flow

obstructions create vortices that are utilized by fish and invertebrates for feeding and other purposes (e.g. Shields et al. 1995; Way et al. 1995). In the present study, the ability of vorticity to quantify complex flow patterns is evaluated near the aforementioned boulder clusters. However, due to the limitations of our 2-D model, only the vertical component of vorticity is considered in this paper.

Figures 6 and 7 illustrate the absolute vorticity values (Crowder and Diplas 2002) computed by the 2-D model for both simulations (with and without boulders) under base and peak discharges. The results show that at base flow, when a small number of boulders are incorporated into the model, higher vorticity values (> 0.1 s^{-1}) are present around the flow obstructions (Figure 6a); whereas these vortices are significantly suppressed in the absence of these boulders at the same flow rate (Figure 6b). In contrast, with a large enough flow rate and a high relative depth (i.e. the ratio of water depth to the obstruction's height), both simulations exhibit similar vorticity contour maps regardless of the inclusion or exclusion of the boulders (Figure 7). To further investigate how the boulder clusters influence the complex flow patterns, absolute vorticity profiles upstream of two selected boulders (cross-section XS in Figures 6 and 7) are compared at base (Figure 8a) and peak flows (Figure 8b). In Figure 8a, pronounced vorticity variability is found near the two boulders, located 12 m and 19 m away from the right bank, respectively. In Figure 8a, the presence of boulders creates a maximum vorticity value, more than 7 times greater than that in the absence of boulders. In Figure 8b, however, the two vorticity profiles almost coincide, with the largest difference been less than 0.04 s^{-1}.

Comparison of habitat modeling

Hydraulic results obtained from 2-D simulations are analyzed using the bioenergetic model to assess potential drift-feeding habitat in the study reach. The results

of optimal fish velocities are compared between the two cases (with and without boulders) at various flows. Suitable habitat is identified as the region within the study reach having velocities between 19 and 27 cm/s, where fish can get a maximum energy intake while keeping a minimum swimming cost.

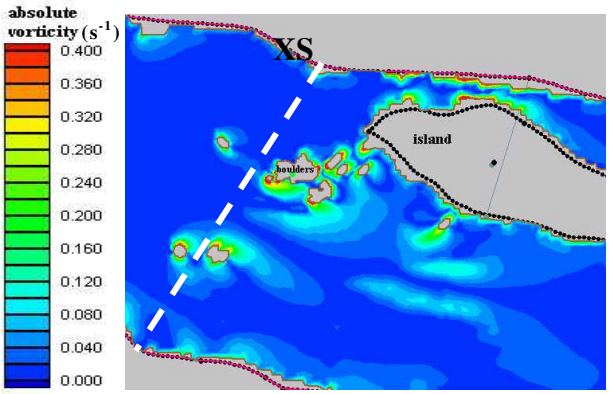

(a) Absolute vorticity contour with boulders at the base flow

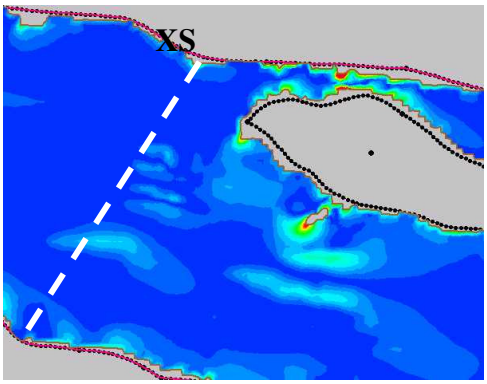

(b) Absolute vorticity contour without boulders at base flow

Figure 6. Plot of the absolute vorticity values at the base flow.

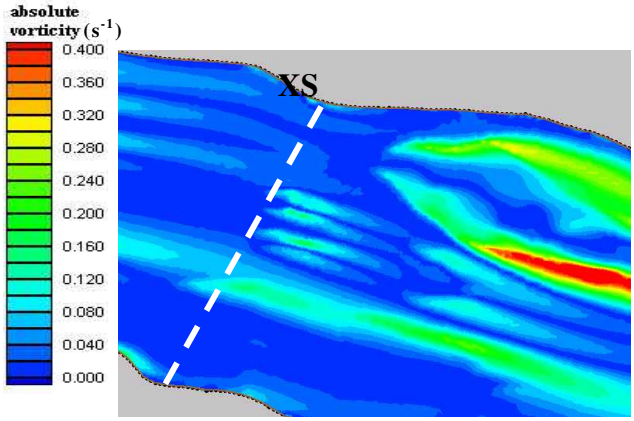

(a) Absolute vorticity contour with boulders at the high flow

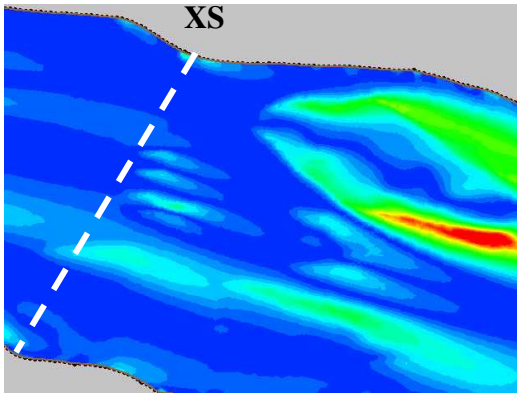

(b) Absolute vorticity contour without boulders at the high flow

Figure 7. Plot of the absolute vorticity values at the high flow.

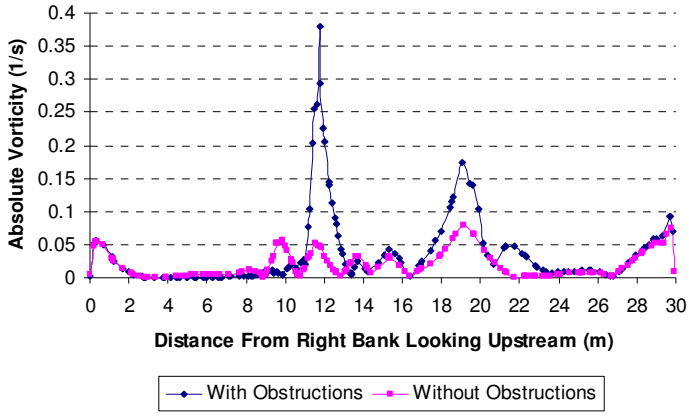

(a) Absolute vorticity profiles along XS at the base flow (shown in Figure 6)

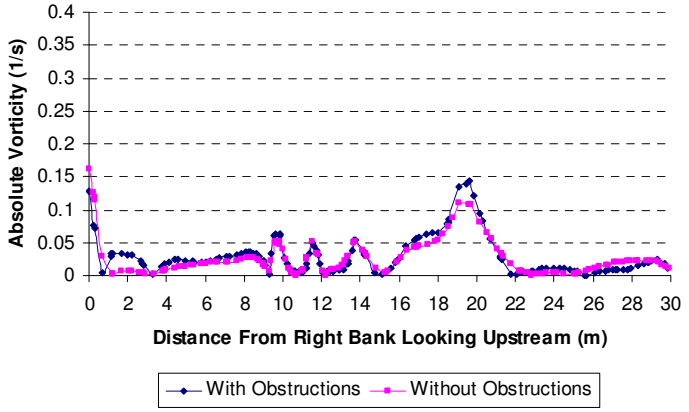

(b) Absolute vorticity profiles along XS at the peak flow (shown in Figure 7)

Figure 8 Vorticity profiles along cross section XS

Figure 9 shows the comparison of predicted drift-feeding habitat over the entire site at base flow conditions. Results show that, at such a low flow rate, the emergent boulders either increase or decrease the surrounding good drift-feeding habitat area, in comparison with the simulation without boulders. In Area A, with the incorporation of four boulders, a total potential drift-feeding habitat of 20 m^2 is predicted before and after

these obstructions. In contrast, when the four boulders are excluded from the model topography, flows in this region are not retarded by any river obstructions and become too fast for supporting drift-feeding fish. In the middle of the reach, excluding the six boulders in Area B, the model results overestimate the potential drift-feeding habitat by 41%. In this portion, the channel width is reduced by the six boulders and a large part of flow is shifted to the left side (looking upstream). Consequently, the local velocities are accelerated, which provides a fast flow area that is difficult for fish to capture prey. However, with the absence of the six boulders, the simulation shows that flow becomes fairly uniform and local velocities are significantly reduced to levels suitable for drift-feeding activity. In contrast to the situation in Area B, the simulation without boulders underestimates the drift-feeding habitat in Area C by 58 m^2. For the peak flow, the present study shows that the inclusion or exclusion of small river obstructions does not affect the predicted drift-feeding habitat. As in such a condition with a high relative depth (at most boulder locations it exceeds 4), trout could not feed because of high energetic cost and inability to withstand the harsh hydraulic conditions (Lagarrigue et al. 2002).

CONCLUSIONS

Simulations using a 2-D hydraulic model (RMA2) have been employed to assess the influence of flow obstructions on physical habitat at various flows. This study shows that the sensitivity of flow patterns to various obstructions, such as boulders, largely depends on the ratio of water depth to the obstruction's height. If the relative depth is less than 1, boulders piercing through the water surface generate complex local flow patterns, manifested through fast moving currents next to the boulders and retarded flow, wakes, behind them. These patterns, together with the resulting vortices are favored by drift-feeding fish. However, when the relative depth becomes large (e.g. >4), the boulders

behave like large roughness elements and have little influence on local depth-averaged velocities.

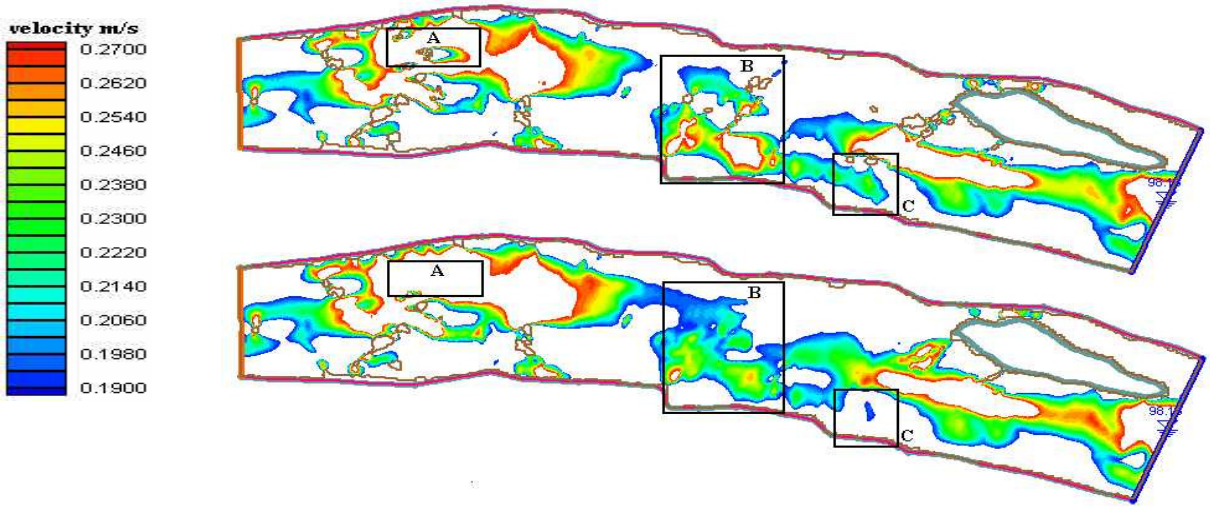

Figure 9. Comparison of the optimal velocity area for the drift-feeding fish at the base flow. Upper graph has the selected boulders and lower graph is without the selected boulders. Areas A, B, and C represent locations where the boulder geometries are modified. White areas have velocities out of the suitable range for the drift-feeding fish. Flow is from left to right side.

The area occupied by the boulders of interest amount to a total area of 38 m^2, only 0.8% of the entire reach. However, the addition of such a small area of boulders augments the local habitat, suitable for drift-feeding fish, by164 m^2 at base flow conditions. These results suggest that under low flow conditions, with a relative depth less than 1, the total amount of potential fish habitat may be dictated, to a large extend, by the presence of flow obstructions, properly placed within the stream, rather than the remaining large flat area of the river reach. Although these river obstructions are difficult to measure and are easily neglected during river restoration studies, it is crucial to correctly evaluate their effects on local flow behavior before proceeding further with fish habitat modeling.

REFERENCES

Crowder, D. W., & Diplas, P. 2000. Using two-dimensional hydrodynamic models at scales of ecological importance. Journal of Hydrology 230:172-191.

Crowder, D.W., & Diplas, P. 2002. Vorticity and circulation: spatial metrics for evaluating flow complexity in stream habitats. Canadian Journal of Fisheries and Aquatic Sciences 59:633-645.

Ghanem, A., Steffler, P. & Hicks. F. 1996. Two-dimensional hydraulic simulation of physical habitat conditions in flowing streams. Regulated Rivers: Research and Management 12:185-200.

Grossman, G.D., Rincon, P.A., Farr, M.D. & Ratajczak Jr, R.E. 2002. A new optimal foraging model predicts habitat use by drift-feeding stream minnows. Ecology of Freshwater Fish 11: 2-10.

Guay, J. C., Boisclair, D. and Rioux D., 2000. Development and Validation of Numerical Habitat Models for Juveniles of Atlantic Salmon. *Can. J. Fish. Aquat, Sci* 57:2065-2075.

Hill, J. & Grossman, G.D. 1993. An energetic model of microhabitat use for rainbow trout and rosyside dace. Ecology 74(3): 685-698.

Lagarrigue, T., Cereghino, R., Lim, P., Reyes-Marchant, P., Chappaz, R., Lavandier, P. and Belaud, A. 2002. Diel and seasonal variations in brown trout (Salmo trutta) feeding patterns and relationship with invertebrate drift under natural and hydropeaking conditions in a mountain stream. Aquat. Living Resour. 15: 129-137.

Ludlow, J.A. & Hardy, T.B. 1996. Comparative evaluation of suitability curve based habitat modeling and a mechanistic based bioenergetic model using 2-dimensional hydraulic simulations in a natural river system. 2nd International Symposium on Habitat Hydraulics, B519-B530.

Munson, B.R., Young, D.F. & Okiishi, T.H. 1990. Fundamentals of fluid mechanics. John Wiley & Sons. Pp. 843

Orth, D. J. 1999. Influences of fluctuating releases on stream habitats for brown trout in the Smith River below Philpott dam. Project Narrative. Richmond, VA., Federal Aid in SportFish Restoration Program, Virginia Department of Game and Inland Fisheries.

RMA2. 1996. *Users Guide to RM2 Version 4.3*, US Army Corps of Engineers-Waterways Experiment Station, Hydraulics Laboratory.

Shields, F.D., Cooper, C. M., & Knight, S. S. 1995. Experiment in stream restoration. Journal of Hydraulic Engineering 121**:**494-502.

Way, C.M., Burky, A.J., Bingham, C.R., and Miller, A.C. 1995. Substrate roughness, velocity refuges, and macroinvertegrate abundance on artificial substrates in the lower Mississippi River. J. North Am. Benthol. Soc. 14: 510-518.

Chapter III: Application of two- and three-dimensional computational fluid dynamics Models to complex ecological stream flows

Yi Shen and Panayiotis Diplas*

This chapter is a modified version of a published article. It is reprinted from Journal of Hydrology, Vol 348, Shen. Y., and P. Diplas, Application of Two- and Three-dimensional Computational Fluid Dynamics Models to Complex Ecological Stream Flows, 195-214, Copyright (2008), with permission from Elsevier Science.

Baker Environmental Hydraulics Laboratory, Department of Civil and Environmental Engineering, Virginia Polytechnic Institute and State University, Blacksburg, VA 24061, USA

ABSTRACT: Complex flow patterns generated by irregular channel topography, such as boulders, submerged large woody debris, riprap and spur dikes, provide unique habitat for many aquatic organisms. Numerical modeling of the flow structures surrounding these obstructions is challenging, yet it represents an important tool for aquatic habitat assessment. In this study, the ability of two- (2-D) and three-dimensional (3-D) computational fluid dynamics models to reproduce these localized complex flow features is examined. The 3-D model is validated with laboratory data obtained from the literature for the case of a flow around a hemisphere under emergent and submerged conditions. The performance of the 2- and 3-D models is then evaluated by comparing the numerical results with field measurements of flow around several boulders located at a reach of the Smith River, a regulated mountainous stream, obtained at base and peak flows. Close agreement between measured values and the velocity profiles predicted by the two models is obtained outside the wakes behind the hemisphere and boulders. However, the

* Corresponding author. Fax: +1-540-231-7532
E-mail address: pdiplas@vt.edu

results suggest that in the vicinity of these obstructions the 3-D model is better suited for reproducing the circulation flow behavior at both low and high discharges. Application of the 2-D and 3-D models to meso-scale stream flows of ecological significance is furthermore demonstrated by using a recently developed spatial hydraulic metric to quantify flow complexity surrounding a number of brown trout spawning sites. It is concluded that the 3-D model can provide a much more accurate description of the heterogeneous velocity patterns favored by many aquatic species over a broad range of flows, especially under deep flow conditions when the various obstructions are submerged. Issues pertaining to selection of appropriate models for a variety of flow regimes and potential implication of the 3-D model on the development of better habitat suitability criteria are discussed. The research suggests ways of improving the modeling practices for ecosystem management studies.

Keywords: Aquatic habitat; CFD; Rivers and streams; Circulation

INTRODUCTION

Fish habitat in streams, including areas for spawning, feeding, covering, and resting, are endangered by flow and river regulation. For example, channelization reduces the complexity of overall stream morphology. Downstream fish displacement may be caused by highly fluctuating flows released from upstream reservoirs (Orth et al. 2004). Rapidly receding water may result in high stranding-related fish mortality. To avoid these problems, measures need to be taken to minimize the detrimental impact of flow and river regulation on local fish communities, in terms of both fish diversity and productivity. Some important remedial works may include fishrock installations,

construction of gravel bars, and design of spur dikes (e.g., Shields et al. 1995). These habitat enhancement structures are often used in stream restoration projects in an effort to mimic natural flow features in creating hydraulic heterogeneity, velocity shelters, turbulent wakes, and overhead cover for aquatic species.

It is well recognized that localized, complex, small-and meso-scale flow patterns created by river flow obstructions are of biological importance and provide favorable environment for many aquatic species (Cullen 1991, Hayes and Jowett 1994, Fischenich and Seal 1999, Kuhnle et al. 2002, Crowder and Diplas 2006). For the past two decades, field measurements, laboratory experiments, and numerical modeling efforts have been performed to investigate the impact of complex flow patterns near habitat structures upon fish and other species. For instance, Kuhnle et al. (2002) conducted a laboratory study on the scour holes generated around spur dikes in clear-water flows. Their results showed that large pools and their associated aquatic habitat could be improved by adjusting the angle of the spur dike to the downstream channel sidewall. Cullen (1991) analyzed the flow field surrounding different fishrocks in a laboratory flume and indicated that the localized vortex mechanism could be useful for the enhancement of fish population. Shamloo et al. (2001) obtained detailed measurements of the flow field and erosion around a simple habitat structure from experiments carried out in a laboratory flume. They found that different erosion patterns were related to different flow regimes.

Nevertheless, laboratory and field investigations are time consuming and labor intensive, because a large number of measurements are needed. These research efforts are often restricted by unavailability of appropriate equipment and difficult field conditions, such as inaccessible terrain or flooding. Recently, much attention has been directed to the development of numerical models as tools to facilitate ecohydraulic studies (e.g. Ludlow and Hardy 1996, Crowder and Diplas 2000, Guay et al. 2000). A typical example is the

development of the Physical Habitat Simulation Method (PHABSIM, see Bovee et al. 1998), a one-dimensional (1-D) hydraulic model that has been widely used in North America for analyzing stream restoration since the 1980s (e.g. Orth and Maughan 1982, Shirvell 1989, Gallagher and Gard 1999). PHABSIM studies have shown good agreement between predicted habitat and observed fish distribution (e.g. Gallagher and Gard 1999), while its limitations have also been well documented (e.g. Scott and Shirvell 1987). One drawback of the model is attributed to the assumption of uniform velocity along the longitudinal flow direction in each cell, which is not always consistent with field observations, particularly near complex river geometry. For example, Guensch et al. (2001) found that three brown trout held positions within the wake of an obstruction in the Blacksmith Fork River, Utah, where flow separation was observed, were difficult to characterize using the standard method.

Compared with 1-D models, two- (2-D) and three-dimensional (3-D) models are more accurate and hold the promise of providing spatially explicit solutions of the flow field. Leclerc et al. (1995) published the first attempt to model fish habitat in a 2-D fashion. Results of their case study in the Moisie River, Québec, illustrated that 2-D approach is more flexible and can achieve higher spatial resolution than traditional 1-D methods. Waddle et al. (2000) used a 2-D hydraulic model, CDG2D, to predict the transverse flows in the Elbow River, Canada. Crowder and Diplas (2000) improved on previous modeling efforts by incorporating stream boulders into a 2-D hydraulic model (i.e. considering them as part of the stream topography rather than simply as roughness elements), RMA2, and analyzed the effects of river flow obstructions on local flow patterns in Feather River, California. Likewise, the habitat assessment based on an in-house 3-D model, SSIIM, was conducted by Booker (2002), whose research further illustrated the significance of 3-D numerical simulations in reproducing better near-bed

hydraulic conditions in natural channels. So far the capabilities and functions of various 2- and 3-D hydraulic models, as well as their applications on different open channel settings have been documented in laboratory flumes (e.g. Salaheldin et al. 2004) and in the field in cases of streams with simple channel geometry (e.g. Tarbet and Hardy 1996, Lane et al. 1999).

The above modeling studies have demonstrated that there is great potential in using computational fluid dynamics (CFD) for representing flow patterns in natural rivers. However, it should be recognized that the application of CFD models to ecological stream flows is not without problems. Although industries and governments usually use the 1-D flow modeling approach for solving large-scale river hydraulic problems, the flow features associated with small- and meso-scale flow obstructions (e.g. boulders and large woody debris) cannot be adequately accounted for by conventional channel scale solutions and therefore are largely ignored. Few modeling efforts have attempted to quantify the local flow structures around such obstructions and the aquatic habitat associated with them (e.g. Crowder and Diplas 2000 and 2006). This issue becomes particularly crucial in mountain streams, like Smith River, Virginia, U.S.A., where the quality and abundance of fish habitat are significantly influenced by the presence of numerous boulders.

In this paper, the performance of a commercial 3-D hydrodynamic model, CFX, based on the steady-state Reynolds-Averaged Navier-Stokes (RANS) equations (CFX-5 2003), is first validated against published experimental results (Shamloo et al. 2001). Next, the impact of boulders on local flow patterns in two selected study areas in the Smith River is assessed using steady-state 2- and 3-D CFD approaches. Field measurements obtained from Smith River are used to test the model simulation results. Complex flow patterns behind the boulders are explored by using concepts of vorticity

and circulation, two spatial metrics proposed by Crowder and Diplas (2006) as measures of flow complexity. The metric values computed by the 2-D and 3-D models are used to examine the degree to which the model simulations can account for the heterogeneity of the local flow field. Considering that fish and invertebrates often utilize boulders and other flow obstructions as refugia and the vortices generated by them for feeding and other purposes, such information is essential for studying the impact of flow complexity on fish habitat and for guiding stream restoration efforts.

MODEL DESCRIPTION

Governing fluid flow equations

The 3-D CFD code, CFX (2003) selected to model the flow field of the Smith River and evaluate local fish habitat solves the three-dimensional RANS equations using the finite volume approach. The governing equations for steady flows may be expressed as:

Continuity equation

$$\nabla \bullet (\rho U) = 0 \tag{1}$$

Momentum equation

$$\nabla \bullet \{\rho U \otimes U - \mu[\nabla U + (\nabla U)^T]\} = -\nabla p - \nabla \bullet \left(\rho \overline{u \otimes u}\right) + B \tag{2}$$

where ρ = fluid density; $\boldsymbol{U}$ = mean velocity vector; μ = molecular viscosity; and $\boldsymbol{p}$ = the total pressure; $\boldsymbol{u}$= fluctuating velocity vector; $\rho\overline{u \otimes u}$ = Reynolds stresses; and $\boldsymbol{B}$ = body force vector.

The 2-D CFD code chosen is RMA2, a program developed by the U.S. Army Corps of Engineers based on the finite element method. The model solves the depth-averaged shallow water (Saint-Venant) equations. It has been successfully applied to various hydraulic and biological projects (e.g. Crowder and Diplas 2000, Mussetter et al. 2001). It computes water surface elevations, water depths, and horizontal depth-averaged velocity components in the streamwise and transverse flow directions. Whether an element is exposed to the air ("dry") or beneath the water ("wet") is determined by two small thresholds of water depth predefined by the user. If any node of the element has a depth less than or equal to 0.01 m, the entire element is deemed to be dry in the model. If projected water depths for all the nodes of that element once again exceed 0.05 m, the element becomes wet. The threshold values must be different in order to prevent the element from oscillating from wet and dry states.

Because the 2-D model neglects vertical velocity and vertical acceleration, the above momentum equation in vertical direction is reduced to a statement of hydrostatic balance. Pressure can then be transformed to water depth to get subsequent water surface elevations based on river geometry. The 3-D model, instead, solves a two-phase fluid domain, usually with water at the bottom and air on the top due to body force $\boldsymbol{B}$ (i.e. gravity and buoyancy force). The volume of fluid (VOF) method (Hirt and Nichols 1981) is used to solve the distribution of air and water for each element, including calculation of the interface between water and air (i.e. free water surface). Over the entire domain, the volume of water occupied within each control volume is assigned with a value called volume fraction, r_{water}, and the remaining fraction of that volume is filled with air, r_{air} (i.e. $r_{air} = 1 - r_{water}$). At the air-water interface, both r_{water} and r_{air} equal 0.5. If r_{water} for an element is 1 (or $r_{air} = 0$) , that element should be under the water surface. Variables such as density ρ and viscosity μ in Eqns (1) and (2) are adjusted accordingly:

$$\rho = r_{water}\rho_{water} + r_{air}\rho_{air}$$
$$\mu = r_{water}\mu_{water} + r_{air}\mu_{air} \quad (3)$$

Turbulence closure

Zero-equation model and Reynolds Stress Model (RSM) are employed here as turbulent stress closure schemes for the governing equations of the 2-D and 3-D formulations, respectively. In the 2-D model, eddy viscosity is prescribed for each element as the product of a turbulent velocity scale and a turbulent length scale, as originally proposed by Prandtl and Kolmogorov. The velocity scale is taken to be the mean velocity within each element and the length scale is defined as the element length in its streamwise direction (Donnell et al. 2001). The Reynolds stresses can then be computed based on the Boussinesq concept. This approach assumes that turbulence kinetic energy is dissipated where it is generated. Because no additional transport equations are solved, the model is termed 'zero equation'. In contrast, the RSM in the 3-D model describes the relationship between Reynolds stresses and time-averaged flow parameters by solving six transport equations for Reynolds stresses and one equation for turbulent kinetic energy dissipation rate. Accounting for the inherent stress anisotropies, vorticity and circulation, theoretically, makes the RSM solver superior to the zero equation method and hence better suited for complex flows. The RSM used in this study does not include the wall-reflection terms and therefore is a simplified version of the formulation introduced by Launder, Reece and Rodi (1975). However, the model is standard in CFD industry where practices have shown it is able successfully to achieve accurate results for 3-D flows while maintaining computational robustness (e.g. Schwarz and Bradshaw 1994, Morvan et al. 2002).

Boundary conditions

Data inputs to the 2-D and 3-D models consist mainly of the boundary conditions and the channel bathymetry, discretized by a finite element mesh and a finite volume mesh, respectively. The boundary conditions generally include solid boundaries at the river bottom and boulder or other flow obstruction surface, and two open boundaries at the upstream and downstream ends of the modeled stream section. In the 2-D model (RMA2), default settings were used that allowed fluid to slip at all solid boundaries. Consequently, the velocities at the boulder surface are identical to those at the adjacent mesh nodes. However, for real fluid flow, non-slip condition should be satisfied at any solid boundary, rendering the velocity equal to zero at the corresponding locations. This requirement is satisfied by the 3-D model (CFX). Furthermore, the non-equilibrium law-of-the-wall extended for flow separation and rough wall was used to simulate the near-wall flow velocity in the 3-D model, in which shear velocity is characterized by the square root of turbulent kinetic energy and wall shear stress is assumed constant throughout the inertial sublayer (Launder and Spalding, 1974):

$$\frac{U_t}{u^*} = \frac{1}{\kappa}\ln\left(\frac{c_\mu^{1/4}k^{1/2}y}{\nu}\right) - \frac{1}{\kappa}\ln\left(1+\frac{0.3k_s c_\mu^{1/4}k^{1/2}}{\nu}\right) + C \qquad (4)$$

where U_t = known velocity parallel to the wall at a normal distance y from it; u^* = friction velocity; κ = von Karman constant; empirical coefficient c_μ = 0.09; k = local turbulent kinetic energy; ν = kinematic viscosity of the fluid; k_s = equivalent grain roughness height and C = log-layer constant depending on wall roughness. In the 2-D model, the upstream boundary is defined using a known discharge and the downstream boundary is specified with a measured water surface elevation. In the 3-D model, a velocity profile and a hydrostatic pressure profile consistent with the measured water surface elevation are assigned to the upstream boundary (i.e. the pressure field is

hydrostatic in the water but zero above the water surface). Another hydrostatic pressure profile, which is consistent with the known downstream water depth, is set at its downstream boundary in the 3-D model.

MATERIALS AND METHODS

First, the 3-D model (CFX) was constructed according to the specifications of a laboratory study published in Shamloo et al. (2001), to assess the model's performance. Second, to evaluate the two models' potential application in steady flow conditions typically encountered in natural streams, two areas selected from the Smith River were surveyed and modeled using both 2-D (RMA2) and 3-D (CFX) codes. Results of the numerical simulations are presented in the next section.

Laboratory assessment

Shamloo et al. (2001) conducted a series of laboratory studies on flows passing around a hemisphere located at the center of a flume in an effort to explore the flow behavior around the simple structure. Three of their experiments were performed over a smooth bed with different discharges mimicking high, medium and low flow regimes. Their schematic diagram of the hemisphere and the three flow regimes is reproduced in Figure 1a. Details of the values adopted for the various flow parameters during these experiments are summarized in Table 1.

To verify the accuracy of the 3-D model, numerical simulations of the above three flow conditions were performed using the Reynolds Stress turbulence closure (RSM). Successful simulation of the complex flow characteristics observed in a well-controlled laboratory experiment by the 3-D model is necessary to develop confidence for its further application to natural stream conditions. Grid sensitivity tests were performed to reduce

potential discretization errors. Hexahedral meshes with three different discretization levels were constructed for each case, where the number of total nodes was incremented

Table 1. Selected flume experiments of flow over a smooth bed in the presence of a hemisphere (Shamloo et al. 2001).

Experiment No.	Discharge (m^3/s)	Average velocity U_0 (m/s)	Water depth d (m)	Flume modeled (width/length)	Longitudinal bed slope ‰	Hemisphere (diameter/height) (D/h)	Relative depth (d/h)
BS1	0.030	0.342	0.072	1.22 m/4 m	1.18	0.13 m/ 0.065 m	1.11
CS1	0.008	0.156	0.042		1.18		0.65
DS1	0.068	0.208	0.268		1.47		4.12

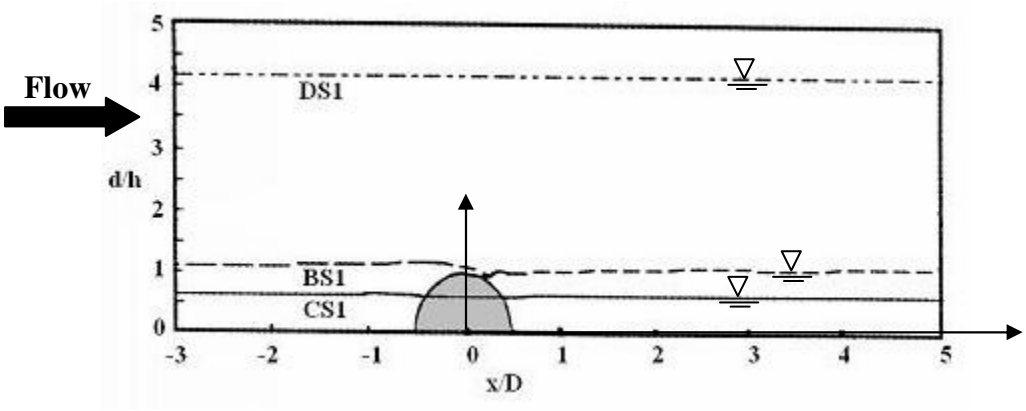

Figure 1(a) Three flow regimes (i.e. CS1, BS1 and DS1) and the hemisphere used in the experiment of Shamloo et al. (2001). The origin of the coordinate system is at the center of the hemisphere. (See Table 1 for more details)

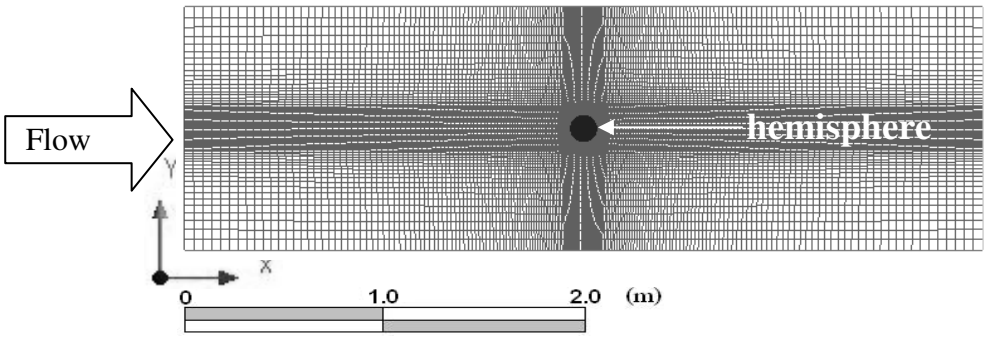

Figure 1(b) Top view of hexahedral mesh (Mesh3 for BS1) that served as the computational domain for the 3-D modeling of the hemisphere experiment of Shamloo et al. (2001). The dimensions modeled flume section are 1.22 m (width) and 4 m (length) with a 0.13 m diameter hemisphere at the center.

by at least 20% for its subsequent grid (Table 2). Hexahedral elements were chosen throughout this study because good mesh quality can be maintained even with high aspect ratio for layers of elements near the boundaries of the hemisphere and boulders. Element sizes were refined near the hemisphere in an attempt to better resolve the rapid variation of flow variables surrounding the obstacle. Mesh refinement level near the hemisphere was monitored through the dimensionless distance of the first node away from the solid boundary, y^+, which is defined as:

$$y^+ = \frac{yu^*}{\nu} \tag{5}$$

where y is the normal distance to the wall.

The upper limit of y^+ is designed to be less than 100 by the user, while the lower limit of y^+ will be determined automatically by CFX as the maximum value between the actually calculated distance and 11.06 during the simulations. Therefore, all mesh points included in the computational domain are technically outside the viscous sublayer so that the wall function can be imposed appropriately (CFX-5 2003). Figure 1b illustrates an

example of a hexahedral mesh with 663029 nodes used for the study case of BS1 (see Table 1).

Table 2. Meshes used in the numerical simulations of the flume experiments (Shamloo et al. 2001).

Case / Mesh	BS1		CS1		DS1	
	Number of Nodes	Average y^+ near the hemisphere	Number of Nodes	Average y^+ near the hemisphere	Number of Nodes	Average y^+ near the hemisphere
Mesh1	441480	21.6	251024	7.99	103578	41.6
Mesh2	540119	20.6	333658	7.92	309452	33.5
Mesh3	663029	19.7	603784	7.42	413201	9.3

After that, three sets of separate flow parameters (see Table 1) were specified at the boundaries to simulate the experiments. For the DS1 case (see Shamloo et al. 2001), the water surface was represented by a solid-lid boundary. In the BS1 and CS1 cases, considering that the local water surface may be affected by strong surface waves, the VOF routine was incorporated into the 3-D model to better simulate the varying water surface.

Field application

Site description

The Smith River reach selected as the study site is 160 m long and is located 4 km downstream of the Philpott Dam (Figure 2). The channel bottom consists of gravel, cobbles, pebbles, sand, but there is little in-channel vegetation. This site ranks the highest in fish reproduction among all twelve fish spawning sites sampled in the Smith River

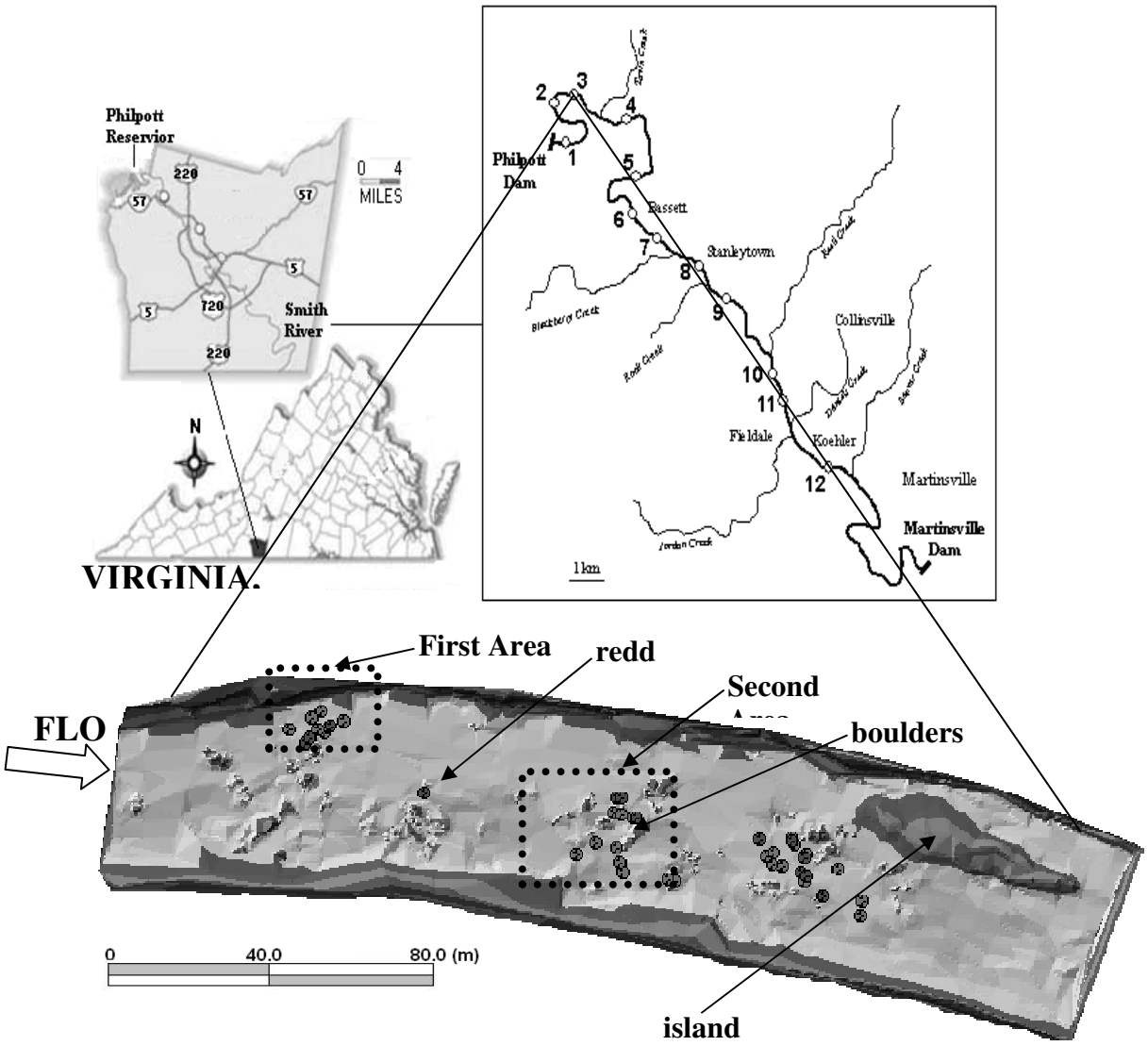

Figure 2. Map of the study reach in the Smith River tailwater below the Philpott Dam with sampling sites numbered upstream to downstream. The rectangles give the location of the two modeled areas. Dots represent redd locations.

(Orth et al. 2004). The mean annual flow released from the reservoir is 8.6 m^3/s, with daily values fluctuating from a base flow of 1.78 m^3/s to a peak discharge of 42 m^3/s.

Data collection

Detailed river topography was georeferenced on a cross-section basis in the form of XYZ coordinates, using a Leica® TC 600 electronic total station. More than 2000 spot elevations were collected over the entire reach, including the two areas, with an average of about two spots per square meter. Boulders were visually identified and measured. To accurately delineate the geometries of the boulders, in terms of both their size and shape, at least nine measurements were made for each boulder. For example, the first four points were taken at the base, the next four points were obtained in the middle, and the last one or two points were located on the top of the boulder. The measured bathymetric data was used to create numerical grids for both the 2-D and 3-D models.

At this site, depth and velocity data were collected when the total channel flow reached its peak value of 42 m^3/s and at base flow conditions when the discharge was 1.78 m^3/s. These two discharges were determined from a USGS gage station located immediately downstream of the Philpott Dam. Measurements of water depth and velocity were taken near selected boulders and along the study site's boundaries. To measure velocities around a boulder, two points with different relative distance from the boulder (i.e. the ratio of actual distance from the boulder to the boulder width normal to the streamwise velocity), were chosen in the plane of symmetry of the boulder (Figure 3). Point A was located within the wake generated by the boulder, while Point B was located further downstream (i.e. outside the immediate wake region). At base flow, water depth was obtained using a wading rod, and velocity magnitude and direction were measured at 5 different locations along the whole water column with a Marsh McBirney® Model 2000

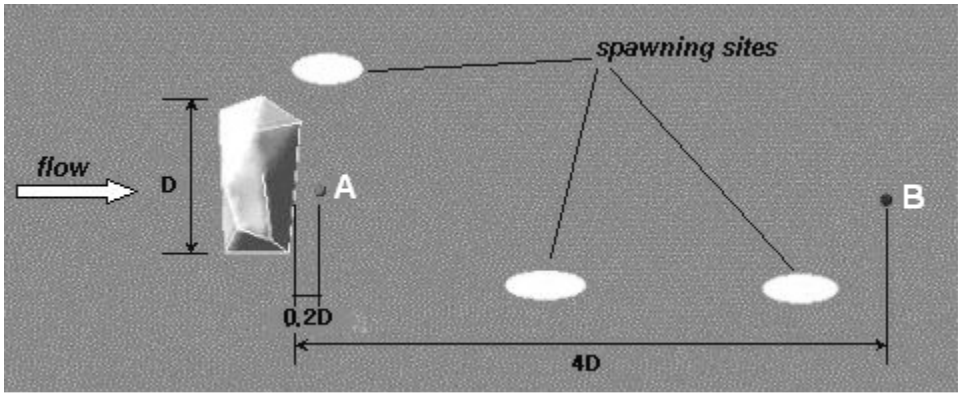

Figure 3. Locations of measured points with respect to the boulder and trout spawning sites. This graph depicts a top view of the single boulder surrounded by three spawning sites (i.e. redds) and two measured points in the first area in the Smith River. The distances of the two points from the boulder are 0.2D and 4D for points A and B, respectively.

flow meter and a compass. At peak flow, when the river became unwadable, a SonTek® ADCP (Acoustic Doppler Current Profiler) was deployed to record the corresponding water depths and velocity profiles. The ADCP was mounted on a catamaran suspended from a cableway that crossed the river and slid to the desired points to obtain measurements (Figure 4). The positions of the ADCP were georeferenced using the total station before and after each measurement. The equipment was operated with a sampling frequency of 3 MHz, which is recommended by SonTek® for shallow water (< 3 m deep). Its transducers' sampling volume for velocity was divided into a maximum of 13 range cells along the water depth, with each cell having a height of 0.15 m. The streamwise, lateral and vertical velocity components were obtained for each cell in the corresponding depth layer. The ADCP was kept stationary at each point for at least 10 minutes and the

collected velocity time-series were time-averaged to get the three mean velocity components for each cell. Because the ADCP assumes the flow field is uniform within the sampling volume, it was not deployed in the immediate vicinity of any underwater obstructions (e.g. boulders) to avoid strong velocity gradients.

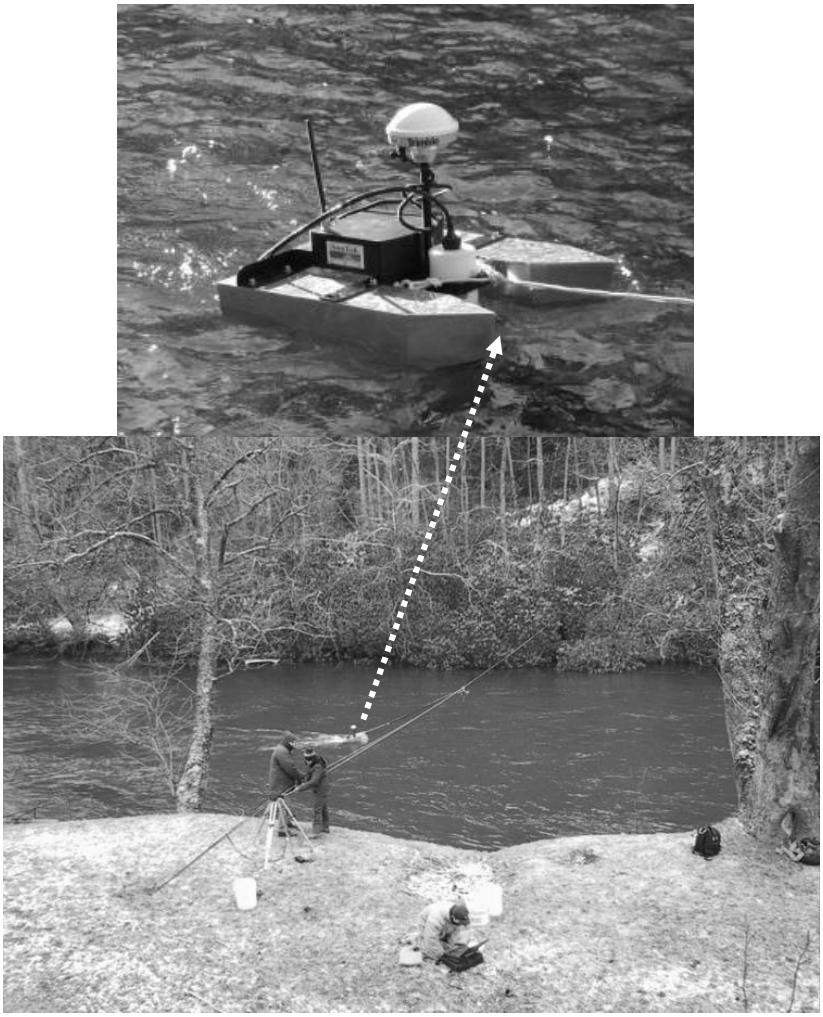

Figure 4. Pulley system setup across the study site in the Smith River, Virginia, with an attached ADCP.

Fishery biologists have been sampling brown trout in the study site for several years. Each fish location was accurately georeferenced immediately after it was visually identified. Most trout fish were spotted in slower water, but close to a fast moving current augmented by the presence of the boulders. Knowing the exact fish location is vital to studying the influence of boulders on local fish habitat.

While the river bathymetry and velocity data were obtained over the entire 160-m reach, only two smaller areas within it were used for the 2-D and 3-D modeling study presented here (Figure 2). Numerical simulation results were compared between the two models and against field measurements, where available. The first area includes an isolated boulder with sufficient distance from other river obstructions, where a velocity wake was developed immediately downstream of the boulder. The second area primarily consists of three large rocks. Swift localized currents and heterogeneous velocity patterns were observed within this boulder cluster. Complex flow patterns and refugia generated by the presence of these obstructions are believed to benefit brown trout spawning sites surrounding them. Their intricate bathymetric features provide an excellent opportunity for evaluating the ability of the numerical models to simulate the small-scale complex flows encountered there, deemed to be of biological importance.

Mesh construction

The first area has a lateral width of 7 m and a streamwise length of 17 m. The second area's width and length are 15 m and 36 m, respectively. Both areas were modeled using approximately 40000 quadratic triangular elements in the 2-D model. For the 3-D model, the same geometries of these two areas, including their boulders, were discretized into structured hexahedral meshes (Figure 5a and b). About 0.8 million finite volume cells were generated for the first area, and 1 million elements were created for the

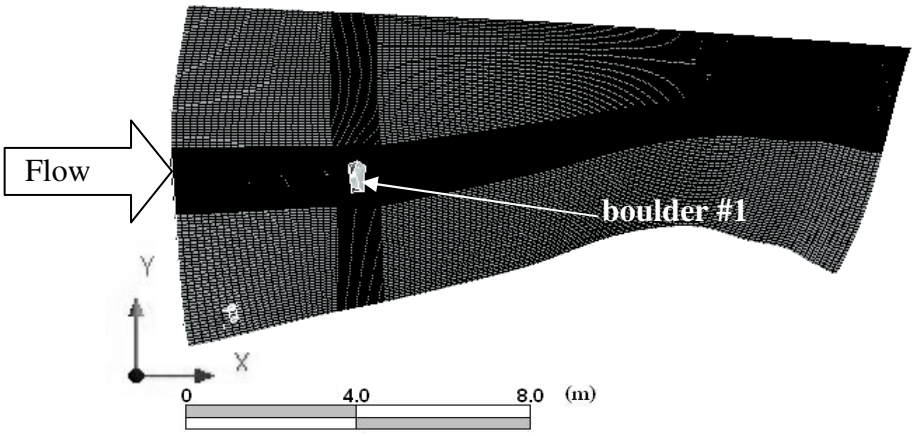

(a)

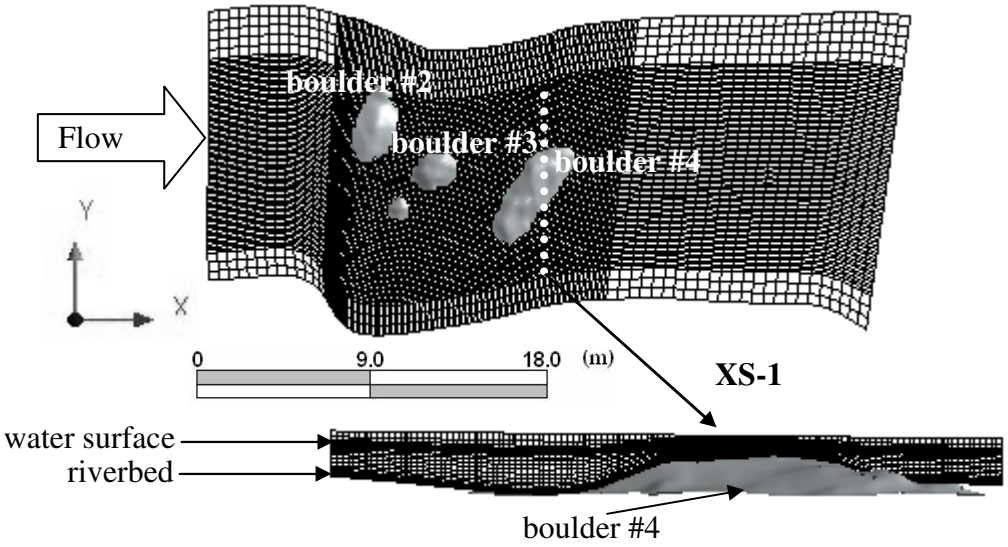

(b)

Figure 5. Top view of the two finite-volume meshes that served as the computational domains for the 3-D modeling of (a) Single boulder in the first study area of the Smith River; (b) Boulder cluster in the second area of the Smith River. Note: Finer grids were set up around the boulders in (a) and (b), as well as the water surface and the riverbed (see XS-1) in (b). Boulder dimensions are listed in Table 2. White dashed line XS-1 is the transect looking upstream (not scaled).

second area. Mesh resolution varies spatially based on topography complexity and the type of fluid solved. For both models, finer elements were assigned near the boulder surfaces to resolve the small-scale turbulent flows surrounding the boulders. Coarser elements were assigned to the air portion modeled in the 3-D model, since the transport of air is not of main concern in this paper.

Appropriate boundary conditions were specified for both models based on field measurements and observations. All the boulder surfaces in the 3-D model were taken as non-slip smooth walls, while the river bottom was treated as a rough boundary and was assigned a roughness height of 0.01 m. This value corresponds to the mean size of sediment particles collected at the study site. In the 2-D model, a Manning's *n* value of 0.04 was specified to account for the river bottom roughness. Finally, at the upstream boundary, a recorded value of the discharge was assigned to the 2-D model, while a measured velocity profile and hydrostatic pressure expression (equivalent to water surface elevation) were set for the 3-D model. At the downstream boundary, measured water surface elevation or its equivalent hydrostatic pressure were defined for the 2-D and 3-D models, respectively.

Model application

To explore the extent to which the boulders impact local flow patterns, the base and peak discharges, at which velocity and depth data were collected, were simulated. The 2-D model was calibrated at base flow and validated against the peak flow. During the calibration procedure, the roughness coefficient and the isotropic eddy viscosity values were adjusted in the 2-D model until the errors of velocities and depths between the predicted and measured data were within 10%. In contrast, for the 3-D model, we decided to validate directly the simulation results without calibration. We adopted such a modeling strategy for the following two reasons. First, because in theory the 3-D code is

more physics based, it is expected that it will be able to model the nature of the flow more accurately and therefore it needs less calibration effort (Lane et al. 1999). Second, the site geometry and boundary conditions, the two most important input parameters for achieving a successful simulation (Donnell et al. 2001), were accurately determined from field measurements. Nevertheless, as described later, good agreement was still obtained between the 3-D model results and field measurements.

For the first area, water surface elevations and velocities near the isolated boulder were compared among the two models and field measurements. Specifically, velocities from the 2-D model were compared against those obtained by the 3-D model at two different points along the streamwise axis of symmetry of the boulder (Figure 3). Point A is located $0.2D$ downstream of the boulder (D = boulder width), within its wake; point B is located $4D$ downstream of the boulder, outside of the immediate wake region. Comparison was also made between the two models at two horizontal planes. The first plane, A, chosen to plot the velocity patterns obtained from the 3-D model is located at $0.4d$ distance above the channel bottom (d = local water depth), where depth-averaged velocities are expected to occur. The second plane, B, is at a vertical distance of 15 cm above the streambed, a location favored by adult brown trout for feeding purposes.

For the second area, due to extraordinary flow complexity in the boulder cluster case, no point velocity measurements and comparison were made here. Instead, two recently proposed spatial metrics — vorticity ξ and circulation Γ (Crowder and Diplas 2006), were adopted as tools for quantifying its local spatial flow complexity. In this paper, the spatial metrics were applied to both areas.

Like focal point velocity and depth, biological implications of vorticity and circulation are well documented. Researchers have reported that fishrocks, spur-dykes, and other flow obstructions create circulation currents that are exploited by fish and

invertebrates for spawning, feeding, resting and hiding, etc. (e.g. Shields et al. 1995, Liao et al. 2003). In this paper, the two metrics were computed in the aforementioned two horizontal planes using results generated by both numerical models.

Vorticity is a measure of the rate of rotation of a fluid element about its three axes, which are *x* (streamwise), *y* (lateral) and *z* (vertical) directions (e.g. Munson et al. 1990). Although the 3-D model is able to compute the vorticity in all three directions, only the *z* (vertical) component can be calculated from the horizontal velocity distribution provided by the 2-D model. Considering that the axes of the wake vortices behind flow obstacles are usually nearly vertical (Salaheldin et al. 2004), an arrangement that appears to be most beneficial for energy extraction by swimming fish (Liao et al. 2003), only the vertical component of vorticity is calculated here, which is denoted as:

$$\vec{\xi} = \left(\frac{\partial v}{\partial x} - \frac{\partial u}{\partial y} \right) \hat{k} \tag{6}$$

where *u* and *v* are velocity components in the *x* and *y* directions, while $\hat{k}$ is a unit vector in the *z* direction. In the 3-D model, *u* and *v* can be calculated at any depth, whereas in the 2-D model, only depth-averaged velocities can be obtained. To investigate the flow complexity within an arbitrary horizontal area, the absolute circulation $|\Gamma|$, which is the integral of absolute values of vorticity $|\xi|$ over a wetted region A_{VOR} surrounding a boulder or a combination of obstructions, is divided by A_{VOR} using the following expression:

$$\frac{|\Gamma|}{A_{VOR}} = \frac{\iint |\xi| dA}{A_{VOR}} = \frac{\sum |\xi| \Delta A}{A_{VOR}} \tag{7}$$

where ΔA represents a small element within A_{VOR}. This is termed “absolute circulation per unit area” or “circulation metric”.

RESULTS

The performance of the 3-D model in a laboratory flume setting, using the experimental results obtained by Shamloo et al. (2001), was evaluated first. Mesh independence study was conducted for assessing the grid sensitivity of the results. Comparisons were made between the velocity data measured during their experiments and our numerical predictions computed from the 3-D model for flow conditions representing both emergent and submerged hemispheres (Table 1). Subsequently, the 2-D and 3-D models were applied to the two study areas in the Smith River, Virginia, in an effort to examine their ability to reproduce the nonuniform flow patterns surrounding the boulders at the two different flows.

Laboratory assessment

Figure 6 compares the simulated velocity profiles against experimental data obtained by Shamloo et al. (2001) at various locations along the centerline of the flume. Comparisons between the coarse and fine meshes are also presented in this figure. Among all the cases, the maximum velocity error is about 16% between Mesh1 and Mesh3 for the CS1 case at the location 4D (D = hemisphere diameter) behind the hemisphere (Figure 6a). The maximum velocity error between Mesh2 and Mesh3 among all the study cases is reduced to 8% for the CS1 case at the location -2D upstream of the hemisphere (Figure 6a). It is worth mentioning that all the y^+ values for Mesh3 are either close to or even below 11.06, which is the lower limit of the inertial layer (Table 2). The grid size dependence study shows that the results obtained with Mesh3 for all the cases are relatively free of mesh discretization error. Hereafter, results computed based on Mesh3 for all the three cases were used for comparisons with the measurements.

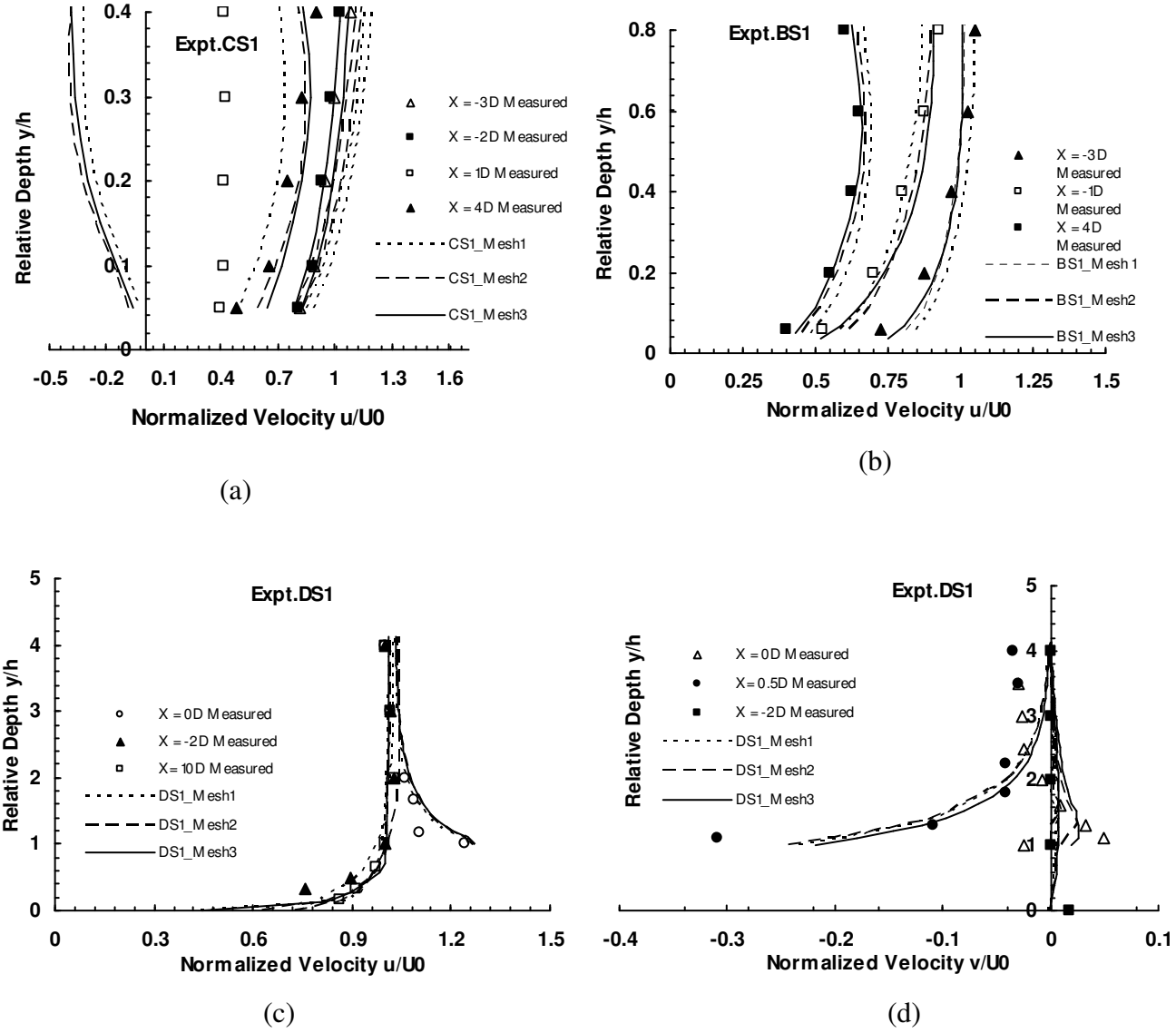

Figure 6. Comparisons of computed (via the 3-D model) and measured velocity profiles (in the plane of symmetry) in the vicinity of the hemisphere. (a)emergent hemisphere (b)shallowly submerged hemisphere (c)deeply immersed hemisphere (d)deeply immersed hemisphere Measured data was retrieved from Shamloo et al. (2001). U_0 is the cross-sectional averaged velocity of the approach uniform flow (see Table 1). RSM = Reynolds Stress Model; **X** is the longitudinal distance from the center of the hemisphere (Figure 1a), expressed through a multiplier of the hemisphere diameter D. A negative sign in **X** value means the velocities were obtained upstream of the obstacle.

For all three flow scenarios (i.e. emergent, shallowly submerged or deeply submerged the hemisphere), the 3-D model successfully reproduces the general acceleration and deceleration trends of the velocity distributions at both upstream and downstream locations of the obstacle. In particular, at locations further away from the hemisphere, the computed streamwise velocities are very close to the measured values (e.g. Figure 6b).

However, some discrepancies exist, especially in the wake region where strong flow circulation is present. In Figure 6a, when the hemisphere pierces through the water surface (relative depth = 0.65, Table 1), positive streamwise velocities were measured by Shamloo et al. (2001) at a distance of 1D downstream of the hemisphere center, where *D* is defined as the hemisphere diameter (Figure 1). In contrast, the 3-D model shows only a negative velocity distribution over the entire water depth at the same location. Similar deviation between numerical results and laboratory measurements has been reported by Salaheldin et al. (2004), for the case of flow modeling around circular piers. The adverse pressure gradient encountered in the flow behind the hemisphere is expected to create a recirculation region dominated by vortices and reverse flow, which could extend several obstacle diameters downstream of the hemisphere (Munson et al.1990). Hence, the difference between the numerical results and the measurements may be attributed to how accurately the turbulent wake size could be captured by the 3-D model. For instance, in the CS1 case, the computed wake length at the water surface level is a bit less than 2D, compared to the 1.5D long region observed by Shamloo et al. (2001).

For the deeply submerged hemisphere case, with a relative depth of 4.12 (Table 1), Figure 6c compares the normalized streamwise velocity profiles generated by the 3-D model with the corresponding laboratory measurements. The model predictions agree well with the measured values. The ability of the 3-D model in reproducing secondary

circulations and vertical velocities affected by the hemispherical object is also considered here for the DS1 case. As demonstrated in Figure 6(d), both the estimated and observed vertical velocity profiles follow similar trends at most locations, with downward velocities shown as negative. Some deviations exist near the top of the hemisphere. Shamloo et al. (2001) detected slightly negative velocities above and behind the hemisphere, whereas the 3-D model does not capture such a feature. Employing a solid-lid boundary approach to model the free surface in this case, rather than an interface between air and water (more accurate approximation that is used for Expts. CS1 and BS1), may be a reason for this disagreement. Consequently, all the flows near this solid-lid boundary are automatically set as parallel to the top surface and no vertical velocity can be expected in the immediate vicinity of the boundary. Nevertheless, because our main interest in this study is on the details of heterogeneous flow patterns typically triggered by bottom river obstructions, it is believed that the influence of such a small velocity deviation (on the order of 10^{-3} m/s) on potential fish habitat could be insignificant.

Field application

Water surface levels in the first area (single boulder case)

Figure 7 depicts the computed and measured water surface elevations near the single boulder in the first area of the Smith River site (Figure 2). The boulder has a base width, D, of 0.5 m normal to the streamwise direction and a height, h, of 0.36 m (Table 3). Close agreement among the water surface levels calculated by the two models and field measurements was obtained for both base and peak flows. Due to uniform bottom roughness, the predicted water surfaces are quite flat. However, at base flow, when the

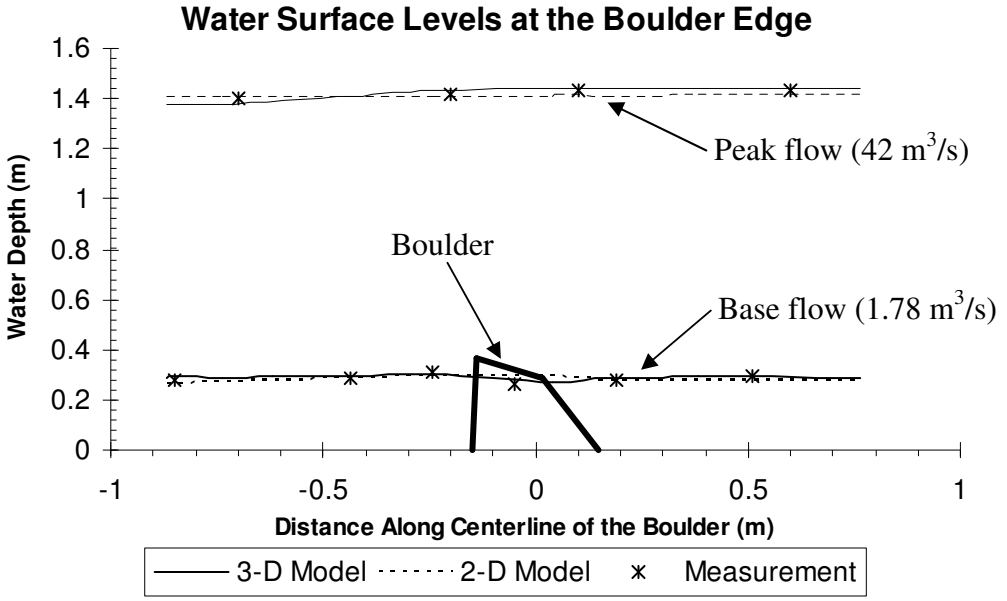

Figure 7. Calculated water levels past the single boulder in the first area of the Smith River at base and peak flows by 2- and 3-D models.

Table 3. The two study areas and the two flow regimes considered for numerical modeling in the Smith River.

Boulder	Boulder height h and width D (m)	Base flow (1.78 m^3/s) Free stream mean velocity (0.25 m/s)		Peak flow (42 m^3/s) Free stream mean velocity (1.2 m/s)	
		Water Depth d (m)	Relative Depth d/h	Water Depth d (m)	Relative Depth d/h
1	h = 0.36 D = 0.5	0.28	0.78	1.42	3.9
2	h = 0.38 D = 3.9	0.31	0.8	1.44	3.8
3	h = 0.35 D = 2.6	0.34	0.97	1.47	4.2
4	h = 0.31 D = 6.3	0.31	1.0	1.44	4.6

Note: Boulder #1 is the single boulder in the first study area; while boulders #2, #3 and #4 are three large rocks in the second study area (see also Figure 2)

boulder is partially dry, the water surface elevation near the boulder obtained by the 3-D model reaches its highest elevation immediately upstream of the boulder. This is consistent with the expected behavior, since as the flow approaches the boulder, part of its kinetic energy should be transferred to pressure head, resulting in a local increase of the water depth. The water level is reduced immediately downstream of the boulder and is restored when the flow moves further away from it. This behavior is in agreement with the field measurements and is similar to the trend observed by Shamloo et al. (2001) during their emergent hemisphere experiment as well as with the water surface levels around a bridge pier calculated numerically by Salaheldin et al. (2004).

Velocity field in the first area (single boulder case)

Figure 8 shows the horizontal velocity vectors around the single boulder simulated by both models for the base flow scenario (relative depth = 0.78, Table 3). Specifically, Figure 8a illustrates the depth-averaged velocities computed by the 2-D model. Figure 8b plots the velocities obtained from the 3-D model on Plane A, located at a distance of 0.4d (= 0.11 m) from the riverbed. Figure 8c depicts the velocity pattern rendered by the 3-D model on Plane B, which is 0.15 m above the bed, considered as a potential trout feeding location. Both Figs 8b and c demonstrate that the 3-D model can predict two small circulation cells trailing immediately downstream of the boulder caused by separated flows. These two cells rotate in opposite directions and create a triangular region immediately behind the boulder dominated by reverse velocities. The 2-D model is not capable of detecting such flow behavior and thus performs poorly for separated flows. Instead, only downstream and lateral velocity components with reduced magnitudes were computed behind the boulder by the 2-D model.

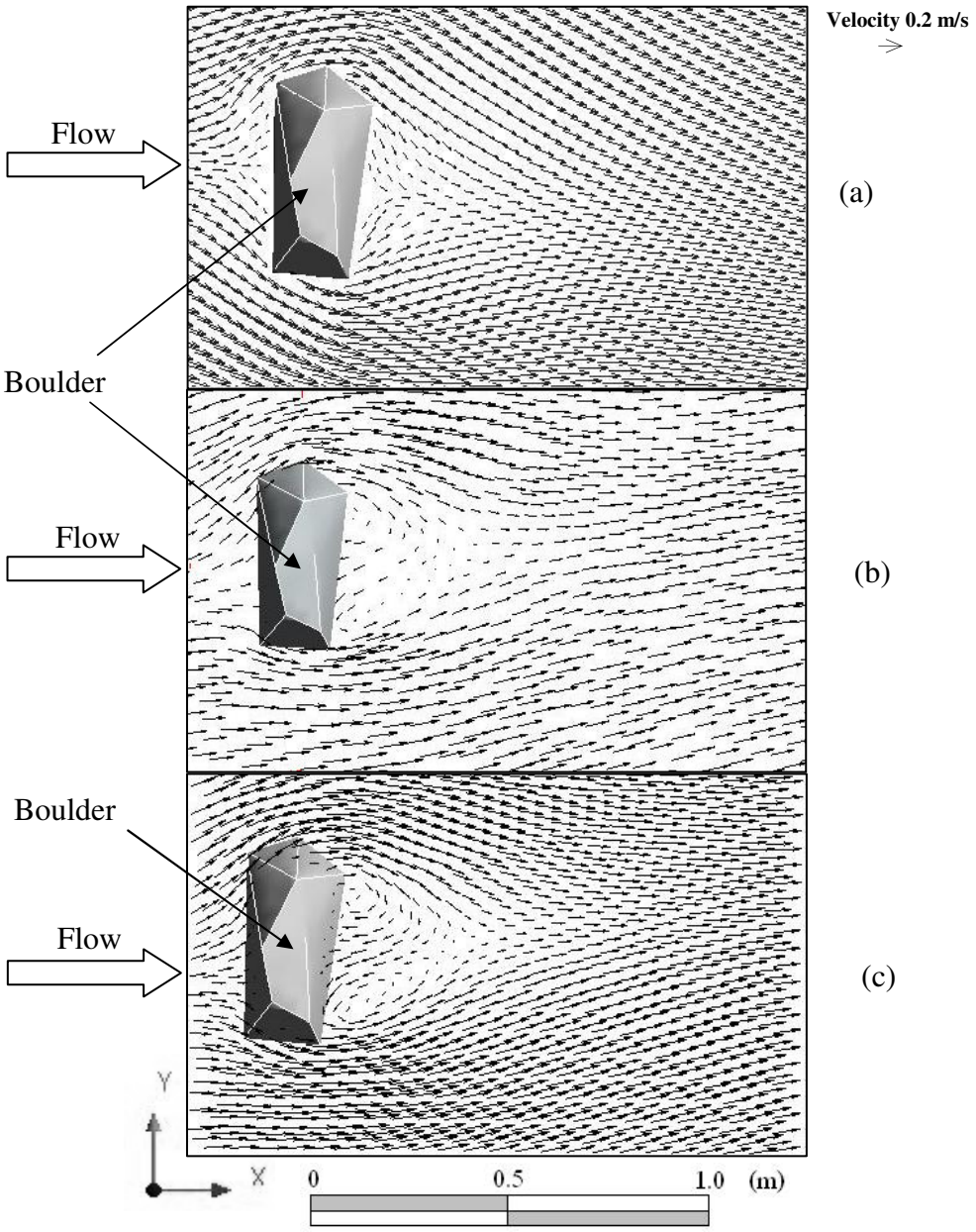

Figure 8. Outputs of horizontal velocity vectors from the 2-D and 3-D models at base flow for the single boulder case in the first area of the Smith River site. (a) depth-averaged velocities provided by the 2-D model. (b) velocity patterns computed on Plane A (0.11 m above the bed) by the 3-D model. (c) velocity vectors calculated on Plane B (0.15 m above the bed) by the 3-D model. Note: velocity units are in terms of m/s and arrows show the direction of flow and are scaled by the mean flow velocity magnitude (see upper right corner).

For the same flow regime, a more detailed comparison of the vertical distribution of streamwise velocity, u, is made between the 3-D model and the field velocity measurements at two different locations behind the boulder (Figure 9a). The depth-averaged velocities obtained by the 2-D model at the same locations are also included in the figure. At point A, located along the centerline of the boulder and at a distance of 0.2D downstream from it (see Figure 3), the velocities obtained from both the 3-D model and the field measurements follow a similar trend, with both profiles facing backward almost over the entire depth (Figure 9a), though the 3-D model results tend to overestimate the negative velocity magnitudes. Such velocity distributions are consistent with the results computed earlier for the corresponding laboratory study case (Experiment CS1). As far as the depth-averaged results are concerned, a large discrepancy is evident between the values calculated by the two numerical models. The 2-D model incorrectly calculated a positive value of 0.09 m/s, while the corresponding 3-D and field depth-averaged velocity values were -0.061 m/s and -0.047 m/s, respectively. At point B, located 4D downstream from the boulder along its centerline, where no reverse flows were present (Figure 9b), the depth-averaged velocity values calculated by the two models are in good agreement with each other and with the field measurement values.

For the peak flow case (42 m^3/s), with a relative depth of 3.9 (Table 3), the results obtained from the 2-D model, depth-averaged velocity values, and the 3-D simulations, velocity vectors at planes A and B, are plotted in Figure 10. It is shown there (Figure 10a) that the 2-D model simply treats the boulder as a large roughness element contributing to the reduction of the cross-sectional area and is unable to detect any backward flows. On plane A, 0.4d or 0.56 m above the riverbed and 0.2 m higher than the top of the boulder, the flow seems essentially uniform (Figure 10b). However, when the plane is lowered to

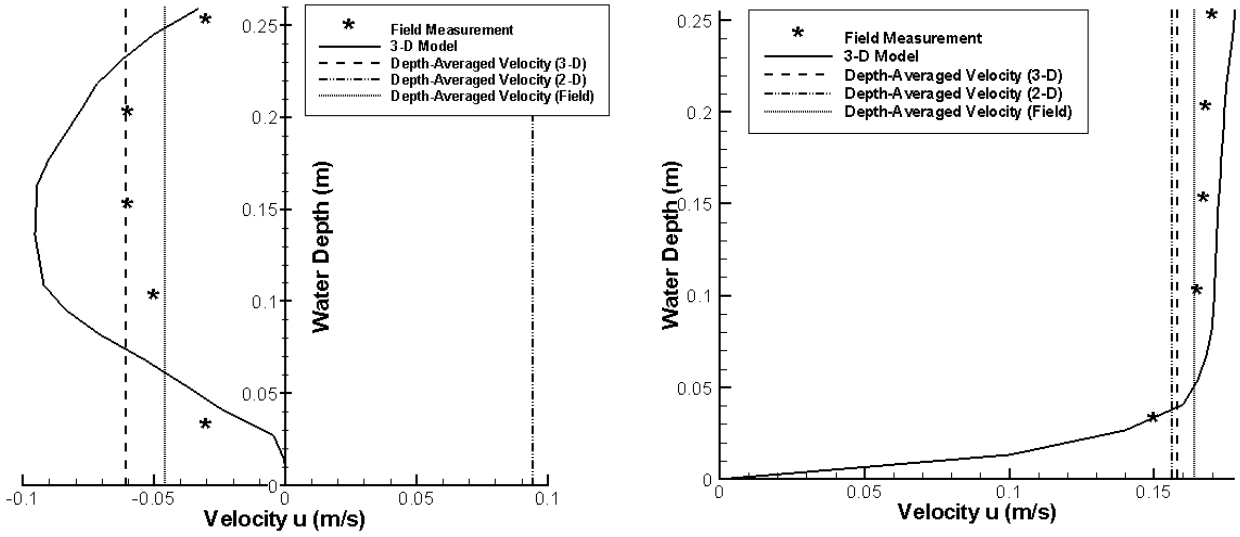

(a) Point A (b) Point B

Figure 9. Comparison among the 2-D, 3-D model results and field measurements for streamwise velocity *u* profiles at the two points behind the single boulder in the first area in the Smith River at base flow. Field data were collected using the Marsh McBirney Model 2000 flow meter.

0.15 m above the bed (i.e. plane B), a pair of counter-rotating vortices is observed behind the boulder (Figure 10c). This is attributed to the existence of an arch vortex bounded by the free shear layers originating from the top and sides of the boulder. Again, these results are in accord with our findings from the 3-D simulations of the DS1 laboratory experiment described earlier.

Figure 11 presents results regarding the streamwise velocity component, *u*, at points A and B (see Figure 3) under peak flow conditions. At point A (Figure 11a), the 3-D model predicts a backward flow region which extends from the river bottom up to an elevation almost equivalent to the boulder height (33 cm). The velocity then changes direction and reaches its maximum value at a depth of 0.55 m above the bed. This reflects

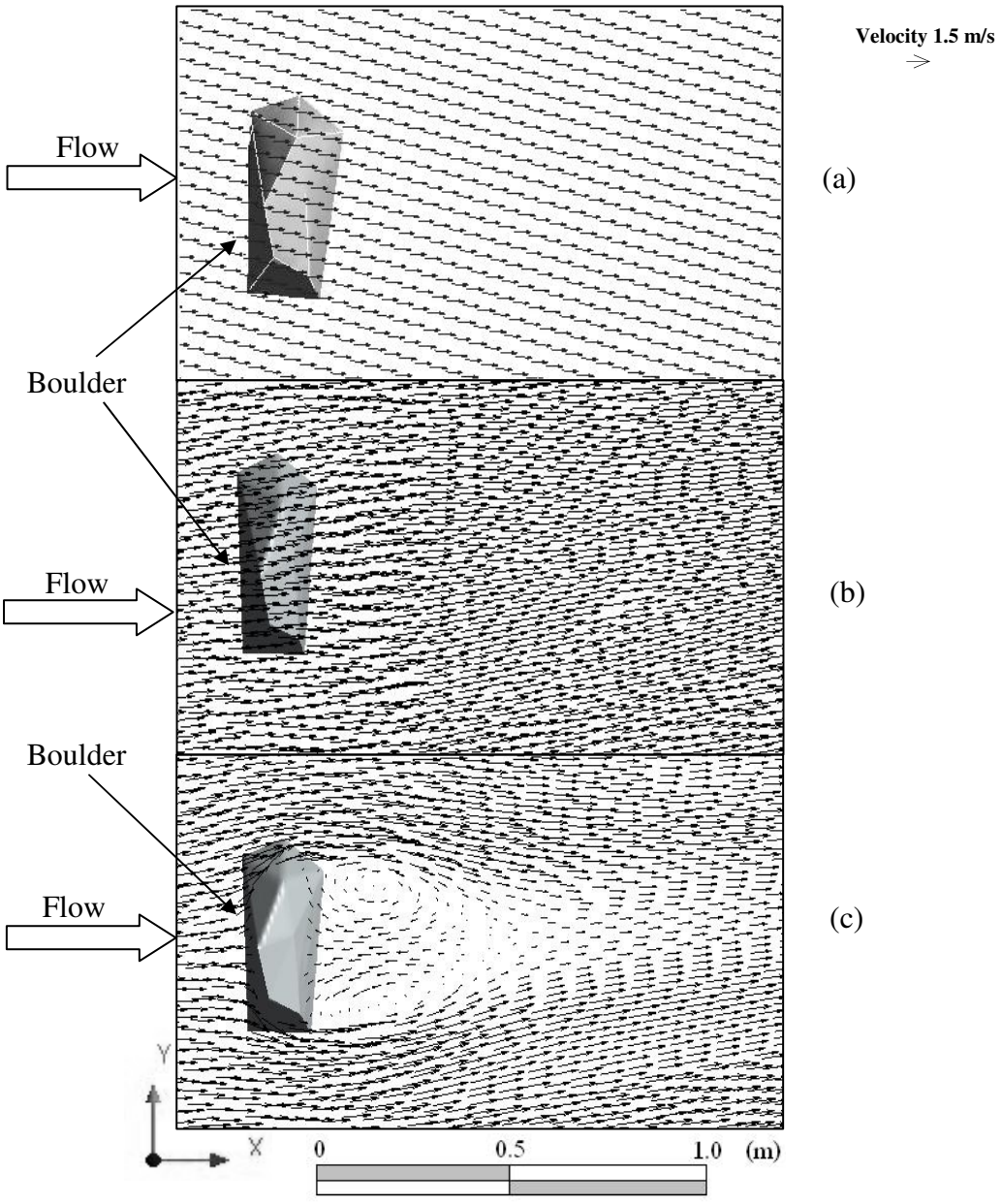

Figure 10. Outputs of horizontal velocity vectors from the 2-D and 3-D models at peak flow for the single boulder case in the first area of the Smith River site. (a) depth-averaged velocities provided by the 2-D model. (b) velocity patterns computed on Plane A (0.56 m above the bed) by the 3-D model. (c) velocity vectors calculated on Plane B (0.15 m above the bed) by the 3-D model. Note: velocity units are in terms of m/s and arrows show the direction of flow and are scaled by the mean flow velocity magnitude (see upper right corner).

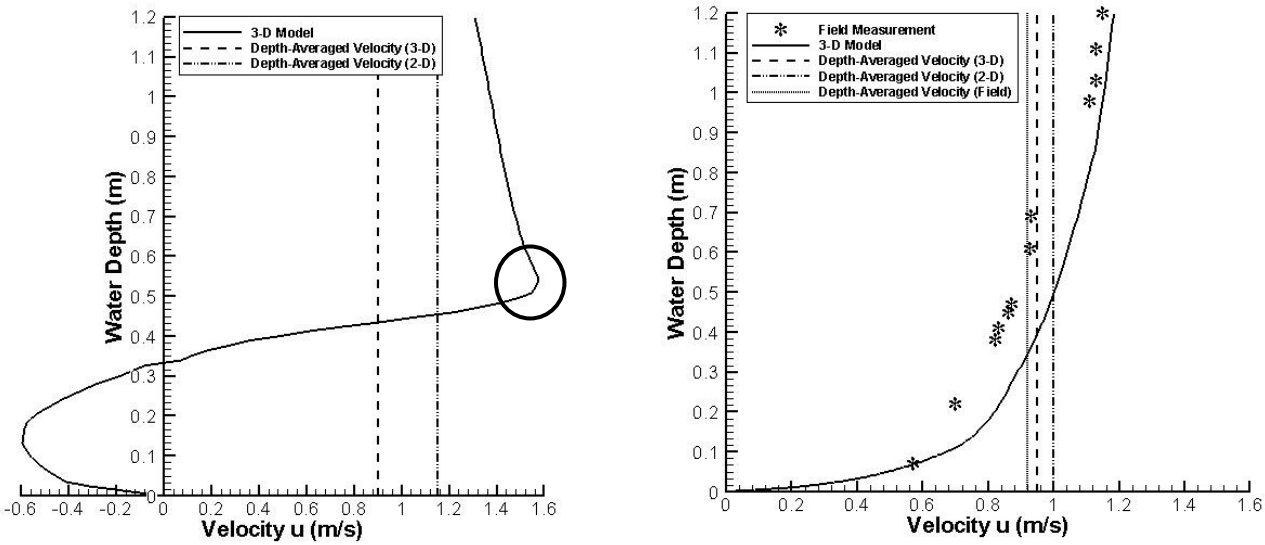

(a) Point A (b) Point B

Figure11. Comparison among the 2-D, 3-D model results and field measurements for streamwise velocity *u* profiles at two points behind the single boulder in the first area of the Smith River at peak flow. Field data were collected using the ADCP. The circle in (a) shows the location where the streamwise velocity *u* reaches its maximum value, immediately above the boulder.

the effect of the convergent flow moving over the boulder. Similar velocity distribution was observed by Hussein and Martinuzzi (1996) in the near wake region behind a cube placed in a channel. Above this level (0.55 m), the calculated flow velocity is relatively uniform. Because of the ADCP's inability to take measurements near flow obstructions, no field data was collected at this point. The 2-D model cannot provide any information regarding the reverse flow at point A; as a result, the depth-averaged velocity computed by this model is about 30% higher compared to the corresponding 3-D model based result. The difference in the velocities calculated by the two numerical models becomes smaller as the location moves further downstream to point B, where the flow is more uniform (Figure 11b). Both the depth-average velocity value and its distribution over the

flow depth computed by the 3-D model slightly overpredict the corresponding field measured values. This might be attributed to the rigid lid approach employed for modeling the free surface boundary.

Vorticity and circulation metrics computed for the first (single boulder) and second (boulder cluster) areas

The circulation metric, Eq. (7), was computed for the two study areas (single boulder and boulder cluster, Figure 2) from the velocity distributions obtained with the two models for base and peak discharge simulations (Table 4). The three large rocks in the second area have an average height of 0.35 m and an average base width of 4.3 m (Table 3). Three cases were considered to examine the ability of each model to capture the degree of flow complexity within each study area as reflected through the circulation metric calculations. The first case dealt with base flow and the second with peak flow circulation metric calculations. The third case drew a comparison between the two flow scenarios based on the circulation values obtained from each model.

At base flow (Table 3), both model simulations generated two high vorticity regions, one on each side of the boulder (Figs. 12a and b). However, pronounced differences exist between the exact vorticity locations predicted from the two models (Figs. 12a, b, d and e). For the 2-D model, the highest vorticity values appear immediately beside the edges of the boulders, but vorticity is absent behind the boulders. The 3-D model computed two much smaller areas of high vorticity on the sides of the boulders, but much longer high vorticity trails directly downstream from the boulders. The distinction may be attributed to the different turbulent mixing processes approximated by the two models and the inability of the 2-D model to satisfy the non-slip condition on solid boundaries. The flow behaviors exhibited by the 2-D simulations

Table 4. Vorticity and circulation metric values from the 2-D and 3-D models for the two study areas in the Smith River.

Model	Boulder	Base flow						Peak flow					
		Area A_{VOR} (m^2)		Absolute Circulation $\|\Gamma\|$(m^2s^{-1})		Circulation Metric $\|\Gamma\|\div A_{VOR}$ (s^{-1})		Area A_{VOR} (m^2)		Absolute Circulation $\|\Gamma\|$(m^2s^{-1})		Circulation Metric $\|\Gamma\|\div A_{VOR}$ (s^{-1})	
2-D Model	1	3.2		0.79		0.25		3.5		0.06		0.02	
	2	13.8		2.74		0.20							
	3	18.6	58.4	2.22	7.56	0.12	0.13	60.8		0.61		0.01	
	4	26.0		2.60		0.10							
3-D Model (Plane A, 0.4d)	1	3.2		1.14		0.36		3.5		0.24		0.07	
	2	13.8		4.41		0.32							
	3	19.5	59.3	3.65	11.35	0.19	0.19	60.8		2.34		0.04	
	4	26.0		3.29		0.13							
3-D Model (Plane B, 15cm)	1	2.8		1.01		0.36		2.8		5.86		2.09	
	2	9.4		2.12		0.22		9.4		2.07		0.22	
	3	12.0	42.1	1.62	5.72	0.14	0.14	12.0	42.4	2.93	7.73	0.24	0.18
	4	20.7		1.98		0.10		21.0		2.73		0.13	

Note: Boulder 1 refers to the single boulder in the first area; Boulders 2, 3 and 4 are the three large rocks in the second area, arranged from upstream to downstream (Figure 5)

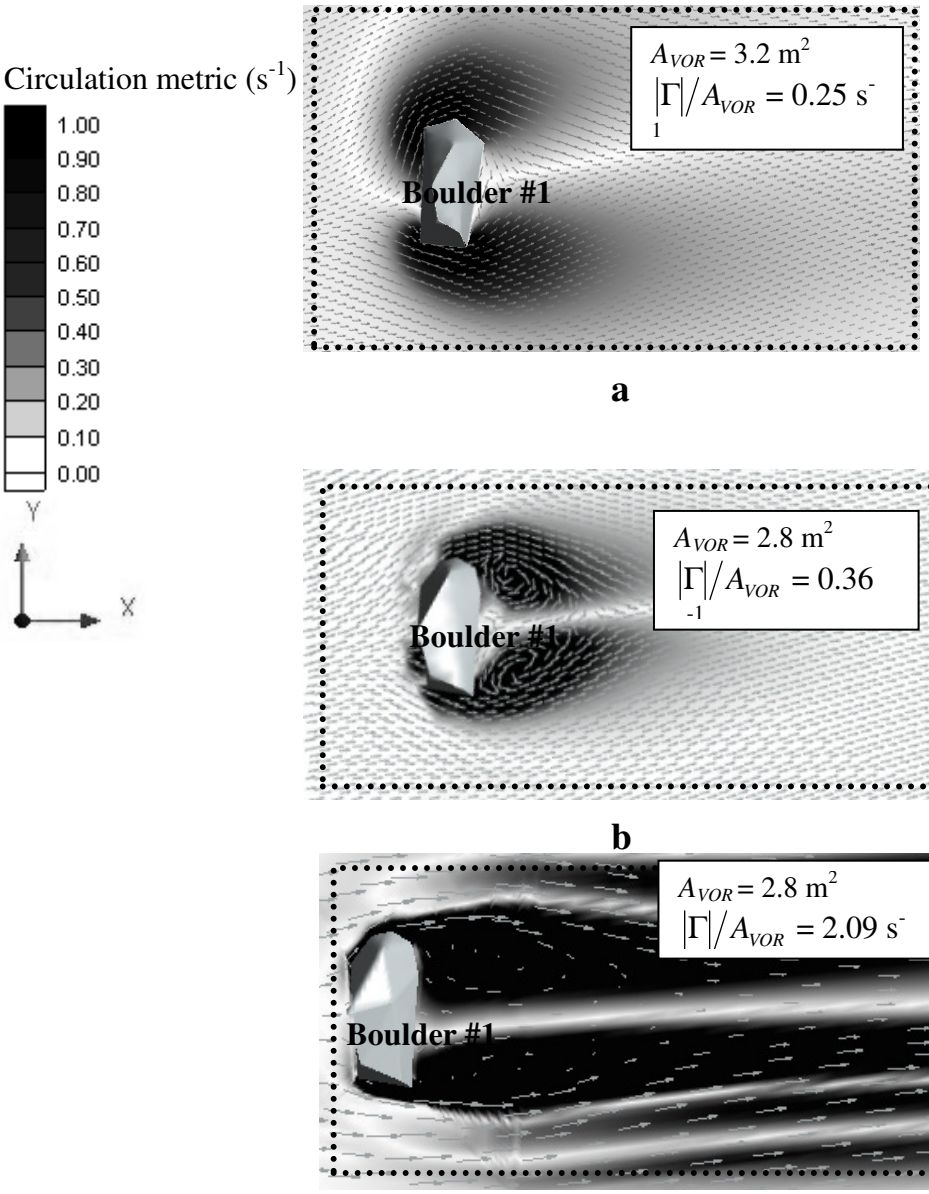

Figure 12. Plot of the absolute circulation metric values $|\Gamma|/A_{VOR}$ within the region AVOR surrounding the boulders in the two study areas. Flow is from left to right. (a) Single boulder in the first area at base flow (2-D model) (b) Single boulder in the first area at base flow on Plane B (3-D model) (c) Single boulder in the first area at peak flow on Plane B (3-D model).

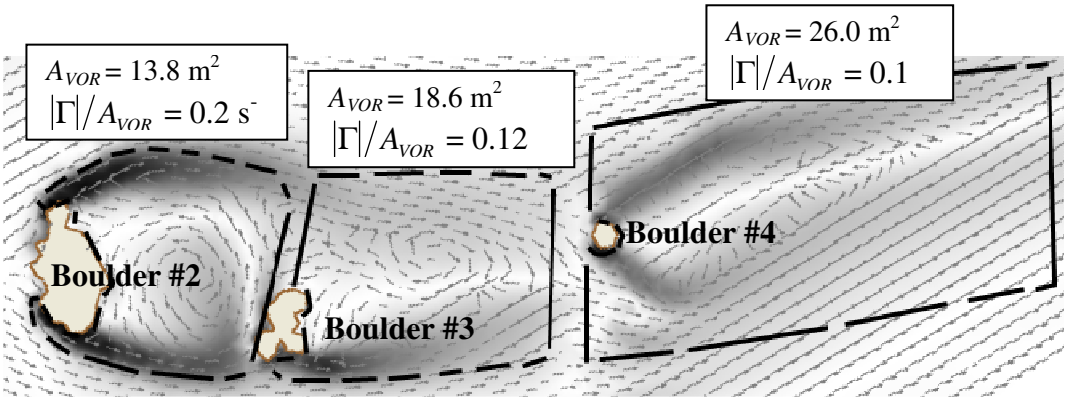
A_{VOR} = 13.8 m^2
$|\Gamma|/A_{VOR}$ = 0.2 s$^-$
A_{VOR} = 18.6 m^2
$|\Gamma|/A_{VOR}$ = 0.12
A_{VOR} = 26.0 m^2
$|\Gamma|/A_{VOR}$ = 0.1
Boulder #2
Boulder #3
Boulder #4

d

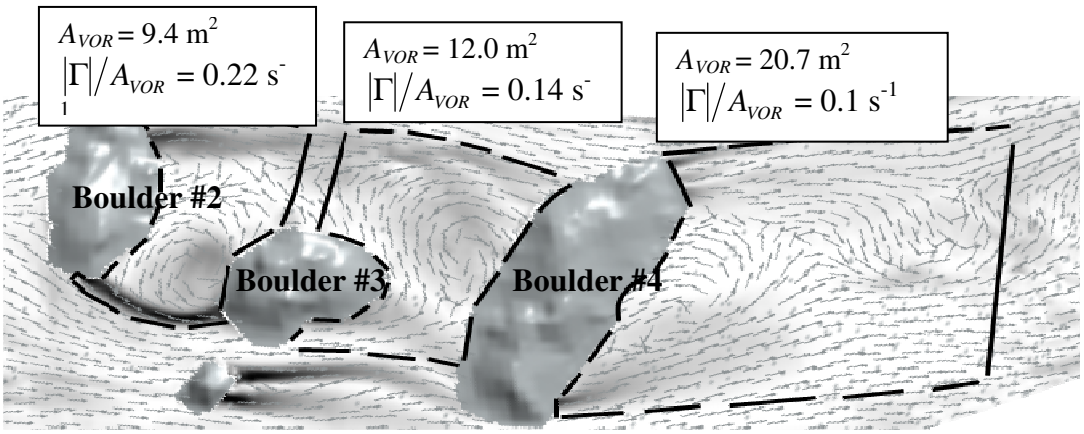
A_{VOR} = 9.4 m^2
$|\Gamma|/A_{VOR}$ = 0.22 s$^-$
1
A_{VOR} = 12.0 m^2
$|\Gamma|/A_{VOR}$ = 0.14 s$^-$
A_{VOR} = 20.7 m^2
$|\Gamma|/A_{VOR}$ = 0.1 s^{-1}
Boulder #2
Boulder #3
Boulder #4

e

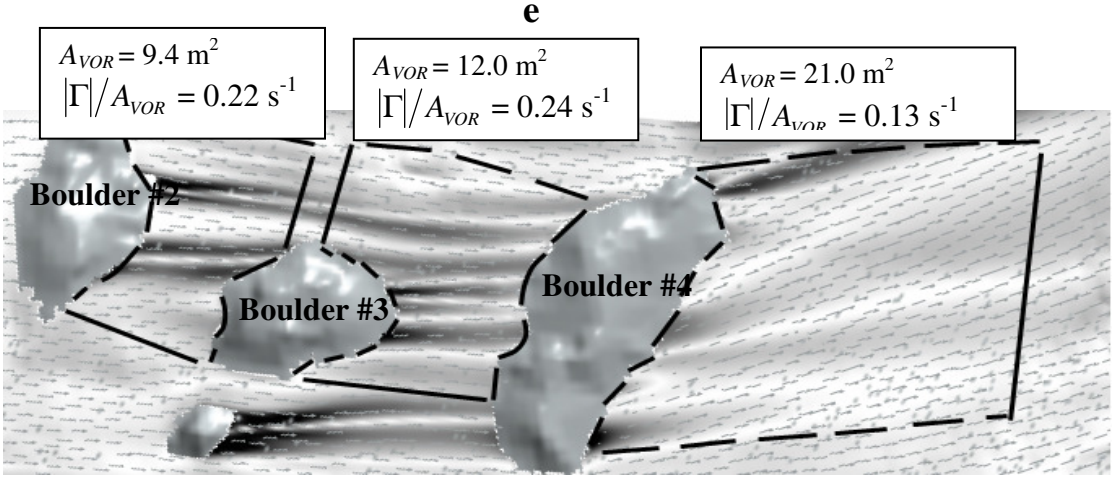
A_{VOR} = 9.4 m^2
$|\Gamma|/A_{VOR}$ = 0.22 s^{-1}
A_{VOR} = 12.0 m^2
$|\Gamma|/A_{VOR}$ = 0.24 s^{-1}
A_{VOR} = 21.0 m^2
$|\Gamma|/A_{VOR}$ = 0.13 s^{-1}
Boulder #2
Boulder #3
Boulder #4

f

Figure 12 (continued). (d) Boulder cluster in the second area at base flow (2-D model) (e) Boulder cluster in the second area at base flow on Plane B (3-D model) (f) Boulder cluster in the second area at peak flow on Plane B (3-D model) Black dashed lines around each boulder represent the areas A_{VOR} considered for the circulation metric calculations. Results from the 3-D model were calculated based on the velocity patterns on Plane B (15 cm above riverbed). The total A_{VOR} for the entire boulder cluster on Plane B in the second area is 42 m^2. The corresponding average circulation metric value $|\Gamma|/A_{VOR}$ for the boulder cluster case is 0.14 s^{-1} at base flow and 0.18 s^{-1} at peak flow. Note: The boulders' shapes outlined in (d) are different from those in (e) due to the proximity of wet/dry algorithm used in the 2-D model (not the free surface algorithm used in the 3-D model). The results from the 2-D model at peak flows were not plotted since vorticity values are too small

(Figure 12a and d) contradict available field and laboratory observations while the 3-D model results (Figure 12b and e) appear to be consistent with such observations (e.g. Tritico and Hotchkiss 2005).

The circulation metric values (Eq. 6) computed by the two models for the areas surrounding the four boulders at base flow were similar, with the numbers calculated by the 3-D model at plane A, located at a distance of 0.4*d* above the stream bed, being consistently higher (Table 4). The way the area associated with a boulder is selected, determines the value of the circulation calculations. In this case, the selected areas include the sides and the region behind each boulder, which explains to a certain degree the similar values obtained by the two models in spite of the different flow patterns predicted by them (Figure 12). For both model simulations, the single boulder in the first area, which is far away from other flow obstructions, consistently creates higher circulation metric values than any single boulder within the cluster (Table 4). This outcome is consistent with well known fluid mechanics experimental results and is attributed to the fact that boulders 3 and 4 are located within the wakes of boulders 2 and 3, respectively (Figure 12d and e).

At peak flow (42 m^3/s), with an average relative depth near 4 for all boulders (Table 3), plane A is located about 20 cm above the boulders. The 3-D simulation at plane A and the depth-averaged values obtained from the 2-D model do not exhibit pronounced vortex patterns at both study areas. As a result, the corresponding circulation metric values are small for these cases (Table 4). In contrast, the vorticity values calculated behind the boulders near the riverbed (plane B) based on the 3-D model simulation were much higher (Table 4, Figure 12c and f). As one would expect, the 2-D model is not capable of capturing the complex local flow patterns present in the vicinity of various flow obstructions during the peak flow conditions. Three-D modeling is mandatory to accomplish that.

The 2- and 3-D model simulations performed here show that even for the same streambed topography the degree of flow complexity varies for different flows. For flows that are sufficiently deep to submerge various obstructions, the location and intensity of vorticity and the magnitude of the circulation metric depend on the distance of the horizontal plane of interest from the streambed compared to the height of the obstructions. The 3-D simulations demonstrated that for a horizontal plane intercepting the obstruction (i.e. plane B in the Smith River case), the circulation metric values are high (Table 4). In this case they came out to be even higher than the corresponding values calculated at the same plane for base flow conditions (Table 4). This result is consistent with the observations of Buffin-Be'langer et al. (2006), obtained from laboratory flume experiments, who concluded that spatial heterogeneity of near-bed flows in the presence of coarse gravel increases at higher discharges. This increase in the flow complexity may be attributed to the interaction of the horseshoe vortices, developed immediately behind the boulders, with the strong arch-type vortices shed from the top of the submerged boulders (Figure 13). However, for deep flows, when the plane of interest is located even

at modest distance above the boulder (i.e. plane A for the peak flow simulation in Smith River) the flow patterns become more uniform and the corresponding circulation metric values very small (Table 4). Likewise, depth-averaged calculations based on 2-D models substantially reduce the flow complexity for deep flows (Table 4, Figure 10a). Therefore, 2-D models may not be suitable for reproducing the intricate near-bed flow patterns exploited by fish and other organisms at large discharge.

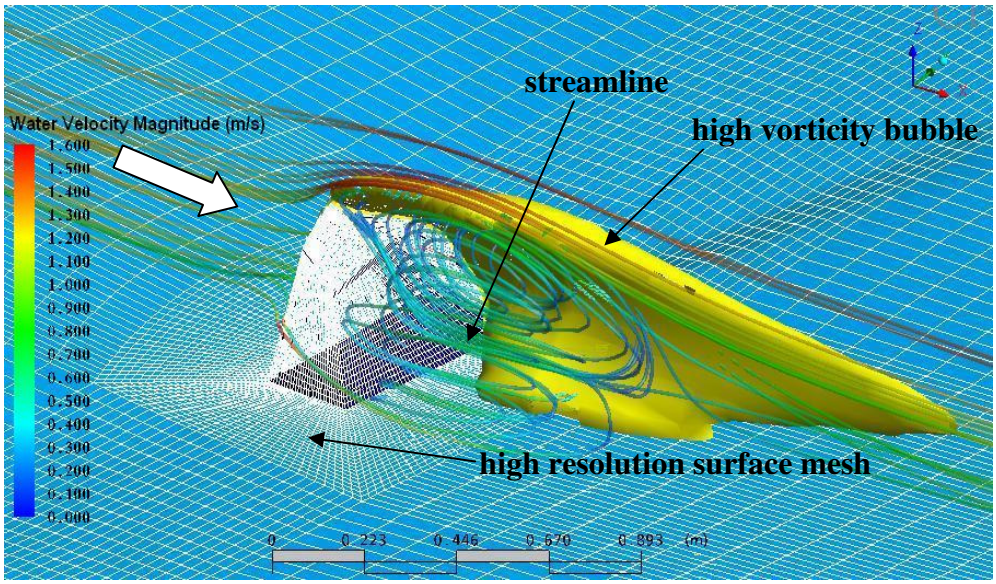

Figure 13 Representation of the three-dimensional velocity streamlines and one of the two high vorticity bubbles ($|\xi| > 0.4\ s^{-1}$) exhibited behind the singe boulder in the first area at peak flow. Results were provided by the 3-D model. The background shows the surface mesh on the boulder surface and streambed.

DISCUSSION

Boulders and rocks constitute fairly common components of a river's topography, especially in mountainous areas. The presence of boulders in streams, along with other flow obstructions, such as woody debris, spur dikes, riprap, bridge piers and weirs can promote complex localized flow patterns favored by many fish and invertebrates. Several studies (e.g. Cooper et al. 1993, Shields et al. 1995, Bouckaert and Davis 1998, Shamloo et al. 2001, Liao et al. 2003, Crowder and Diplas 2006) suggest that these natural and manmade hydraulic structures can play a key role in supporting food production, augmenting habitat diversity, increasing fish biomass, and providing feeding and rearing sites for various aquatic species. Experiments show that vortices shed from a cylinder can be exploited by trout in reducing its swimming energy cost (Liao et al. 2003), while elevated wake turbulence behind boulders was observed to enhance substantially macroinvertebrate population through retention of organic particles and augmentation of dissolved oxygen (Bouckaert and Davis 1998). In Smith River, brown trout redds were observed at the periphery of the recirculation regions of the boulders (Figs. 2 and 3), where vortex trails generated by the boulders were strong enough to entrain air and purge fine sediments from the streambed, a process that contributes to high embryo survival (see also Crowder and Diplas 2002). In recent years, advances in CFD technology have allowed simulation of these complex ecological stream flows in a diverse range of applications and have made numerical models an attractive analysis and design tool for ecosystem restoration (e.g. Salaheldin et al. 2004, Crowder and Diplas 2006).

CFD performance validation plays a pivotal role in 3-D habitat modeling. Compared with the hemisphere experimental results from Shamloo et al. (2001), the 3-D model, coupled with RSM turbulence closure, is proved reliable and has the ability, to a certain extent, to characterize the vortex shedding mechanism behind the obstacle at both

shallow and deep open channel flows. The underlying numerical techniques were previously tested successfully by Salaheldin et al. (2004) for a bridge pier at base flow, Morvan et al. (2002) on a meandering compound channel and Chu et al. (2005) using a backward-facing step for pipe flow. If a CFD model is used without validation, an inappropriate numerical function could be applied and in turn deliver unexpected results. As an example, the zero-equation turbulence model, a standard feature in many CFD codes, when implemented for simulation of flow around obstructions, may dramatically underpredict flow separation and thus generate spurious velocity values. The model implies turbulent stress approaches zero for a low flow field behind the boulder. Consequently, recirculation flow patterns present in the prototype may be oversimplified as uniform flows in the model outputs.

No comparison was made regarding eddy-viscosity or two-equation turbulence models in this study, because they are either not available in the current version of 2-D RMA2 software (Donnell et al. 2001) or theoretically inferior to RSM in the 3-D CFX package (CFX-5 2003). This does not mean that these models, like k-ε model and its variants, are not important in academic research and the industry. Rather, there may be limits to the extent to which these models can be applied without losing accuracy. For flow separation, secondary flows or swirling flows encountered in this study, the RSM turbulence model can facilitate a good prediction for their inherent anisotropic turbulence features, where eddy-viscosity assumption is not suitable (e.g. Salaheldin et al. 2004). Nevertheless, compared to RSM model, several studies have indicated that the two-equation models exhibit high stability and numerical robustness and can offer a good compromise in terms of accuracy and efficiency (e.g. Lane et al. 1999, Morvan et al. 2002), particularly for a less complex geometry. Further study about the applicability of two-equation models to complex ecological flows is warranted.

Achieving effective river restoration and ecosystem management will require addressing as many types of channel geometries (from boulder to pool and riffle) as possible which support various life stages of aquatic biota (from hatching insects to fish feeding) under a full range of flows (from base to peak flow). However, hydrologists and biologists are often challenged in their efforts to choose appropriate tools to run physical habitat simulations that deal with these issues. To model general flow characteristics of a river reach that is tens or hundreds of miles long, the use of 1-D models remains the most appropriate methodology to follow. If flow exchange between the riparian area and the main channel is significant, a 2-D model should be employed to better characterize the lateral velocities along the pertinent section of the river. A 2-D model would also be useful to resolve complex meso-scale flow patterns surrounding partially submerged flow obstructions, conditions typically encountered under low flows, as long as the computed areas can be carefully defined and the 2-D model satisfies the non-slip boundary condition and is coupled with an appropriate turbulence closure. However, if these flow obstructions become deeply submerged, conditions typically encountered during high flows, only velocities well above the obstacles may be quantified by a 2-D model, while the near-bed velocities affected by the obstructions should be computed using a 3-D model. The present study indicates that these near-bed small to medium-scale flow structures often involve reverse, upward and downward velocities, negative pressure and three-dimensional vortex shedding, which cannot be accurately reproduced from empirical equations using depth-averaged velocities in either a 1-D or a 2-D model. Moreover, for secondary flows near a channel bend, resolving the transfer between transverse and vertical velocities requires a 3-D flow model representation. Nevertheless, 2-D models can be adopted to determine water surface elevations and discharges at sections located at sufficient distance from boulders, which in turn can be applied as

inputs for upstream and downstream boundary conditions to a 3-D model used to resolve the localized flow patterns around a boulder or a boulder cluster.-

Three-dimensional flow structure and turbulence features obtained from 3-D models can be of great benefit for physical aquatic habitat assessment. Habitat Suitability Criteria (HSC) used in physical habitat studies that only consider standard metrics (e.g. depth-averaged velocity and water depth) would be improved by encompassing measures of spatial variation of local flow patterns (e.g. velocity gradient and kinetic energy). Several studies show that certain fish species activities may not be correlated with only local velocity or water depth, but instead can be connected with those measures reflecting heterogeneous flow pattern surrounding the fish location (e.g. Hayes and Jowett 1994, Crowder and Diplas 2002 and 2006). Quantifying these non-uniform flow structures will render the HSC more complete. Another advantage of the 3-D model is its ability to compute vorticity in all three directions. Aside from the circulation metrics examined on horizontal planes in this study, field data collected by Shields et al. (2003) indicate that stronger circulations in vertical planes were present near meandering bends in Little Tallahatchie River, Mississippi, that contributed to greater levels of species diversity. In the Smith River, three-dimensional bubbles of high vorticity were found behind boulders. For instance, there existed two lateral symmetrical high vorticity (>4 s^{-1}) bubbles behind the single boulder in the first area at the peak flow (Figure 13), with a total volume of 0.22 m^3, nearly 5 times as large as the boulder itself. Information on the volume, shape and location of these bubbles may influence the distribution of macroinvertebrates, dissolved oxygen, sediment entrainment or fish resting space within the water column during high flows. Fish typically use their genetic intelligence to find the location within the water column with the most favorable flow conditions, which is affected by the availability of food, bubbles, protection from predators and other factors. Obviously, any

single spatial or combined metric value estimated at a certain depth may not be sufficient to explain the ecologically significant flow complexity along the whole water column. A 3-D model is a useful tool in examining the three-dimensional circulation metric or other habitat parameters in any specific direction essential for aquatic biodiversity or benthic organism studies at a broader range of flow conditions.

The total area occupied by boulders may constitute a small portion of a stream reach. However, it should be noted that localized non-uniform velocity patterns and flow complexities augmented by the presence of these boulders may influence stream behavior for a considerable distance and represent a significant part of the total suitable aquatic habitat available in that stream (Shen et al. 2004). Although existence of these flow obstructions could influence a stream's overall health and should not be treated as simple channel roughness (Crowder and Diplas 2000), incorporation of boulders into instream flow studies or river restoration projects is not straightforward. Thus, it is often neglected because of the difficulty in acquiring the necessary field measurements and pursuing the required intensive numerical modeling. Conducting a proper physical habitat study near obstructions under different flow conditions presents a challenge for ecosystem restoration because it requires application of existing and emerging modeling methodologies, in combination with innovative surveying strategies. This is crucial for river engineers, fish biologists and water managers in determining how various types of geometric features should be considered in instream flow studies based on a project's goals, available tools and budget, so that the influence of river obstructions on flow behavior can be correctly evaluated to obtain a more complete picture of the stream's condition. Further studies may include 3-D unsteady flow simulations to model the alternating von Karman vortices exploited by fish and other species. Better understanding of the interaction between fish behavior and instantaneous fluid hydrodynamic

characteristics would provide insights into the development of better habitat suitability criteria for complex ecological stream flows.

CONCLUSION

Numerical simulations using 2- and 3-D CFD models were conducted to assess their ability to reproduce micro- and meso-scale complex flow patterns triggered by the presence of a hemisphere or boulders at various discharges. Compared to measured data, results show that the 3-D model, coupled with RSM turbulence closure, can provide a more satisfactory prediction of the reverse velocities and predominant circulation patterns near the flow obstructions. Moreover, results from the Smith River field study at base and especially at peak flows reveal that the 3-D model is capable of quantifying more accurately spatially varying flow features important to aquatic species for a wide range of stream flow conditions. Such information can assist the efforts of properly accounting for the role of flow obstructions on fish habitat enhancement in the design of stream restoration projects.

ACKNOWLEDGEMENT

The support of the Virginia Department of Game and Inland Fisheries and the U.S. Army Corps of Engineers for this study is gratefully acknowledged.

REFERENCES

Booker, D.J. 2002. Hydraulic modelling of fish habitat in urban rivers during high flows. Hydrol. Process. 17: 577-599.

Bouckaert, F. and J. Davis. 1998 Microflow regimes and the distribution of macroinvertebrates around stream boulders, Freshwater Biology 40: 77-86

Bovee, K.D., Lamb, B.L., Bartholow, J.M., Stalnake, J. Taylor, and Henriksen, J. 1998. Stream habitat analysis using the instream flow incremental methodology. U.S. Geologicial Survey, Biological Resources Division Information and technology Report USGS/BRD 1998-0004, 1.

Buffin-Be´langer, T., Rice, S., Ian Reid, I. and Lancaster, J. 2006. Spatial heterogeneity of near-bed hydraulics above a patch of river gravel. Water Resources Research. Vol 42. W04413, doi:10.1029/2005WR004070

CFX-5 Solver Theory (2003). CFX Ltd. Didcot Oxfordshire, U.K.

Chu A.K.M., Kwok R.C.W. and Yu K.N. 2005. Study of pollution dispersion in urban areas using Computational Fluid Dynamics (CFD) and Geographic Information System (GIS). Environmental Modelling & Software 20: 273-277.

Cooper, C.M., Testa, S., and Shields, F.D. Jr. 1993. Evaluation of invertegrate habitat created by rock introduced for stream bank stabilization (abstract number 412). Bull. North Am. Benthological Soc. 10(1), 202.

Crowder, D.W. and Diplas, P. 2000. Using two-dimensional hydrodynamic models at scales of ecological importance. Journal of Hydrology 230: 172-191.

Crowder, D.W. and Diplas, P. 2002. Vorticity and circulation: Spatial metrics for evaluating flow complexity in stream habitats. Can. J. Fish. Aquat. Sci. 59:633-644.

Crowder, D.W. and Diplas, P. 2006. Applying spatial hydraulic principles to quantify stream habitat. River Research and Applications, 22(1), 79-89.

Cullen, R.T. 1991. Vortex mechanisms of local scour at model fishrocks. Proceedings of American Fisheries Society Symposium 10: 213-218.

Donnell, Barbara P., Letter, Joseph V., McAnally, W.H. 2001. User's Guide for RMA2 Version 4.5 [http://chl.wes.army.mil/software/tabs/docs.htp]

Fischenich, C. and Seal, R. 1999. Boulder clusters. EMRRP Technical Notes Collection (ERDC TN-EMRRP-SR-11), U.S. Army Engineer Research and Development Center, Vicksburg, MS.

Gallagher, S.P. and Gard, M.F. 1999. Relationship between Chinook salmon (*Oncorhynchus tshawytscha*) redd densities and PHABSIM-predicted habitat in the Merced and Lower American rivers, California. Can. J. Fish. Aquat. Sci. 56:570-577.

Guay, J.C., Boisclair, D., Rioux, D, Leclerc, M., Lapointe, M. and Legendre, P. 2000. Development and validation of numerical habitat models for juveniles of Atlantic Salmon. Can. J. Fish. Aquat. Sci. 57: 2065-2075.

Guensch, G.R., Hardy, T.B. and Addley, R.C. 2001. Examining feeding strategies and position choice of drift-feeding salmonids using an individual-based, mechanistic foraging model. Can. J. Fish. Aquat. Sci. 58:446-457.

Hayes, J.W. and Jowett, I.G. 1994. Microhabitat models of large drift-feeding brown trout in three New Zealand rivers. North Am. J. Fisheries Mgmt 14: 710-725.

Hirt, C. and Nichols, B. 1981. Volume of fluid methods for the dynamics of free boundaries. Journal of Computational Physics 39: 201-225.

Hussein, H. J. & Martinuzzi, R. J. 1996, Energy Balance for the Turbulent Flow Around a Surface Mounted Cube Placed in a Channel. *Phys. Fluids.* **8**, 764-780

Kuhnle, R.A., Alonso, C.V. and Shields Jr, F.D. 2002. Local scour associated with angled spur dikes. Journal of Hydraulic Engineering. Vol. 128, No. 12: 1087-1093.

Lane, S.N., Bradbook, K.F., Richards, K.S., Biron, P.A. and Roy, A.G. 1999. The application of computational fluid dynamics to natural river channels: three-dimensional versus two-dimensional approaches. Geomorphology 29: 1-20.

Launder, B.E., Reece G.J. and Rodi, W. 1975. Progress in the development of a Reynolds-stress turbulence closure. J. Fluid Mech. 68: 537-566.

Launder, B.E. and Spalding, D.B. 1974. The numerical computation of turbulent flows. Comp Meth Appl Mech Eng, 3:269-289.

Leclerc, M., Boudreault, A., Bechara, J. and Corfa, G. 1995. Two-dimensional hydrodynamic modeling: a neglected tol iin the instream flow incremental methodology. Transactions of the American Fisheries Society. 124(5): 645-662.

Liao, J.C., Beal, D.N., Lauder, G.V., and Triantafyllou, M.S. 2003. The Karman gait: novel body kinematics of rainbow trout swimming in a vortex street. J. Exp. Biol., 206, 1059-1073.

Ludlow, J.A. and Hardy, T.B. 1996. Comparative evaluation of suitability curve based habitat modeling and a mechanistic basd bioenergetic model using 2-dimensional hydraulic simulations in a natural river system. 2nd International Symposium on Habitat Hydraulics, B519-B530.

Morvan, H., Pender, G., Wright, N.G. and Ervine, D.A. 2002. Three-dimensional hydrodynamics of meandering compound channels. Journal of Hydraulic Engineering 128(7): 674-682.

Munson, B.R., Young, D.F. and Okiishi, T.H. 1990. Fundamentals of fluid mechanics. 2nd ed. John Wiley and Sons, Inc., New York.

Mussetter, R.A., Harvey, M.D., Zevenbergen, L.W. and Tenney, R.D., 2001. A Comparison of one- and two-dimensional hydrodynamic models for evaluating Colorado pikeminnow spawning habitat, Yampa river, Colorado. "Applying Geomorphology to Environmental Management", Water Resources Publications, LLC.

Orth, D.J. and Maughan, O.E. 1982. Evaluation of the Incremental Methodology for recommending istream flows for fishes. Transactions of the American Fisheries Society 111: 413-445.

Orth, D. J., Diplas, P., Dolloff, A. and Newcomb, T. 2004. Influences of fluctuating Releases on Stream Fishes in the Smith River below Philpott Dam. Final Report (Contract No. 08220203). Richmond, VA., Federal Aid in Sport Fish Restoration Program Federal Aid Grant F-121-R-5, Virginia Department of Game and Inland Fisheries.

Salaheldin, T.M., Imran, J. and Chaudhry, M.H. 2004. Numerical modeling of three-dimensional flow field around circular piers. Journal of Hydraulic Engineering Vol 130, No.2:91-100.

Schwarz, W.R. and Bradshaw, P. 1994. Term-by-term tests of stress-transport turbulence models in a three-dimensional boundary layer. Phys. Fluids 6 (2): 986-998

Shamloo, H., Rajaratnam, N. and Katopodis, C. 2001. Hydraulics of simple habitat structures. Journal of Hydraulic Research, 39(4): 351-366

Shen, Y., Diplas, P. and Crowder, D.W. 2004 Two-dimensional hydraulic modeling: a tool for stream restoration studies. In: Proceedings of the 5th International Symposium on Ecohydraulics, Madrid, Spain.

Shields, F. Jr., Cooper, C.M. and Knight, S.S. 1995. Experiment in stream restoration. Journal of Hydraulic Engineering. Vol. 121, No.6: 494-502.

Shields, F. Jr., Knight, S.S., Testa, S.III and Cooper, C.M. 2003. Use of acoustic doppler current profilers to describe velocity distributions at the reach scale. Journal of The American Water Resources Association, 39(6): 1397-1408.

Shirvell, C.S. 1989. Ability of PHABSIM to predict Chinook Salmon spawning habitat. Regulated Rivers: Research & Management 3: 277-289.

Scott D and Shirvell CS. 1987. A critique of the instream flow incremental methodology and observations on flow determination in New Zealand. In: Craig JF, Kemper JB

(eds). Regulated streams: Advances in Ecology. Plenum Press, New York and London.

Tarbet, K. and Hardy, T.B. 1996. Evaluation of one-dimensional and two-dimensional hydraulic modeling in a natural river and implications in instream flow assessment methods. In: Leclerc, M., Capra, H., Valentin, S., Boudreault, A., Cote, Y. (Eds.), Ecohydraulics 2000 Proceedings of Second International Symposium on Habitat Hydraulics B. INRS-Eau & FQSA, IAHR/AIRH, pp. B395-B406.

Tritico, H.M. and Hotchkiss R.H. 2005. Unobstructed and Obstructed Turbulent Flow in Gravel Bed Rivers. Journal of Hydraulic Engineering. Vol. 131, No.8: 635-645.

Waddle, T., Steffler, P., Ghanem, A. Katopodis, C. and Locke, A. 2000. Comparison of one and two-dimensional open channel flow models for a small habitat stream. Rivers 7: 205-220.

Chapter IV: Modeling Unsteady Reservoir Releases and Their Potential Effects on Stream Habitat

Yi Shen[1] and Panayiotis Diplas[*2], M. ASCE

This chapter is a modified version of an earlier manuscript submitted to Journal of Hydraulic Engineering, ASCE.

ABSTRACT: Reservoir releases for generating power need to be reconciled with efforts to maintain healthy ecosystems in regulated rivers. Time-dependent flow features affecting channel morphology and aquatic physical habitat are investigated here using one-, two- and three-dimensional hydrodynamic models for a gravel-bed reach in Smith River, Virginia, USA. Temporal variation measurements of water surface elevation and velocity profile obtained in the field during a reservoir release are in good agreement with the three numerical simulation results. However, the one-dimensional model significantly overestimates the local bed shear stresses. In addition, a hypothetical "staggering" flow release scenario simulated by the three-dimensional model resulted in reduced erosional area and longer refugia availability for juvenile brown trout during hydropeaking. Issues related to the adoption of either a truly dynamic flow approach or a quasi-steady flow method for modeling unsteady flows in terms of a proposed unsteadiness parameter β are discussed. The insights obtained from this study can assist the efforts of properly accounting for the impact of unsteady flow fluctuations on fish habitat in the design of instream flow strategies.

[1] Hydrologist, Texas Parks & Wildlife Department, Austin, TX 78744. E-mail: yi.shen@tpwd.state.tx.us
[2] [*]Professor and Director, Baker Environmental Hydraulics Laboratory, Civil and Environmental Engineering Department, Virginia Tech, Blacksburg, VA 24061.E-mail: pdiplas@vt.edu

INTRODUCTION AND OBJECTIVES

In regulated rivers, it is common that base flow periods are disrupted by pulsing or rapidly changing flows resulting from hydropeaking, abrupt rainstorms and reservoir flood-control operations. The fluctuating flow regime plays a complicated role that has the potential to control the ecological integrity of a regional ecosystem through shaping river morphology, affecting wetland functions and altering species reproduction. In Switzerland, 30% of the monitored river ecosystems are affected by hydropeaking operations (FOEN 2008). In Virginia, U.S.A., frequent hydropeaking operations in the Smith River have caused the erosion of upstream gravel addition and catastrophic failure of young-of-the-year (age-0) fish species (Orth et al. 2004). On the contrary, in Australia, an increase in flood frequency is recommended in an effort to sustain the health of Barmah-Millewa Forest along the River Murray (Gordon et al. 2004, p.303). Therefore, a better understanding of the impact of rapidly changing flows on stream morphology and ecology is crucial for developing proper reservoir release rules, as attempts are made to restore previously altered ecosystems.

Information regarding unsteady, fluctuating flow behavior has been documented in the literature based on laboratory experiments and field measurements. On one hand, the velocity profiles in unsteady open-channel flows can be accurately described by the law of the wall (Tu and Graf 1992, Nezu et al. 1993). Quasi-steady state friction term is often used in the calculation of unsteady pipe flows and open-channel flows (Eichinger and Lein 1992). On the other hand, during the passage of a pulsing flow or flood, bed shear stresses and sediment transport processes can change significantly with time. For example, Song and Graf (1996) conducted unsteady velocity measurements in a laboratory flume using an acoustic Doppler velocimeter (ADV) and observed that the time-dependent depth-averaged velocity reached its maximum value earlier than the flow

depth. However, similar time lags between the arrivals of the peak values of the basic flow properties are rarely reported from field studies (Graf and Qu 2004). Nezu et al. (1997) investigated the unsteady velocity profiles over a smooth bed flume with a laser Doppler anemometer (LDA) and found that the value of instantaneous bed shear stress τ was not constant, but rather increased in the rising branch of the hydrograph, attained a maximum value before the peak depth was reached, and decreased in the falling branch. More recent experimental evaluations of the shear stress (or the friction velocity) during unsteady flows have been extended from well-controlled laboratory environments to streams and rivers. Rowinski et al. (2000) derived an expression of unsteady friction velocities from the Saint-Venant equations. Parameters in the expression, such as water surface slopes and velocities, were measured during the passage of flood waves in sandy streams in Poland. The so obtained unsteady shear velocities were found to significantly exceed those calculated with steady uniform flow formulae. It was found that results were greatly improved through the substitution of the bed slope in the uniform flow formulae by the instantaneous water surface slope. De Sutter et al. (2001), based on their results from flume erosion experiments and field measurements of artificial flood events in a small brook in Germany, recommended that unsteady friction velocity developed from the Saint-Venant equations be used to examine suspended sediment transport behavior during unsteady flows.

Many studies on the impact of fluctuating flows (e.g. hydropeaking) on physical habitat suitability are mainly focused on changes of riverbed geometry and response of fish behavior to peak flow conditions. The degree to which flows affect fish behavior varies depending on fish life-stages. For example, although fluctuating river levels seem to influence little the movement of adult brown trout (*Salmo Trutta*) in the Kananaskis River, Alberta (Bunt et al. 1999), fry displacement under hydropeaking was observed in

mountain streams by Liebig et al. (1999) and Orth et al. (2004). Reduction of the fish population may also be induced by high embryo mortality, which is linked to redd scouring under hydropeaking events (Montgomery et al. 1996, Orth et al. 2004).

Laboratory and field measurements are often restricted due to lack of suitable instruments, harsh weather and dangerous flow conditions. Development of proper numerical modeling methodologies is a viable alternative for understanding the impact of hydropeaking on natural river ecosystems. To date, ecological applications of hydraulic models to stream habitat have been used to design spawning gravel configuration in natural channels (Pasternack et al. 2004), examine local meso-scale flow structures around boulders and other obstructions (Crowder and Diplas, 2000 and 2006; Shen and Diplas, 2008), assess refugia habitat during high flows (Booker, 2003), and calculate spatial patterns of energy gain for drift-feeding (Guensch, et al. 2001). However, efforts for modeling the morphologically and biologically important transient flow, such as a regime component that occurs as the river level rises from the base to peak flow discharge, as well as quantifying its impact on physical fish habit during that period remain rare.

In this study, a historical unsteady flood pulse released from Philpott Reservoir in Smith River, Virginia was first measured during the rising branch of the discharge hydrograph. The unsteady flow was simulated using the three-dimensional (3D) hydrodynamic model CFX, based on the Unsteady Reynolds-Averaged Navier-Stokes (URANS) equations (CFX-5, 2003). A numerical sensitivity study for assessing the influence of different roughness height values on predicted flow properties was conducted using the 3D model. Next, the time-dependent flow features and shear stresses in selected riffles and pools near brown trout spawning sites computed by the 3D model were compared with field data, as well as those obtained using one-dimensional (1D

HEC-RAS) and two-dimensional (2D RMA2) dynamic approaches to evaluate the models' performance. As part of this objective, the feasibility of extending steady state shear stress formulae to unsteady flows was examined. Third, to explore potential effects of varying reservoir release patterns on gravel erosion and fish displacement during the flood period, a second 3D simulation was conducted using a hypothetical reservoir release scenario and compared with the 3D simulation results of the historical reservoir release. Considering that fish recruitment is often limited by hydropeaking events in the Smith River and other mountain streams, the information acquired through this study is important for understanding the effects of unsteady flows on physical fish habitat and for water managers to design appropriate instream habitat treatments.

ONE-, TWO- AND THREE-DIMENSIONAL HYDRODYNAMIC MODELS

A robust 3D hydrodynamic solver, CFX, is adopted for this study (CFX-5, 2003). The model solves the unsteady 3D Reynolds-averaged Navier-Stokes (URANS) equations. The governing equations consist of conservation of mass and momentum equations, which are expressed as:

$$\frac{\partial \rho}{\partial t} + \nabla \bullet (\rho \mathbf{V}) = 0 \tag{1}$$

$$\frac{\partial \rho \mathbf{V}}{\partial t} + \nabla \bullet \{\rho \mathbf{V} \otimes \mathbf{V} - \mu[\nabla \mathbf{V} + (\nabla \mathbf{V})^T]\} + \nabla p + \nabla \bullet \left(\rho \overline{\mathbf{v} \otimes \mathbf{v}}\right) - \mathbf{B} = 0 \tag{2}$$

where ρ = fluid density, t = time, $\mathbf{V}$ = 3D mean velocity vector, μ = dynamic viscosity, p = the total pressure, $\mathbf{v}$ = 3D fluctuating velocity vector, $\rho \overline{\mathbf{v} \otimes \mathbf{v}}$ = Reynolds stresses, and $\mathbf{B}$ = body force vector. Turbulence is simulated using the standard k-ε model. The governing equations are discretized using the finite volume approach. The First Order Backward Euler scheme approximates the transient term and the Upwind Difference

Scheme is used for discretising the advection term. The free water surface boundary is determined by using the Volume of Fluid (VOF) algorithm (Hirt and Nichols 1981). This method estimates the free water surface by calculating the volume fraction and velocities of both water and air in each element over the entire domain. Because the 3D CFX can account for vertical velocity and vertical acceleration, both hydrodynamic and hydrostatic pressures can be calculated. The solver is fully implicit. Boundary shear stress is calculated via a modified form of the law of the wall (Launder and Spalding 1974) and is given by:

$$\frac{U_t}{u^*} = \frac{1}{\kappa}\ln\left(\frac{c_\mu^{1/4}k^{1/2}y}{\nu}\right) - \frac{1}{\kappa}\ln\left(1+\frac{0.3k_s c_\mu^{1/4}k^{1/2}}{\nu}\right) + C \qquad (3)$$

where U_t = known instantaneous velocity parallel to the wall at a normal distance y from it, u^* = shear velocity, empirical coefficient $c_\mu = 0.09$, k = local turbulent kinetic energy, ν = kinematic viscosity of the fluid, $\kappa = 0.41$ (von Karman constant), k_s = equivalent grain roughness height and C = log-layer constant depending on wall roughness.

The 2D hydrodynamic model evaluated in this study is RMA2 (Donnell et al. 2001). The 2D model solves the depth-averaged form of the unsteady Navier-Stokes equations (i.e. also called shallow water equations) by assuming a hydrostatic distribution of pressure, since vertical velocity and vertical acceleration are neglected. The hydrostatic pressure distribution assumption is valid for gradually varied non-uniform unsteady flows and is often acceptable for rapidly unsteady flows (Hicks et al. 1991). Turbulence is accounted for by using a simple zero-equation model. Its governing equations are solved by the finite element method using the Galerkin Method of weighted residuals. Time derivatives are approximated by a nonlinear finite difference scheme. At the end of each time step, elemental elimination method is employed for the process of "wetting and drying" so that the instantaneous water surface boundary can be determined.

The solution is fully implicit and solved by Newton-Raphson nonlinear iteration scheme. Local instantaneous boundary shear stress is represented using the Manning friction approach and can be expressed as:

$$\tau = \rho g h S_f \cong \frac{\rho g V^2 n^2}{h^{1/3}} \tag{4}$$

where τ = local instantaneous bottom shear stress, S_f = local instantaneous friction slope, ρ = water density, g = gravity acceleration, V = local instantaneous total depth-averaged velocity, h = local instantaneous water depth and n = time-dependent roughness coefficient. Equation 4 was originally developed for steady uniform flows, but has been commonly applied in non-uniform (gradually varied) flows for practical purposes. In this study, it is assumed within each element or section and during every time step, the energy loss per unit length in the steady uniform flows is close enough to that in the unsteady non-uniform flows. The instantaneous value of S_f was updated through the Manning formula at every time step during the simulations of the unsteady reservoir releases.

The 1D simulations were performed using the UNET package from HEC-RAS developed by US Army Corps of Engineers (Brunner 2008). This model solves the full 1D St Venant equations for unsteady open channel flow. However, turbulence effects do not appear explicitly in the model equations. The governing equations were approximated using the implicit finite difference method and solved with the Newton-Raphson iteration technique. Instantaneous boundary shear stress in the 1D model was still calculated using equation (4).

STUDY SITE DESCRIPTION AND MEASUREMENTS

Field measurements of depth, velocity and shear stress were made in a 30 m wide by 160 m long gravel bed channel in the Smith River, Virginia (Figure 1a). The study site

is located 4 km downstream of the Philpott Reservoir, which is being operated in a hydropeaking mode using two 6700 kw turbines. Tailwater peak discharge released from the turbines is characterized by long periods of steady low discharge (1.78 m^3/s), interrupted daily by short-term pulses of much higher flows (38 m^3/s) (Figure 2). The discharge rises from base to peak flow over a period of approximately 20 minutes. The study site is critical for supporting wild brown trout population, where highest redd densities, juvenile abundance and spawning biomass were found (Orth et al. 2004). It is thought that the pulsing nature of the released flows has substantially affected the quality of local trout spawning (i.e. redds) and rearing habitats through redd scouring and fry displacement, and constrained the full potential of trout fishery. From 1999 to 2004, fish biologists and river engineers conducted a series of studies in this river exploring the feasibility of enhancing physical habitat of wild brown trout through the adjustment of reservoir operating rules (Orth et al. 2004).

The selected reach has a mild longitudinal channel slope, S_0 = 0.02%. The majority of boulders and pools in the reach are located on the right side (when looking downstream), while the left side mainly consists of riffles and an island. The detailed three-dimensional topography of the study reach, including the boulders and the island, was surveyed using a Leica® TC600 electronic total station that resulted in an actual field accuracy of <1 cm. Streambed materials are largely composed of gravels and pebbles and were sampled with a McNeil sediment core sampler from 5 different locations within the study site, including trout spawning locations. The collected sediments were dry sieved to determine the particle size distribution. The obtained median grain size d_{50} was 0.02 m, with a geometric standard deviation σ_g = 2.58 (Figure 3).

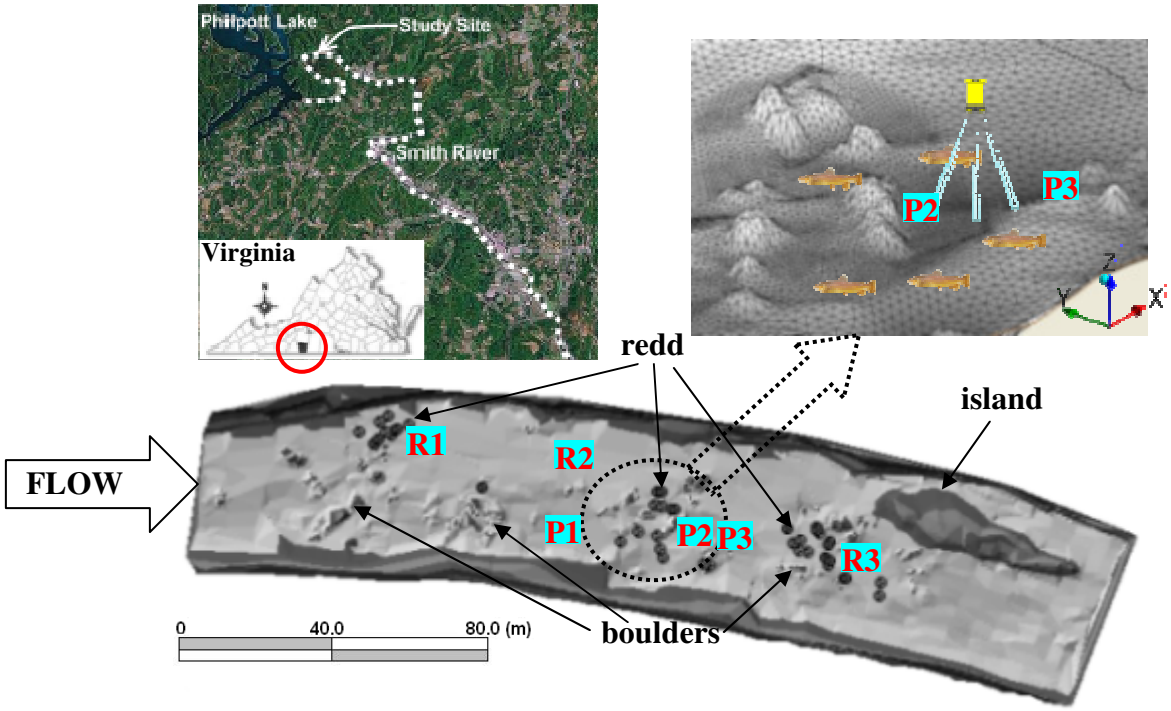
Philpott Lake
Study Site
Smith River
Virginia
P2
P3
redd
island
FLOW
R1
R2
P1
P2
P3
R3
0
40.0
80.0 (m)
boulders

(a)

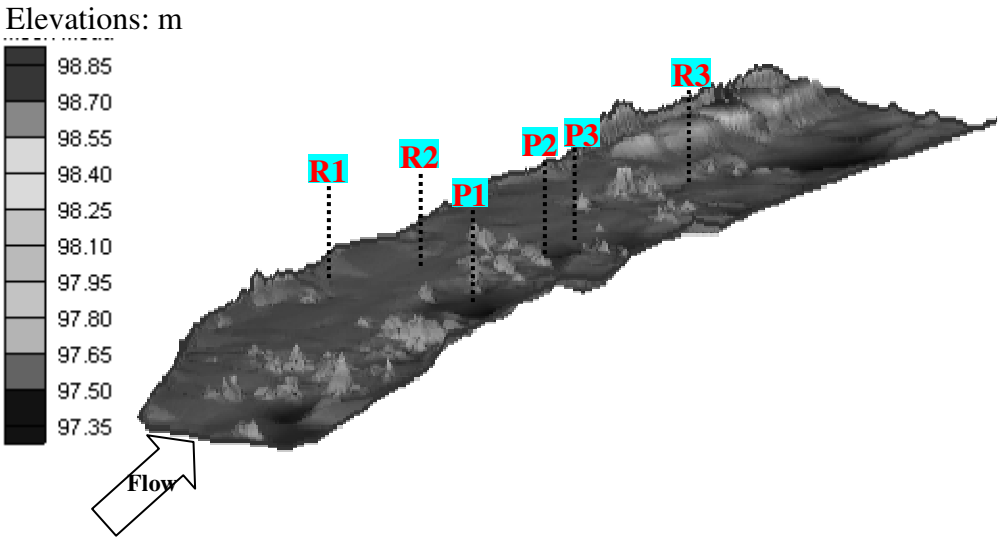
Elevations: m
98.85
98.70
98.55
98.40
98.25
98.10
97.95
97.80
97.65
97.50
97.35
R3
R1
R2
P2
P3
P1
Flow

(b)

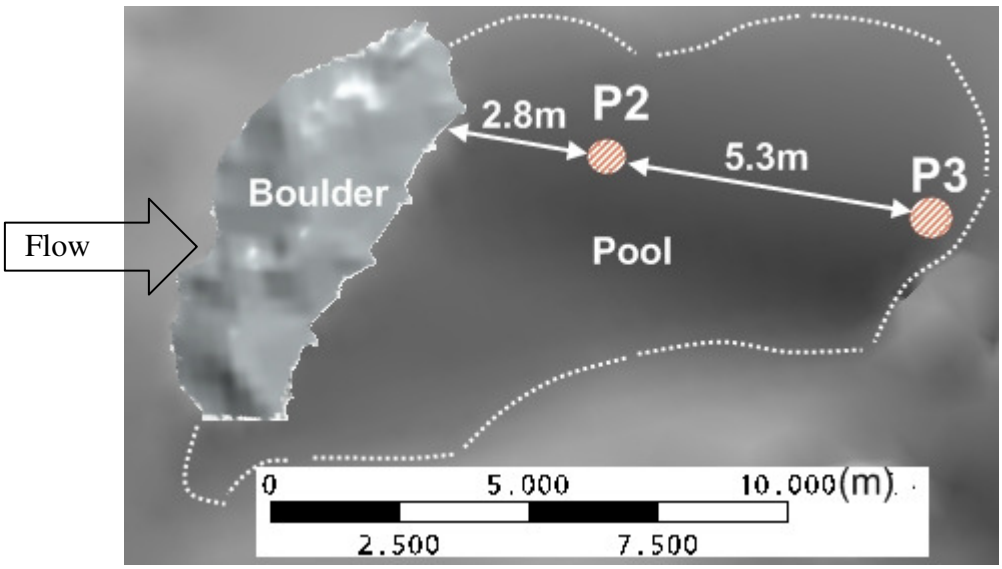

(c)

Figure 1 (a) Topographic map of the study reach in the Smith River tailwater below the Philpott Dam with brown trout spawning locations (represented by dots) and ADCP measurement points behind the boulder; (b) Locations of the six points used for comparison in the simulations (points R1, R2 and R3 are in the riffles; points P1, P2 and P3 are in the pools); (c) Approximate locations of points P2 and P3 with respect to the boulder. The white dotted line delineates the shape of the pool behind the boulder.

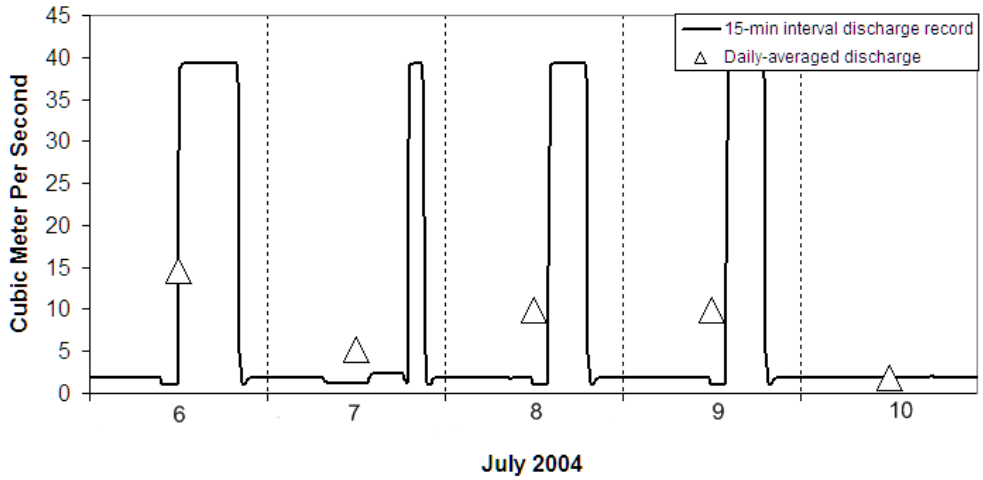

Figure 2 Typical 15-minute interval discharge records (USGS Gage# 02072000) at the Philpott Dam in the Smith River.

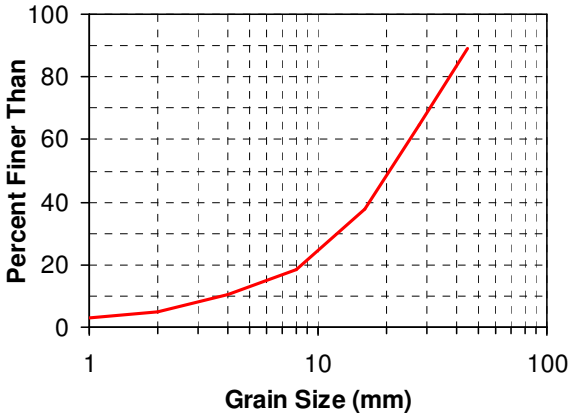

Figure 3 Cumulative logarithmic probability size-frequency graphs for the substrate sampled in the study site. Note: d_{50} = 0.02 m, d_{84} = 0.04 m, geometric standard deviation σ_g = 2.58.

The rising branch of the released discharge hydrograph was recorded at the upstream boundary of the study site using a SonTek® 3 MHz acoustic Doppler current profiler (ADCP) mounted on a catamaran suspended from a cableway over the river. The ADCP utilized three sensor heads for measuring the streamwise, lateral and vertical velocity components within each cell. Every profile was divided up to 13 cells along the water column, with each cell having 0.15 m depth. At the downstream boundary, the stage hydrograph was determined using a staff gauge and a stopwatch. Since the released flood wave receded very slowly after its peak, it is believed that the falling branch of the hydrograph can be approximated as a quasi-steady state flow using conventional modeling methodology. Therefore, only the rising limb of the discharge hydrograph was measured and modeled in the present study.

A total of 6 locations, 3 at riffles (points R1, R2 and R3) and 3 at pools (points P1, P2 and P3), were selected for comparison (see Figure 1b), either between measurements and numerical models, or among the numerical models only. These points

were randomly distributed over the entire site. All three points R1, R2 and R3 were located at the center of their individual riffles but were surrounded by different geo features. The upstream riffle, where point R1 was located, was a brown trout spawning site located between the left bank (looking downstream) and a boulder. Point R2 was about 30 meters downstream from point R1, but far away from other river obstructions. Point R3 was on a riffle between two boulder clusters where a spawning site was identified. Swift currents and uniform velocity patterns were observed on these riffles. On the other side, points P1 and P2 were at the deepest part of their individual pools covered by wakes generated by the upstream boulders, while point P3 was located in the same pool with P2 but further downstream from it at the pool tail (Figure 1c).

A major challenge in this study was the deployment and control of the ADCP during the flood. Consequently, only limited field data were obtained. During the rising limb of the flood wave, time-series of vertical velocity profile and water depth measurements were recorded using the ADCP at points P2 (in the near wake region) and P3 (in the far wake region) behind a boulder for validating the numerical models (Figure 1c).

To evaluate potential erosion problems at fish habitat under the reservoir release, bed shear stress, τ, was estimated from the measured velocity data. Traditionally, τ can be determined from the slope of a vertical velocity profile that follows a logarithmic distribution near the riverbed, the log-law. Nezu et al. (1997) demonstrated that the wall shear stress in unsteady flows in a water flume can be calculated accurately using the log-law developed in steady flows. Nevertheless, this method requires extensive velocity point measurements within a small log-layer, which may be difficult to collect at base flow (or shallow water) with large relative roughness elements in natural channels.

Hence, in this study, the log-law is modified so that the point velocity is replaced by a depth-averaged velocity. The equation then becomes:

$$\tau = \rho \frac{\kappa^2}{\ln^2\left(\frac{h}{ez_0}\right)} V^2 \quad (5)$$

where V = the local total instantaneous depth-averaged velocity; h = instantaneous water depth; e ≈ 2.718 (an irrational constant); and z_0 is roughness length, a small height above the bed where local near-bed velocity is zero and is assigned to be $0.1d_{84}$ in this study. This method assumes V occurs at depth h/e and was previously tested successfully for estimating steady shear stress in gravel-bed rivers using conventional flow meters and ADCP (e.g. Sime et al. 2007). In this study, the measured real-time values of V and h were used to calculate the instantaneous τ value using equation 5.

MODEL SETUP AND APPLICATIONS

A Digital Elevation Model (DEM) was created using ArcGIS® Desktop software based on the surveyed geometry of the study site. For the 3D CFX model, the DEM was imported into ANSYS ICEM CFD® to generate a total of 1,875,456 3D hexahedral cells. The average grid size in the horizontal plane is about 0.3 m × 0.3 m. The node spatial distribution along vertical edges follows the BiGeometric bunching law and varies from 0.015 m near the bottom and the water surface, to 0.05 m in the air portion above the water surface. The same DEM was processed and discretized into 54,297 2D triangular elements in the 2D RMA2 model. Efforts were made to setup the cross sections and elements in a way that can accurately describe major abrupt topography changes near boulders and the downstream island. For the 1D HEC-RAS model, the geometric boundary of the study site was setup using 57 cross sections extracted from the DEM.

The cross-sections were more closely spaced at those locations where more drastic changes in channel slope and shape occurred. Additional cross sections were added through interpolation so that the interval distance between any two transects was less than 4 m. Figure 4 illustrates the meshes for the three different numerical models.

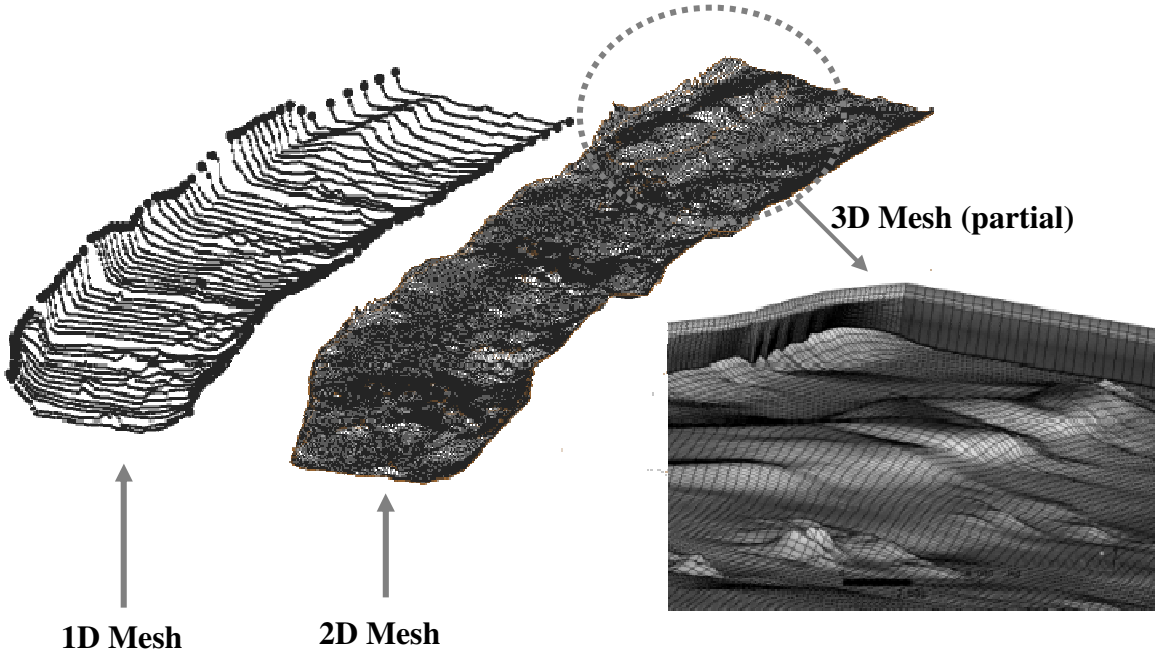

Figure 4. Oblique visualizations (looking at the downstream) of the complete 1D HEC-RAS and 2D RMA2 meshes. Only partial 3D mesh near the downstream end is shown in this figure. No meshes are scaled.

Within each time step during the simulations of the observed unsteady release, uniform roughness parameters were applied over the entire site for all three models' simulations. However, the discharge-dependent Manning's n values in the 1D HEC-RAS and the 2D RMA2 models were gradually reduced between time steps when the discharge increased to ensure that the errors of the stage hydrograph between the predicted and measured ones at points P2 and P3 were less than 10% (Figure 5). As far as the 3D CFX model, a constant roughness height, k_s, value was used throughout the simulation of the above measured reservoir release. In addition, roughness sensitivity

analysis was conducted for the 3D model to investigate the effects of bed roughness on the depths, velocity profiles, and bed shear stresses through testing three different roughness height values (i.e. $0.5d_{50}$, $2d_{50}$, $3d_{84}$). Nicholas (2001) used a k_s value of $0.5d_{50}$ (= 0.01m in this study) to quantify grain roughness in two gravel-bed rivers in UK. This value could also be valid in the Smith River, since for gravel-bed rivers, grain roughness is the primary cause of flow resistance (Chang 1998). Ge et al. (2005) modeled the scour patterns around a bridge foundation with an equivalent roughness of $2d_{50}$ (= 0.04 m in this study). A third k_s value of $3.5d_{84}$ was recommended by Hey (1979) for estimating bed shear stress in large gravel bed rivers. Because the log law layer is deemed to generally extend over the bottom 20% of the flow depth (the range of the total flow depth is 0.6~1.7 m during most of the simulation period of the unsteady reservoir release in this study), the value of $3.5d_{84}$ was adjusted to be $3d_{84}$ (=0.12 m = 0.2×0.6) in this study to ensure that the roughness height (or the first grid point off the wall in the mesh) is inside the log layer where the law of the wall is valid.

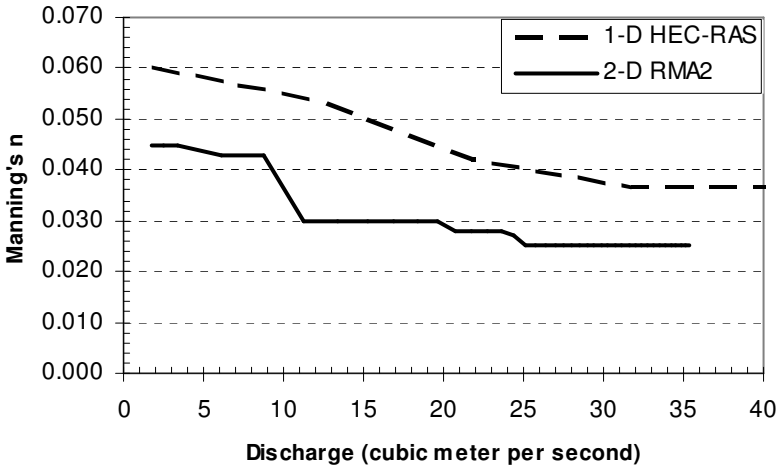

Figure 5 Discharge-dependent Manning's *n* values used in 1D HEC-RAS (Case A) and 2D RMA2 (Case B) models.

The measured boundary conditions were imposed on the three numerical models. Turbulence quantities at the upstream boundary in the 3D model were specified with a zero gradient option by assuming fully developed turbulent boundary layer. Small time step was adopted in all three models (Table 1) to preserve mass conservation and to avoid numerical shocks when cells change between wet and dry conditions (e.g. 2D RMA2 model). Nevertheless, the Courant number, representing the average ratio of the distance traveled by the flow to computational space interval (1D model) or an element size (2D and 3D model), may be allowed to be greater than 1, since all three models use implicit solvers and convergence was achieved within each time step. Our experience showed that stable solutions were obtained in the 2D RMA2 model, even with a Courant number as high as 10. Press et al. (1992) also reported stable numerical solutions with large Courant numbers when using implicit schemes. Table 1 summarizes major model parameters used in grid constructions, boundary conditions and simulations in this study.

Table 1. Main parameters used for 1D, 2D and 3D unsteady model simulations.

Case	Model	Grid/Transect number	Unsteady discharge [m^3/s]	Roughness parameter	Time step	Average courant number	Total Run Time (order of time magnitude)
A	1D	57	1.78→35	n=0.060→0.037	1[sec]	1.24	seconds
B	2D	54,297	1.78→35	n=0.045→0.025	3.6 [sec]	10	weeks ~ months
C1	3D	1,875,456	1.78→35	$k_s=0.5d_{50}$=0.01m	0.1[sec]	0.40	months*
C2				$k_s=d_{84}$=0.04m			
C3				$k_s=3d_{84}$=0.12m			
C4	3D	1,875,456	1.78→35	$k_s=3d_{84}$=0.12m	0.1~0.2[sec]	0.75	months*

*Note: all the 3D simulations were computed using 4 Intel Pentium® 4 CPU in a parallel computing environment.

SIMULATIONS OF THE HISTORICAL UNSTEADY RESERVOIR RELEASE

The performance of the 3D CFX model, using flood data gathered from the Smith River, is evaluated first. Sensitivity studies are conducted to examine the impact of three different roughness height, k_s, values on the computed values of depth, velocity and shear stress (Cases C1, C2 and C3, see Table 1). Comparisons were made only for the first 400 seconds period during the passage of the flood wave to save further computational efforts. Next, the 1D HEC-RAS (Case A), 2D RMA2 (Case B) and 3D CFX (Case C3) models were used to simulate the rising stage of the flood wave over an extended 20 min-long period. The 1D and 2D models were calibrated against measured water surface elevations at points P2 and P3. The 3D simulation was implemented using a roughness height of 0.12 m. Comparisons of the temporal variations of depth, velocity and shear stress obtained by the three models were also made.

Validation and numerical sensitivity studies with the 3D model

Figure 6 compares the simulated streamwise velocity profiles obtained with the 3D model against measured field data at 7 consecutive time instants during the rising stage of the flood wave at points P2 and P3, in the near and far wake regions of a boulder located in a pool (see Figure 1c). Comparisons among the simulations with three different roughness height k_s values are also presented in Figure 6. It is illustrated that at any time instant, the flow depth calculated for all three roughness scenarios is about the same. It is therefore concluded that, for the 3D model, the prediction of water surface elevation in the present unsteady flows is not as sensitive to the choice of the roughness values considered here. In addition, the 3D model reproduces the growth and evolution of the velocity profiles reasonably well, especially at location P3. At location P2 better predictions are obtained at the beginning (at time = 60 seconds) and when the velocity

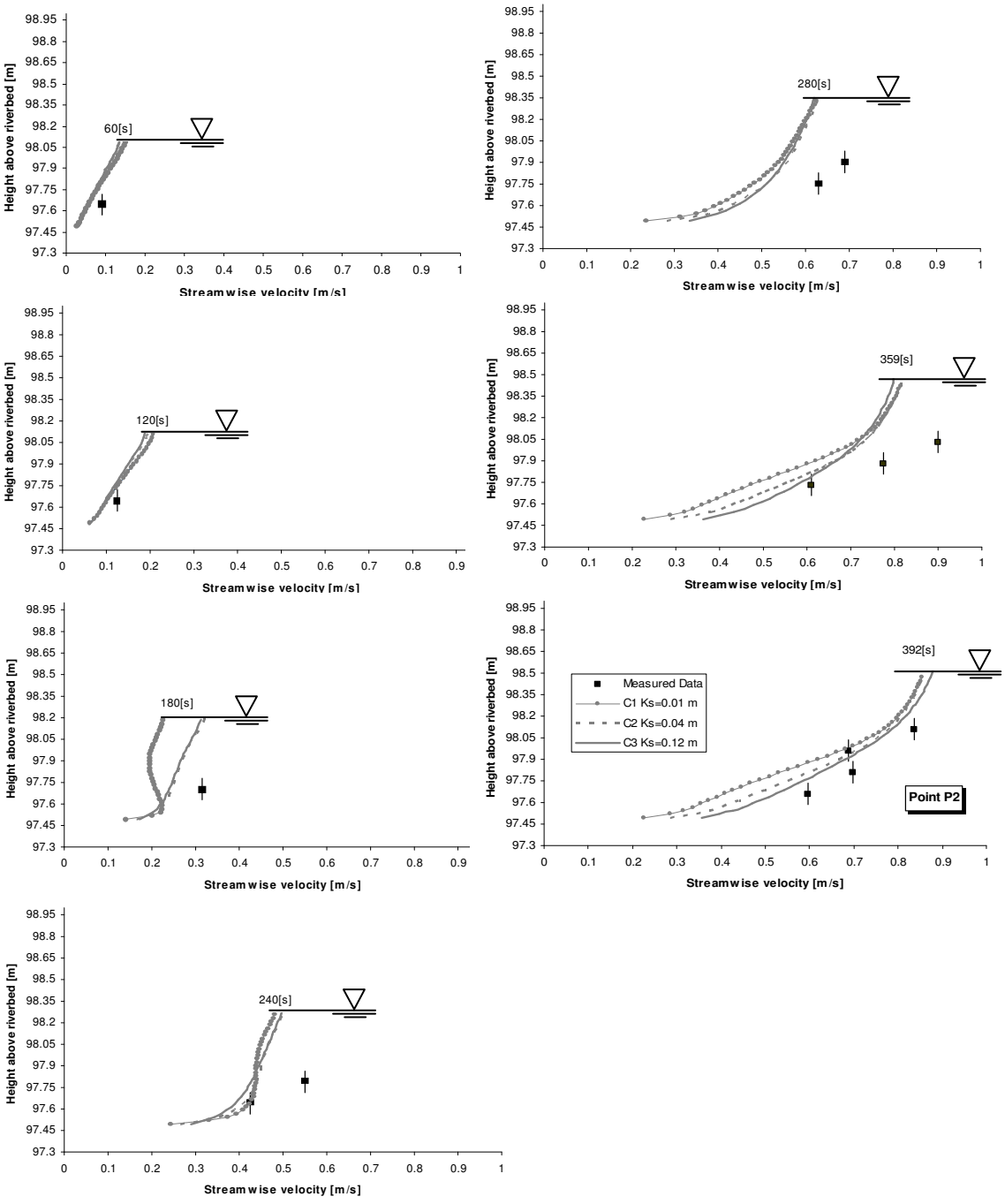

Figure 6(a) Comparisons of measured and calculated time-dependent streamwise velocity profiles using the 3D model (Cases C1, C2 and C3) at point P2. Error bar disclosed the measurement uncertainty of each height location within the water column, which is equivalent to a 0.15 m ADCP cell thickness. Velocities before the time = 60 seconds and after the time = 392 seconds are not shown when flow conditions were essentially near steady-state.

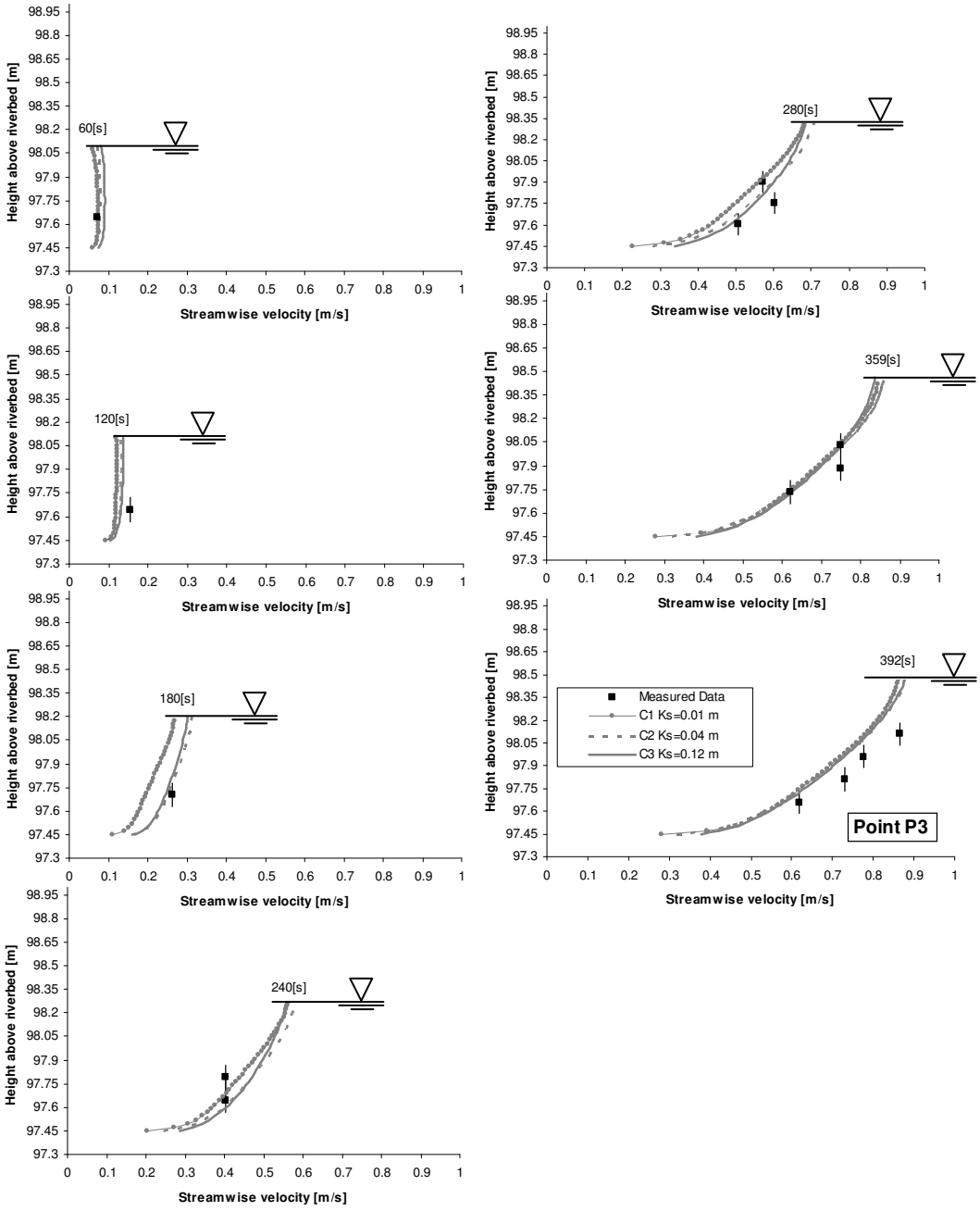

Figure 6(b) Comparisons of measured and calculated time-dependent streamwise velocity profiles using the 3D model (Cases C1, C2 and C3) at point P3. Error bar disclosed the measurement uncertainty of each height location within the water column, which is equivalent to a 0.15 m ADCP cell thickness. Velocities before the time = 60 seconds and after the time = 392 seconds are not shown when flow conditions were essentially near steady-state.

nearly reaches its peak value (at time = 392 seconds). Velocity discrepancies exist at the other 5 time instants, all of which are within the period of higher rate of water level rise. For example, at t = 180 s, the depth-averaged velocities computed in Case C1 ($k_s=0.5d_{50}=0.01$ m) are smaller by 26% at point P2 and by 22% at point P3 than those from Cases C2 and C3 with larger k_s values. On the other hand, the simulation results from C2 and C3 with k_s values of $2d_{50}$ (=0.04 m) and $3d_{84}$ (=0.12 m) are nearly indistinguishable throughout the entire simulation period at both points. This may be attributed to the role of bed roughness on the wake size and velocities behind bluff bodies (like boulders) located on rough beds. An increase in the bed surface roughness (represented by k_s value) may result in a decrease in the wake area behind the obstruction and limit the velocity reduction there for a certain Reynolds number range ($4.7\times10^6<Re<6.9\times10^6$ in this study) (e.g. Munson et al. 2002). Ingram and Chu (1987) also found that higher bed roughness could make the impact on velocities in the wakes behind islands less pronounced. In this study, the low roughness scenario, Case C1, has a smaller impact on the momentum loss for the flow approaching the boulder. This results in higher separating velocities near the edges of the boulder and a larger velocity defect region in the wake behind it. Compared to C1, the rougher surfaces in Cases C2 and C3 result in smaller wake regions and reduced impact on the velocity behind the obstruction.

Further roughness sensitivity study shows that although the computed shear stress values in all three cases are lower than the ones based on field measurements, the bed shear stress curve at point P3 obtained in Case C3 is closest to the field data (Figure 7). Babaeyan-Koopaei et al. (2002) found similar difference, when measuring shear velocities for steady overbank flows in River Severn, United Kingdom. The reason for such a difference is that τ values calculated from measurements (by equation 5) reflect all the energy losses due to bottom friction and complex turbulence patterns, whereas the τ

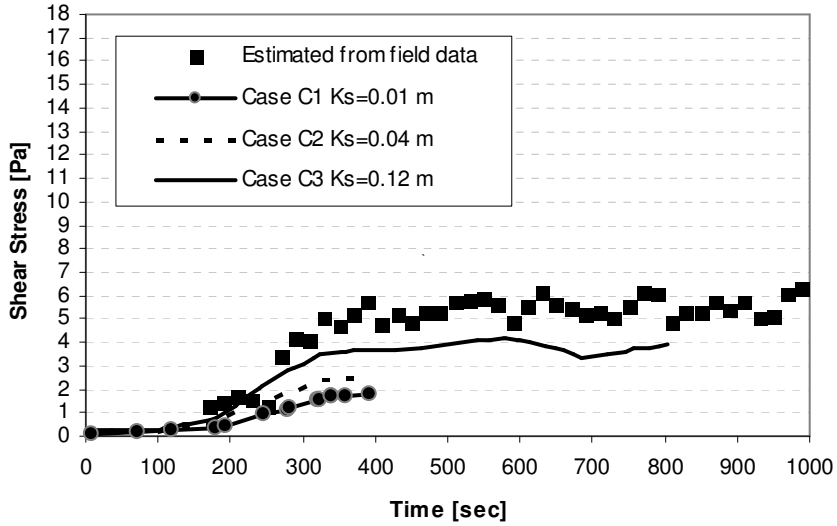

Figure 7 Comparisons of time variations of shear stress values computed by the 3D model with three different k_s values at point P3 (Cases C1, C2 and C3) and estimated from the field during the first 400 seconds period. *Note: No simulation was made beyond time = 400 seconds for Cases C1 and C2.

values obtained from equation 3 in the 3D model only account for the bottom skin friction (Morvan et al. 2008). In the remaining of this paper, Case C3 is chosen to represent the simulation results of the observed reservoir release by the 3D model.

Comparisons of flow field and riverbed shear stress among the 1D (Case A), 2D (Case B) and 3D (Case C3) models

Water surface elevations

Figure 8 shows comparisons of modeled water depth and streamwise velocity hydrographs at the six points R1, R2, R3, P1, P2 and P3 (see Figure 1). The field-measured data is also plotted in this figure for points P2 and P3. The water depth curves calculated by the three models based on either hydrostatic assumption (1D and 2D models) or non-hydrostatic VOF method (3D model) not only overlap with each other at the six points, but also compare quite favorably with the measured stage hydrographs at

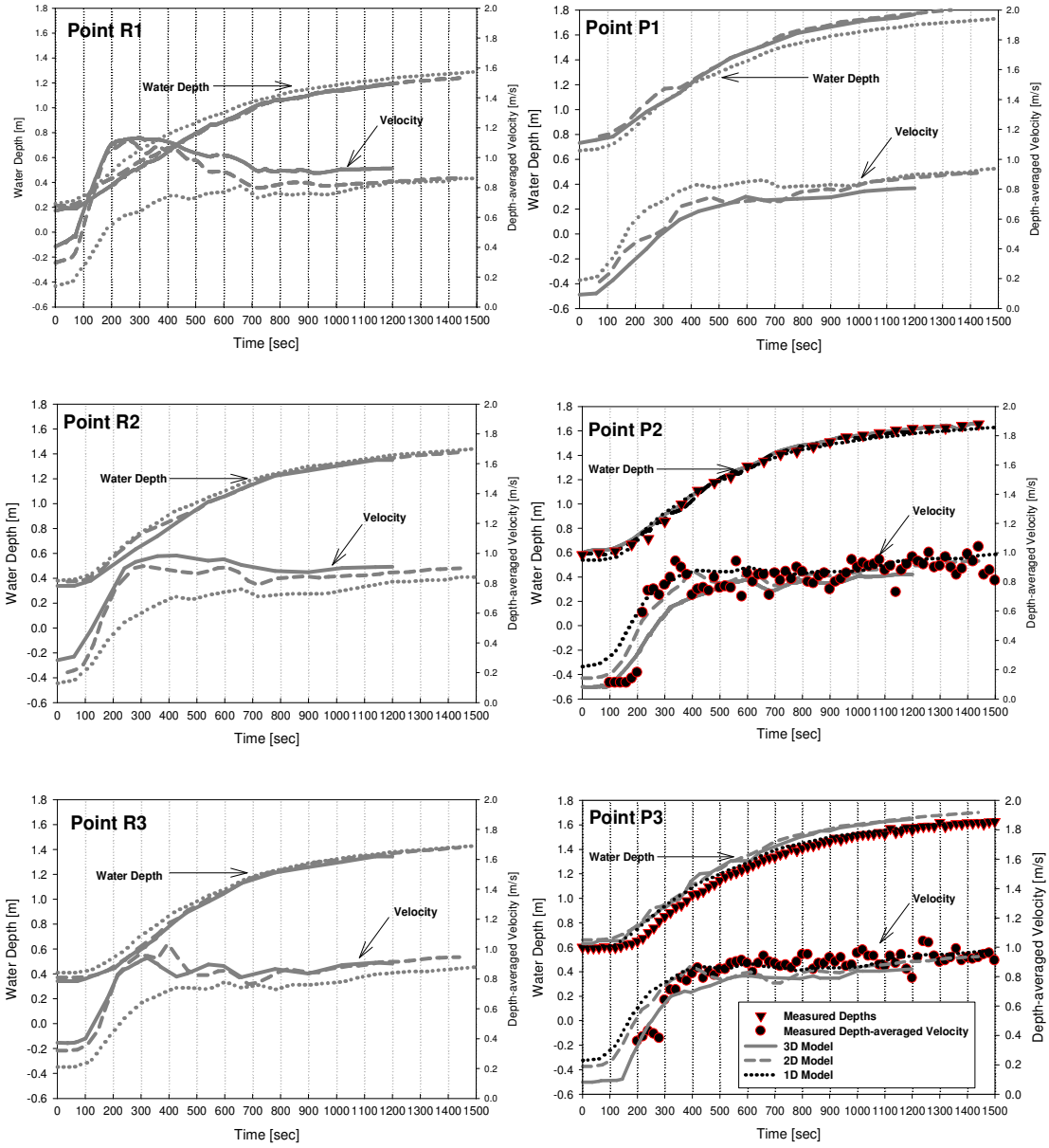

Figure 8 Time variations of streamwise velocities and water depths computed by the numerical models (Cases A, B and C3) at the selected six points and measured in the field (points P2 and P3 only) during the first 1500 seconds period.

points P2 and P3. It is worth mentioning that traditional rigid-lid treatment for the free water surface boundary in many 3D approaches, which imposes a fixed flat boundary on the free surface over the entire computational domain, neglects vertical surface velocities during the periods of flow rising and receding stages and therefore is not appropriate for simulating unsteady open-channel flows. Furthermore, previous studies have pointed out that free surface boundary near complex geometries is not flat owing to transformation of kinetic to potential energy (e.g. Shen and Diplas 2008). Additionally, efforts of mesh regridding for correcting any pressure discrepancy at the surface are impractical for a significantly deformed water surface that varies both temporally and spatially. In this regard, VOF method may be the only effective approach for this study.

Time variations of velocity

Figure 8 also indicates good agreement between the depth-averaged streamwise velocity values obtained from the 2D and 3D models. These results are consistent with the field measurements obtained at P2 and P3. Both the computed (2D and 3D simulations) and measured depth-averaged velocities reach their peak values much earlier than the maximum water depths do. At all six points, the velocities reach their peak values between t = 250 s and 400 s, while the water depths seem to continue to increase beyond 1500 s. Consequently, the time lag between the velocity and water depth peaks may exceed 1100 seconds. Song and Graf (1996) observed a similar feature from their flume experiments but with a much shorter time lag (approximately 3 seconds), which is reasonable given the much smaller scale of their model.

On the other hand, temporal velocity changes computed by the 2D and 3D models at points R1, R2 and R3 in the riffles are different from those at points P1, P2 and P3 in the pools. After reaching the peak values, the velocities in the riffles decrease in a slightly

more pronounced way compared to that in the pools. This may be attributed to the different topographies typically present in these two areas. In riffles or other similar simple geometries, the local streamwise velocities are mainly affected by the water surface slope. The relationship can be described by the Manning Formula. The decreased water surface slope after the passage of the flood wave could result in reduced velocity values. On the other hand, compared with the riffles, water surface slopes over pools remain relatively flat since the pools normally have large storage capacity and thus can moderate the impact of abrupt changes in water level. Velocities in pools may be mainly controlled by the effects of 3D flow patterns such as secondary circulation and turbulence eddies behind the boulders (e.g. Shen and Diplas 2008). These complex flow patterns appear to persist over the entire simulation period.

Finally, Figure 8 indicates that the velocity hydrographs in the pools are slightly overestimated by the 1D HEC-RAS model, compared to those from the 2D and 3D models. This may be attributed to the over-simplified geometry for the pool areas considered in HEC-RAS. Deep pools in the field were entered as flat topographies in the 1D model. As a result, HEC-RAS yields a bit shallower but somewhat faster flows. On the other side, unlike the 2D and 3D models, the 1D model does not predict the velocities in the riffles to peak between t = 250 s and 400 s. Consequently, the discharges in the riffles may be underestimated during this time window compared to those from the 2D and 3D models.

Shear stress comparisons among the values predicted by 1D (Case A), 2D (Case B) and 3D (Case C3) models

Figure 9 depicts the temporal variation of the local riverbed shear stress at the six points. The shear stresses predicted by the 2D and 3D models follow the identical trends with the

velocity changes. The computed shear stresses approach their peak values at approximately the same time as those of the depth-averaged velocity curves in Figure 8. For the points P2 and P3 in the pool, the curves computed by the 2D and 3D models are in reasonable agreement with the shear stresses based on the field data and estimated using Equation 5. However, it appears that the shear stresses calculated by the 2D model are higher than those from the 3D model during the initial rising stage of the hydrograph. For the three points within the riffles (points R1, R2 and R3), the peak shear stress values from the 2D and 3D models are about 1.5 ~ 3 times as high as those at subsequently higher flows. A similar finding was reported by De Sutter et al. (2001) from flood measurements at the Olewiger Bach Basin, Germany. This is consistent with the rapid increase in the water surface slope typically observed during the initial phase of the reservoir release and the successive decrease and move towards the channel bed slope at subsequent times. It appears that the shear stress changes in the pools are not as pronounced as those in the riffles, in agreement with the more limited water surface slope changes experienced at the pool areas.

The 1D model yields considerably higher bed shear stresses than those obtained from the 2D and 3D models, especially in the pools. The main reason is the Manning's n values used in the 1D model are larger than those in the 2D model and the equivalent k_s values in the 3D model (Table 1 and Figure 5). This is due to the different underlying boundary roughness concepts and formulations employed in the various models. The 1D model cannot account for the effects of secondary currents and turbulence on energy dissipation or flow resistance commonly encountered in the pools. The energy head loss or friction associated with these complex 3D flow patterns is accounted for through the calibration effort of empirical Manning's n coefficient, which was originally developed

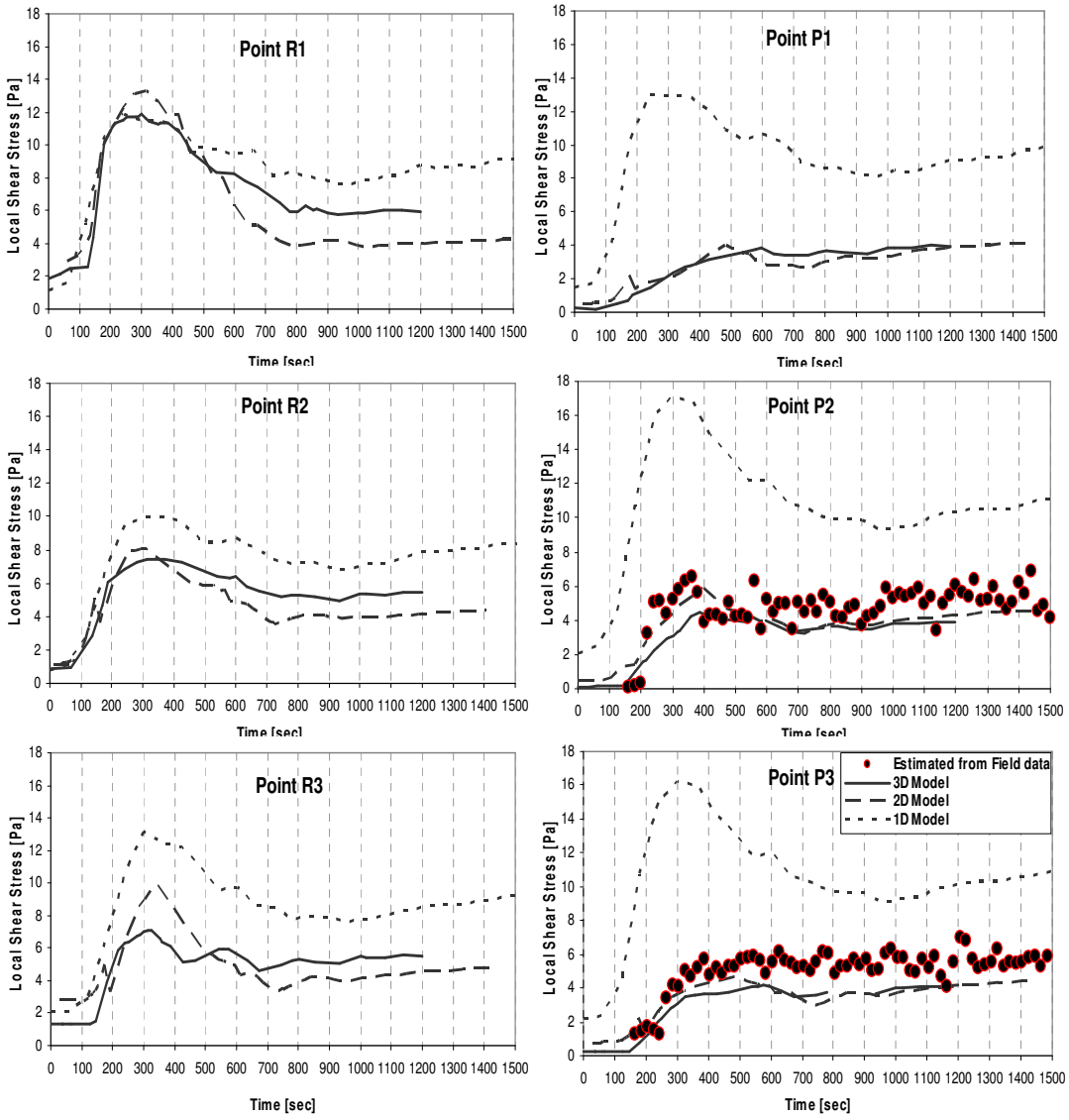

Figure 9 Time variations of shear stress values computed by the numerical models (Cases A, B and C3) at the selected six points and measured in the field (points P2 and P3 only) during the first 1500 seconds period.

from uniform flows. In the 2D model, the turbulence, to a limited extent, can be represented by the zero-equation turbulence model. Consequently, the Manning's n coefficient in Equation 4 in the 2D model is smaller than that in the 1Dmodel (Table 1 and Figure 5), and is not used to address the contribution of turbulence structures to flow

resistance. Similarly, the friction parameter k_s in the 3D model used for calculating the skin friction plays a less significant role in quantifying the overall flow resistance when compared to the Manning's n parameter in the 1D and 2D models, since the impact of 3D turbulence structure on momentum and energy losses is much better accounted for by the k-ε model.

ECOLOGICAL APPLICATIONS OF THE 3D MODEL TO PHYSICAL FISH HABITAT

Since 1953, the daily fluctuating releases from hydropower peaking operations in the Smith River have constrained fish recruitment and depressed brown trout population, especially for age-0 trout because of flow-associated redd scouring during spawning season and fish displacement in fry rearing period (Orth et al. 2004). Consequently, federal government and state agencies together with local communities are interested in developing a new and more effective flow management strategy for enhancing the trout fishery.

To explore what changes in flow regime could be beneficial, a new hypothetical unsteady reservoir release scenario was developed in addition to the aforementioned measured release. Specifically, this was designed so that the reservoir would start releasing flow through one turbine for the first half hour, then the second turbine would be added into operation for the next half hour. After one hour, both turbines would operate at their peak capacities. In other words, the peak flow will be reached after approximately one-hour operation instead of the twenty-minute period that we observed historically (Figure 10). The purpose of this new scheme is to make the transition between base and maximum flows more gradual and is called "staggering" scenario or Case C4. This case was compared to the aforementioned historical unsteady flow simulated using the 3D model in Case C3. The 1D and 2D models were not employed for

the comparison study of different release scenarios, since their roughness coefficients require extensive calibration before being applied to other flow regimes (Donnell et al. 2001, Brunner 2008) and they lack robust turbulence model to address 3D flow patterns in complex river geometries (e.g. pools, boulders and islands).

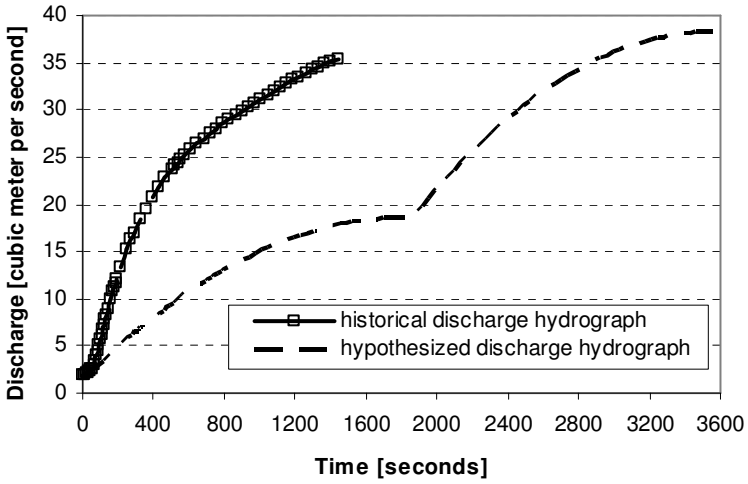

Figure 10 Discharge hydrographs of measured historical and hypothesized reservoir release scenarios.

To address the effects of different unsteady reservoir releases on entrainment of stream gravels or redd scouring, estimation of bed material movement was determined by comparing the dimensionless bed shear stress τ^* obtained in Cases C3 and C4 to the critical stress, τ^*_c, values determined from the Shields diagram. A similar concept was employed by Pasternack et al. (2004) for assessing spawning gravel entrainment for chinook salmon (*Oncorhynchus tschawytscha*) in California's Central Valley. A typical value for τ^*_c suggested in the literature for gravel is 0.045. Lower values for τ^*_c have been used by several investigators. For example, Parker et al. (1982) suggested that the minimum value for incipient motion of the surface material median size is $\tau^*_c = 0.03$. In

this study, the degree of susceptibility to gravel erosion is divided into three categories: $\tau^*>0.045$ denotes significant erosion; $0.045>\tau^*>0.03$ represents a condition for potential erosion; while there is no erosion for $\tau^*<0.03$.

To evaluate the availability of suitable habitat where fish will not be flushed away during the reservoir releases, appropriate measures of fish swimming performance under the hydropeaking conditions need to be devised. It is expected that a fish must hold its position long enough (i.e. endurance time) or be swimming against surrounding lotic water to avoid being displaced. In the present study, the level of "sustained speed", defined as the minimum fish swimming speed that can be maintained for at least 200 minutes of endurance time (Clough and Turnpenny, 2001), was adopted because records indicate that most historical peak flow events below the Philpott dam can last more than 180 minutes (Orth et al. 2004).

The information of fish swimming speeds is crucial for many aspects of fish survival, such as design of fish ladders, prevention of fish entrainment at water intakes and estimation of fish habitat during high flows (e.g. Booker 2003). Clough and Turnpenny (2001) conducted an extensive study on the swimming performance of several freshwater fish species in a laboratory water tunnel. Their results show that for small and large brown trout, their median sustained speed at cold water (<9°C) is 7.5 bl/s (bl = body lengths) and 7 bl/s, respectively. The mean total body length of juvenile trout sampled in our study site was 0.0304 m (Orth et al. 2004). Since adult brown trout could typically grow to at least 0.15 m, the equivalent sustained speed can be determined to be 0.228 m/s and 1.05 m/s for juvenile and adult fish in the study site, respectively. These sustained speed criteria were compared against the velocity fields computed in Cases C3 and C4 for determining the availability of suitable habitat during unsteady reservoir releases. Once again, we should emphasize that in this study, suitable habitat are defined as refugia

spaces, with flow velocities slower than a fish's sustained speed. These spaces are three-dimensional in nature where the fish can hide from fast currents without being displaced.

In the following two sections, the hypothetical reservoir release scenario Case C4 was simulated by the 3D model using k_s = 0.12m. The results obtained are then compared to those computed in Case C3 to examine their different impacts on stream gravel erosion based on Shields criteria and fish displacement in reference to sustained fish swimming speed in the study site.

Redd scouring

Figure 11 illustrates maps of the calculated erosion areas at different time instants for the two simulation cases. In both cases, most areas predicted with significant erosion (τ^*>0.045) are near exposed boulders and submerged rocks. No significant erosion occurs in the spawning locations within the study site. During their entire simulation periods, the maximum total area subject to significant erosion is only 2.26% and 0.3% of the entire reach for Cases C3 and C4, respectively. In contrast, the areas susceptible to potential erosion (0.045>τ^*>0.03) are significantly different. For Case C3, the maximum total area subject to potential erosion is equivalent to 15.4% of the study reach, and includes a major upstream spawning habitat in this reach (Figure 1a). Compared to C3, the maximum potential erosion area computed in Case C4 is reduced by 7 times and is concentrated near boulders and the downstream island. No potential erosion is predicted in any spawning locations.

Figure 12 shows that for both simulation cases, potential erosion area is not always proportional to the discharge. In Case C3, large area subject to potential erosion occurs from t = 200 s to t = 700 s, which coincides with the period when the peak shear stress is obtained (see Figure 9). Both shear stress values and potential erosion area increase and reach their peak values simultaneously first, then both values begin to

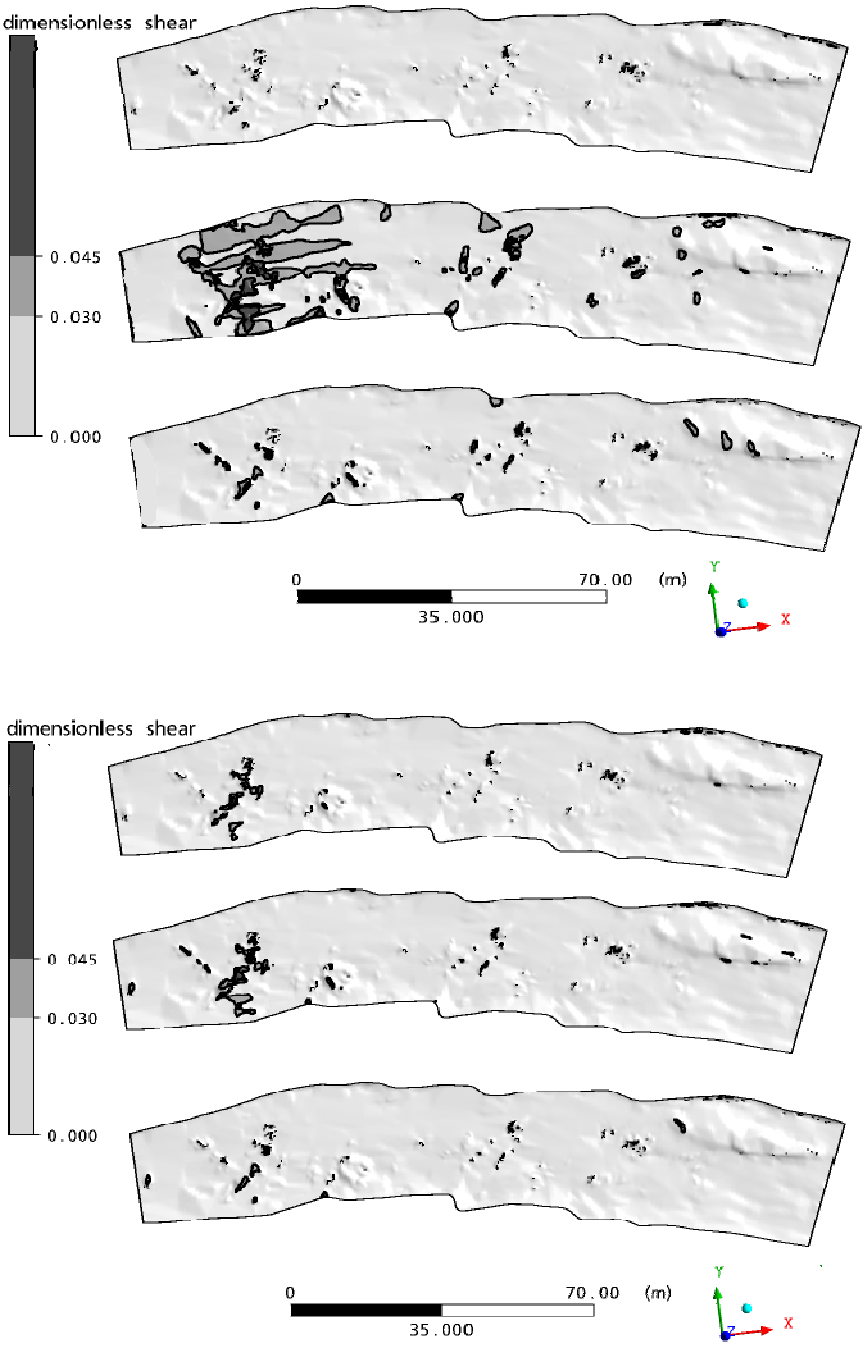

Figure 11 Maps of calculated erosion areas at different time instants for Cases C3 and C4. Different color represents different erosion degree. White (τ^* <0.03) — no erosion; gray (0.03<τ^* <0.045) — potential erosion; black (τ^* >0.045) — significant erosion. *Note: Maximum potential erosion area occurs at time = 354 sec in Case C3 and time = 700 sec in Case C4.

decrease, even though the corresponding discharge continues to rise. In Case C4, there are two peaks for the predicted total potential erosion area during the two consecutive discharge rises. From their fieldwork at the Olewiger Bach basin, Germany, De Sutter et al. (2001) observed similar features regarding the temporal variations of friction velocity and suspended solids concentration between two discharge increase steps. Results obtained here imply that during the rising stage of certain unsteady pulsing flows, subsequent higher flows may not necessarily lead to more erosion than earlier lower flows. Therefore, any investigation for a complete understanding of bed scour impacted by reservoir releases or flood waves should include analysis of the transition component between base and peak flow regimes during the passage of flow pulses but not just limited to the steady of peak flows.

Flow records from the nearest upstream U.S. Geological Survey gage (#02072000) below Philpott dam show that during the year 2003, due to frequent rain and mountain snowmelt, fluctuating hydropeaking events similar to those simulated in this study happened 84% of the time, or 51 days during the November and December peak spawning season (Orth et al. 2004). Although the actual period that may potentially cause gravel scouring in each event is much shorter (≈500 s), frequent occurrence of spawning gravel mobilization could still dramatically disrupt adult spawning activities, damage the nests and cause higher egg mortality during spawning and incubation stages.

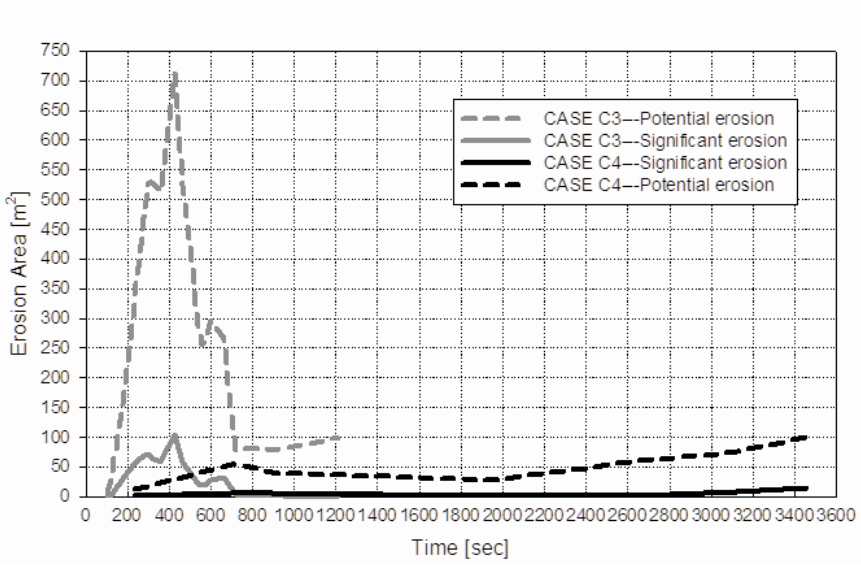

Figure 12 Time variations of potential and significant erosion areas predicted using the 3D model in Cases C3 and C4.

Fish displacement

Figure 13 shows maps of refugia habitat for age-0 brown trout at selected time instants in Cases C3 and C4. During the initial base flow period, suitable spaces with velocities less than the juvenile's sustained swimming speed (<0.228 m/s) are mainly present along the banks, around the downstream island and in wakes behind boulders. No refugia habitat is predicted in riffles where redds are constructed. At t = 120 s, both simulation cases show that shallow and small pools in the middle of the channel would no longer be suitable for juvenile trout, whereas the spaces of refugia in some large deep pools increase as the water level rises. Refugia spaces adjacent to the banks are also quickly reduced. At t = 300 (C3) and 400 s (C4), both simulations reveal that only a few discrete zones near small bank depressions and downstream of the island still remain as shelters for the juvenile trout. This means displacement of age-0 brown trout can occur in

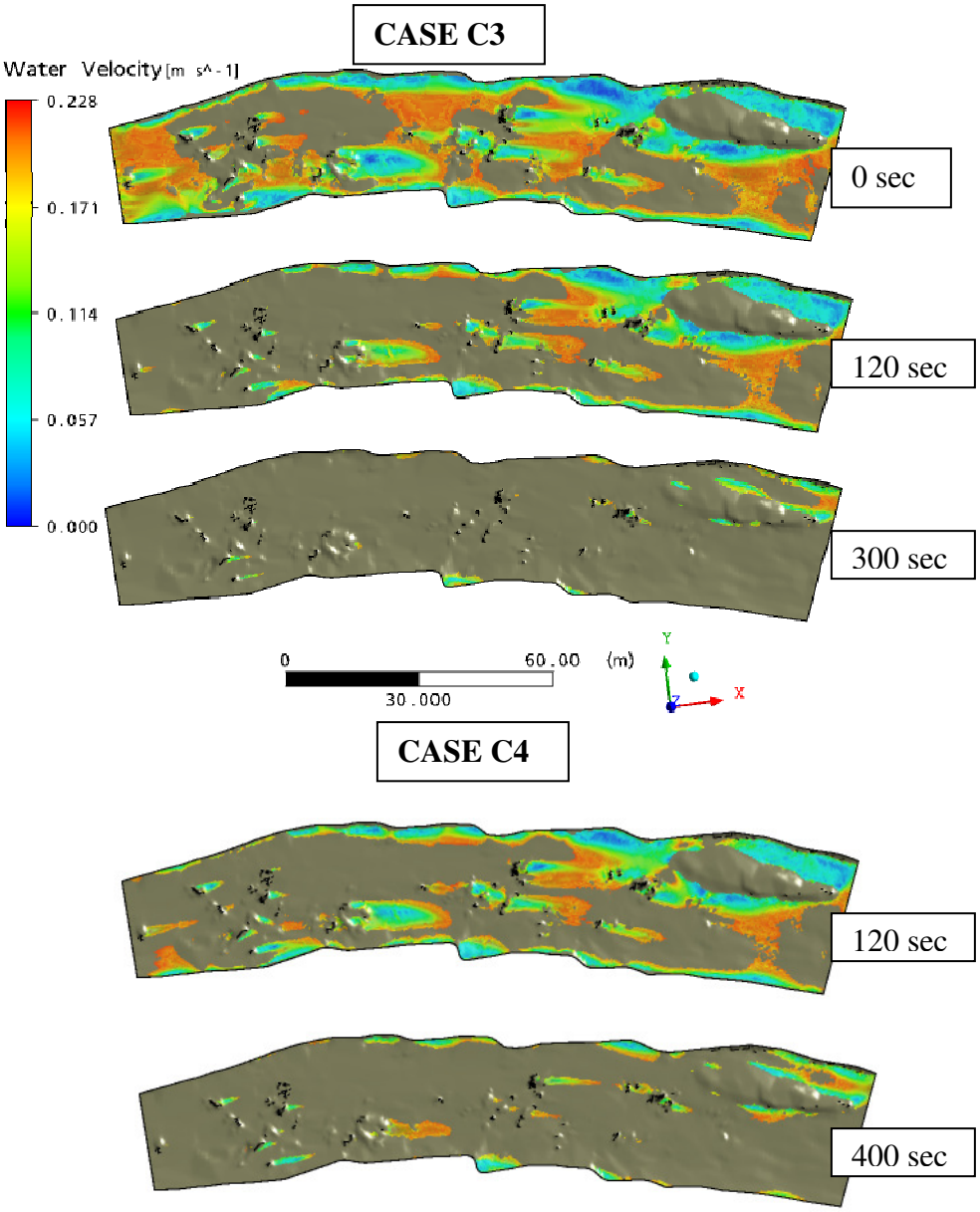

Figure 13 Color maps of refugia habitat for age-0 juvenile brown trout at selected time instants in Cases C3 and C4. Grey areas are those having velocities exceeding age-0 sustained speed 0.228 m/s and hence not suitable to hide.

the early stage of the reservoir release with a much smaller discharge than the final peak flow.

It is hypothesized that one role the boulders in the river play is to create wake regions in pools adjacent to the nests in riffles. The wakes could not only provide temporary shelters for fry or juvenile brown trout after they emerge at base flow, but function as retreat paths between the redds and refugia spaces along the banks in case either the flow increases or recedes. This probably may explain the field sampling results obtained in 2003, in which several fries recently emerged from redds were discovered behind rocks, while the majority of juveniles were found near the banks (Orth et al. 2004).

Figure 14 illustrates the temporal variations of available refugia for juvenile and adult brown trout in early spring (temperature < 9°C) derived from Cases C3 and C4. For juvenile brown trout, both scenarios show that their refugia shrink rapidly to a substantially smaller size within the first 400 s, regardless of how the flow has been released. The available habitat at t = 400 s is only 6.8% and 13.6% of the initially available suitable space (=514 m^3) for Cases C3 and C4, respectively. After that, the available refugia decrease gradually to less than 10 m^3 within the next 800 s in Case C3; whereas in Case C4, the available refugia for the juvenile fish remain at 50 m^3 for another half an hour before they finally reduce to the identical level as that in Case C3. The reason that Case C4 has higher and longer refugia availability for juvenile fish than Case C3 is clearly attributed to the "staggering" strategy in Case C4. On the other hand, in both cases, the declining trends of refugia habitat for juvenile trout are in contrast with the climbing tendencies of refugia space for adult brown trout. This is because the adult is able to sustain a much faster swimming speed (up to 1 m/s in this study) and thus can endure a wider range of flow variations. As the discharge increases and water level rises, the potential refugia habitat for adult fish generally expands. Near the ends of both

simulation periods, high velocities (>1 m/s) produced by convergent flow moving over some submerged boulders may somewhat decrease available refugia.

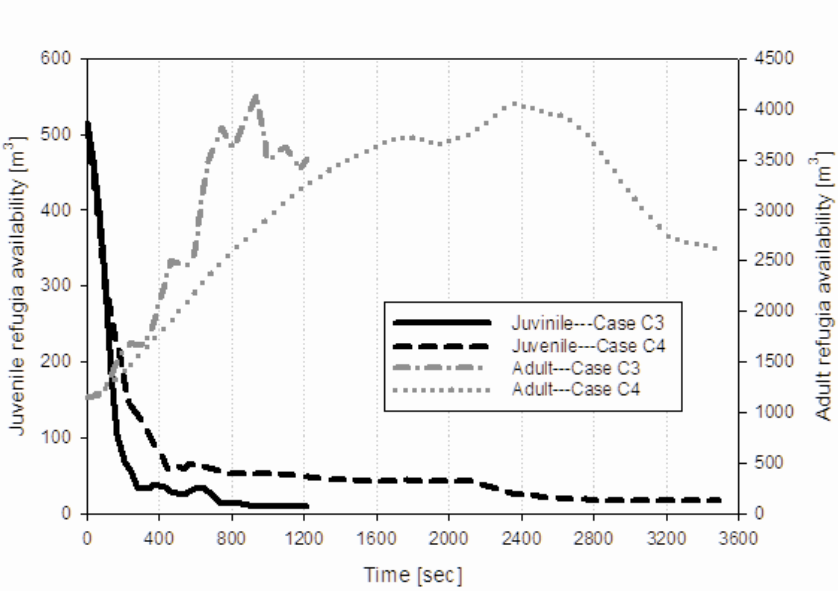

Figure 14 Time variations of refugia habitat for juvenile and adult brown trout predicted using the 3D model in Cases C3 and C4.

DISCUSSION

Current assessment of the effects of hydropower-induced flow perturbations on stream fishes relies exclusively on the Instream Flow Incremental Methodology (IFIM, see Bovee 1982). This method is designed to account for the long-term impacts of steady instream flows on physical fish habitat, but fails to address the morphological and behavioral impacts (e.g. biological response of fish) of rapid changes in flows over short periods (Hunter 1992). To fully understand the effects of unsteady flow on stream ecology it is vital to properly simulate the passage of the flood wave or the transition process from low to high flow conditions. Unfortunately, it is difficult to construct an

appropriate environment in the laboratory since brown trout has a long migration behavior and needs several years to become mature and spawn. Real-time data surveyed under natural field conditions is always preferable. In this paper, we collected field data and conducted numerical studies on two unsteady reservoir releases below a hydropower dam in a mountain river. Results obtained here can assist the efforts of developing surge mitigation measures or adopting proper environmental flow criteria.

The 3D CFX model used in this paper employs a modified wall function with a roughness length concept. In general, use of the wall function method would retain the identical accuracy as other alternative boundary treatments (e.g. the porosity treatment of the bed, Carney et al. 2006) when the relative roughness (d_{84}/h) is small. However, possible inaccuracies may arise if the relative roughness is high. This is because the model requires the first element off the riverbed boundary to be larger than the riverbed roughness value, and there may not be enough nodes allocated near the bed to resolve the boundary layer (bottom 20% of the water depth) if relative roughness (d_{84}/h) becomes too high, especially at base flows. The maximum relative roughness values estimated in this study at base flow conditions are 0.067 in pools and 0.2 in riffles (d_{84} is the same over the entire computational domain). Through the comparisons between field data and simulation results (e.g. Figures 6, 8 and 9), it is evident that it is acceptable to use the wall function approach for modeling the flow patterns in the pools where local depths normally exceed 0.6 m. As far as the riffles are concerned, the depth-averaged velocities calculated by the 3D model are similar to those obtained through the calibrated 2D model solutions. In Case C3, most of the riverbed area is represented by small relative roughness (<0.1) for about 85 percent of the time during the whole 20 min-long simulation period. For streams having extended shallow water area dominated by high relative roughness, however, additional research needs to be conducted to seek the

feasibility of incorporating other special boundary treatments (e.g. porosity approach or low-Reynolds number integration) into the unsteady 3D flow simulations.

Equation 4 used in the 1D and 2D models can provide appropriate shear stress values for steady non-uniform flows, but does not consider the effects of dynamic evolution of the flood wave. A more complete representation of the time-dependent shear stress may employ the full St. Venant equation:

$$\tau = \rho g h[\ \underbrace{\underbrace{\underbrace{S_0}_{\substack{bed\\slope}} - \underbrace{\frac{\partial h}{\partial x}}_{\substack{pressure\\force}}}_{water\ surface\ \ slope} - \underbrace{\frac{V}{g}\frac{\partial V}{\partial x}}_{\substack{convective\\acceleration}} - \underbrace{\frac{1}{g}\frac{\partial V}{\partial t}}_{\substack{local\ acceleration\\(unsteadiness)}}}_{friction\ \ slope\ \ S_f}\ ] \tag{6}$$

where x is the streamwise distance along the channel. In this equation, the convective and local acceleration terms account for the non-uniformity and unsteadiness features of the flood wave, respectively. Figure 15 presents examples showing the variations of the above individual terms during the passage of the rising limb of the observed flood wave as obtained by the 3D model at points R2 and P2. The velocity in this equation was taken as the local depth-averaged velocity along the streamwise direction from the 3D simulation results. At both locations, the dominant term is the pressure force (or water surface slope), while the convective and local acceleration terms appear to be important as well. The maximum values of the local acceleration term $\frac{1}{g}\frac{\partial V}{\partial t}$ are 2 and 1.5 times larger than S_0 at points R2 and P2, respectively. Furthermore, in contrast to the convective acceleration term, the local acceleration term has stronger effect on the riffle (point R2) than on the pool (point P2).

Accurate estimates of unsteady shear stress in the 1D and 2D models require formulas in the form of equation 6, while the range of accuracy of equation 4 in

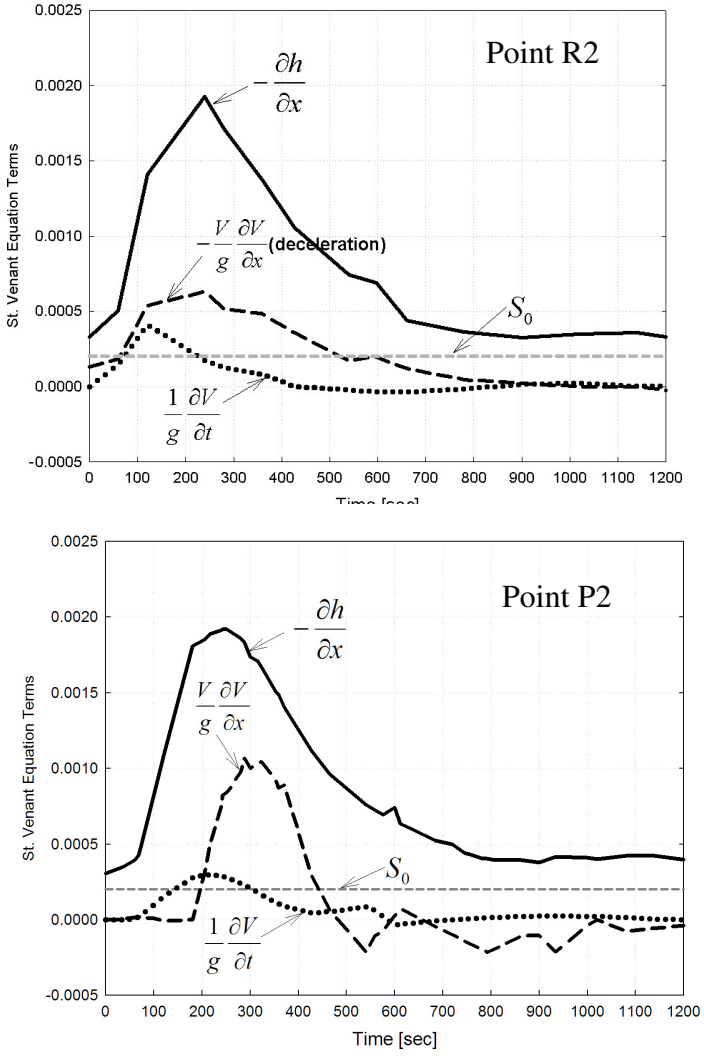

Figure 15 The time variations of the Saint-Venant equation terms (equation 6) calculated based on the results of the 3D model simulation at points R2 and P2 in the Smith River.

calculating unsteady shear stress through the Manning formula depends on the contribution of $\frac{1}{g}\frac{\partial V}{\partial t}$ on the total S_f value. In this study, an unsteadiness parameter β is proposed to represent the ratio of the stress due to local acceleration/deceleration of the fluid (i.e. unsteadiness) to the shear stress corresponding to the same flow but under steady non-uniform state condition:

$$\beta = \frac{\frac{\partial V}{\partial t}}{g(S_0 - \frac{\partial h}{\partial x}) - V\frac{\partial V}{\partial x}} \tag{7}$$

In the literature, two other parameters used to characterize the influence of unsteadiness on flow properties are α (Nezu et al. 1997) and Φ (Shuy 1996):

$$\alpha = \frac{1}{V}\frac{\partial h}{\partial t} \approx \frac{2}{V_p - V_b}\frac{h_p - h_b}{T_d} \tag{8}$$

$$\Phi = \frac{8h}{f_s V^2}\frac{dV}{dt} = \frac{8h}{f_s V^2}\left[\frac{\partial V}{\partial t} + V\frac{\partial V}{\partial x}\right] = \frac{\frac{\partial V}{\partial t} + V\frac{\partial V}{\partial x}}{\tau_0/\rho h} = \frac{\frac{\partial V}{\partial t} + V\frac{\partial V}{\partial x}}{g(S_0 - \frac{\partial h}{\partial x})} \tag{9}$$

where the subscripts b and p denote the values at the base and peak flows, respectively. Td is the flood duration time. τ_0 denotes quasi-steady shear stress and can be calculated using Darcy-Weisbach formula with the quasi-steady friction factor fs. It is noted that the Φ parameter reflects a similar physical concept as β, but moves the convective acceleration term to its numerator. Figure 16 depicts comparisons of the time variations of the three parameters at points R2 and P2 (the α values in this figure were calculated using the instantaneous V and h values). It is seen that their trends are not the same over the entire simulation period. At point R2, both β and α attain their largest values at t = 100 s, whereas the absolute value of Φ becomes the largest one at t = 427 s. This is because the absolute value of the convective acceleration term continues to increase beyond t = 100 s and is still large even when the local acceleration approaches zero at t = 427 s. The dominant influence of the convective acceleration term on the behavior of Φ can be confirmed at point P2 in Figure 16, where both $\frac{V}{g}\frac{\partial V}{\partial x}$ and Φ reach their peak values

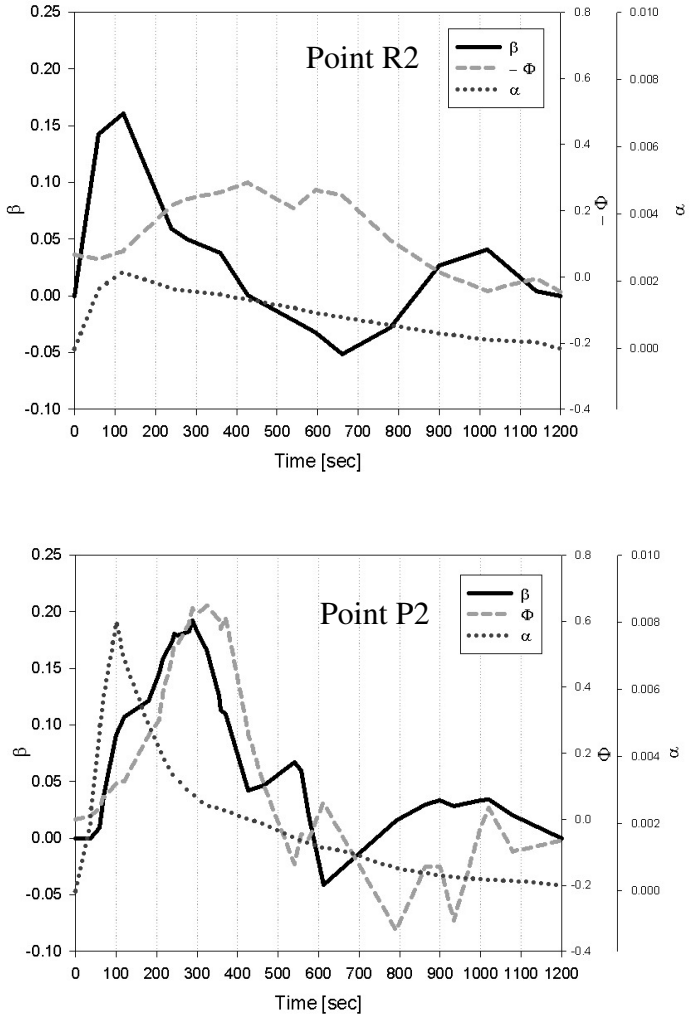

Figure 16 Comparisons of the time variations of the three parameters α, β and Φ at points R2 and P2.

around t = 300 s. Obviously, the effect of flow unsteadiness (or local acceleration) on the Φ value is considerably masked at both locations. On the other side, although the parameter α is generally correlated with the flow unsteadiness, it cannot measure the relative importance of the local acceleration to the other terms in equation 6. For this reason, the parameter β may provide a more unified treatment of the role of unsteadiness

and explain partially the overestimates of shear stresses by the 1D and 2D models at the initial rising stage of the flood wave in Figure 9.

Nezu and Sanjou (2006) found that the law of the wall (equation 3) used in the 3D model is satisfied in unsteady open-channel flows regardless of the degree of flow unsteadiness. However, studies showed the integral constant C (=8.5) may vary by as much as 15% for unsteady flows, if the degree of unsteadiness is high (e.g. $\alpha = 0.0063$, calculated using the velocities and depths at their base and peak flows only, see Qu 2002, Nezu and Sanjou 2006). When $\alpha \leq 0.001$, the integral constant remains the same as that for steady flows. Considering that $\alpha = 0.0013$ in this study if calculated in the same way, we believe that equation 3 is still valid for estimating unsteady shear stress (Bares et al. 2006, Nezu and Sanjou 2006).

The above proposed parameter β not only can assess the validity of the Manning formula in quantifying the effect of flow unsteadiness on shear stress in 1D and 2D models, but it also may help examine whether it would be acceptable to approximate an unsteady flow regime as a quasi-steady state. To elaborate this issue, Case C3 was re-run by a sequence of seven incrementally increasing steady flow discharges using the 3D model, each of which continued for a specified period. This is referred to as a quasi-steady flow approach. Figure 17 compares the results of three basic flow characteristics (depth, streamwise depth-averaged velocity and shear stress) at point P2 obtained by the quasi-steady flow approach and the truly dynamic flow simulation (Case C3). The discrepancies calculated at each discharge and the corresponding β values are listed in Table 2. At any discharge between the base (1.78 m^3/s) and peak flows (35 m^3/s), the unsteady simulation (Case C3) always results in a lower depth, a higher velocity and a higher shear stress than those obtained using the quasi-steady flow approach. Case C3

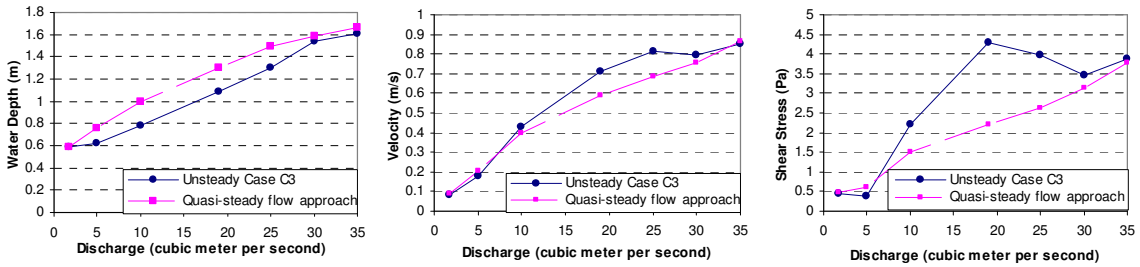

Figure 17 Comparisons of three basic flow characteristics at point P2 between Case C3 (truly unsteady flow approach) and quasi-steady flow approach using the 3D CFX model. Each discharge in the quasi-steady flow approach corresponds to an instantaneous cross-sectional discharge where point P2 is located in Case C3.

Table 2. Unsteadiness parameter β and percentage differences of computed basic flow characteristics (depth, velocity and shear stress) at point P2 between Case C3 (truly unsteady approach) and the quasi-steady flow approach using the 3D CFX model. For Case C3, each discharge listed on the first column corresponds to an instantaneous cross-sectional discharge where point P2 is located.

Discharge [m^3/s]	Unsteadiness β	Depth [m]	Depth-averaged Velocity [m/s]	Shear Stress [Pa]
1.78	0	0.00%	-8.54%	-3.04%
5	0.11	-22.42%	-12.61%	-56.00%
10	0.17	-27.72%	7.56%	32.13%
19	0.06	-19.69%	17.14%	48.65%
25	-0.04	-14.51%	16.32%	33.53%
30	0.028	-3.06%	4.65%	9.80%
35	0	-2.94%	-1.56%	2.83%

*Note: percentage difference = (TU-S)/TU×100; where TU = truly unsteady flow approach and S = quasi-steady flow approach.

predicts a peak shear stress at a discharge of 19 m^3/s, whereas the quasi-steady flow approach presents a monotonically increasing shear stress as the discharge rises. It is evident that the quasi-steady flow approach does not reflect the loop behavior in the

stage-discharge relation that is commonly exhibited by unsteady open-channel flows (Henderson 1966). In general, higher β values are associated with larger discrepancies of predicted flow characteristics between the two modeling strategies. When $|\beta| < 0.04$ at the initial base and final peak flows, all the discrepancies are either less than 10%. For this study, this implies that a discharge hydrograph could be modeled using the 3D model as a sequence of steady flows of variable durations if the unsteadiness contribution compared to those from the water surface slope and non-uniformity is less than 4%.

In industry, it is common practice to use 1D and 2D hydraulic models like UNET package within HEC-RAS (Brunner 2008) and RMA2 for unsteady flood routing and geomorphic evolution because of their simplicity and shorter run times. However, calibration of the 1D and 2D models over a range of flows encountered in an unsteady flow presents a big challenge, while the 3D model is more physics based and therefore needs less calibration effort. Moreover, 1D models discretize stream topography into a series of transects along the channel rather than 2D and 3D elements. The cross sectional spacing is normally much larger than the typical sizes of elements created for the 2D and 3D models. On one side, this will allow the 1D model simulation to use a much larger time interval without having numerical stability issues. On the other side, computational inaccuracy may arise since small-scale geometrical features of biological importance could be missed and sudden changes of flow features with a time-scale smaller than the defined time step not resolved. Although the 2D RMA2 model can accommodate a much more refined mesh, the elemental elimination method employed may occasionally cause too many elements becoming dry (disabled elements) or wet (reactivated elements) within a time step over large flat areas like wetlands or flood plains during a passage of a flood wave, thus inducing mass conservation errors and numerical shocks. In the 3D CFX model, no element becomes disabled or reactivated during the unsteady flow simulation

since the model solves the transport processes of both air and water simultaneously. Overall, to model long-term, yearlong hydraulic conditions in a river or over a watershed, 1D and 2D models remain the most suitable methodologies to choose. For short-term event simulation, the 1D model can be used to determine the temporal variation of water levels for simple channel topographies, which in turn can be applied as boundary inputs to a 2D (if sufficient measured data is available for calibration) or 3D model to resolve the details of rapid changes of flow characteristics at a time-scale of minutes to seconds.

Previous efforts studying temporal changes in physical habitat at either high or low flows have been determined using quasi-steady flow approach based on Habitat Suitability Criteria (HSC) (e.g. Booker and Dunbar 2004). As the HSC is developed from surveys conducted at flows under steady conditions, this type of criteria cannot describe how the fish may respond to a rapidly changing environment. Instantaneous flow information provided by unsteady hydrodynamic modeling approach, integrated with bioenergetic data derived directly from rigorous experiments, may advance our fundamental understanding of the impact of unsteady flow physics on aquatic habitat. In addition, conventional quasi-steady flow approaches may fail to reveal the real peak impact of an unsteady flow event on downstream habitat. In cases of pulsing flows or floods with high degree of unsteadiness, this type of method may significantly underestimate the severity of the situation they could produce. It is estimated that, if Case C3 was simulated with a steady 3D model, the maximum potential erosion area predicted could only be $1/7^{th}$ of the actual area. If the scale at which a legitimate conclusion needs to be made were not consistent with the model temporary resolution, the effectiveness of any subsequent channel protection plan would be in doubt. The non-monotonic, nonlinear relationship between discharge and habitat quality at unsteady flow conditions makes it

necessary to adopt a truly unsteady flow modeling methodology, particularly for hydrographs with high degree of unsteadiness.

Short-term hydrological fluctuations have more immediate impact than long-term base flows on the quality of physical habitat and aquatic organisms' adaptation to their surrounding environment. Complete stream restoration measures should consider the physical consequences that the unsteady transition period may have on a stream's morphology and ecology. Future research should include 3D unsteady flow simulations to model the falling limb of the flood waves where fish stranding can be examined. Better understanding of the interaction between habitat availability and instantaneous fluid patterns can assist in designing proper water management strategies.

CONCLUSIONS

Unsteady numerical simulations of a measured pulsing flow released by the Philpott Reservoir using 1D, 2D and 3D hydraulic models were conducted to assess their ability to reproduce time-dependent depths, velocities and shear stresses in the Smith River. Estimation of the unsteady shear stress using the modified log-law in the 3D model is demonstrated to be acceptable for flows associated with moderate unsteadiness. However, the quasi-steady state shear stress equation based on the Manning formula in the 1D and 2D models may overestimate the unsteady shear stresses if unsteadiness is high. Compared to field measurements, the prediction of water surface elevation exhibits very low sensitivity to the use of different roughness values k_s in the 3D model and to the choice of different dimensional models. However, use of smaller k_s values in the 3D model tends to increase the wake sizes behind flow obstructions, reduce local velocities and result in smaller shear stresses. On the other side, compared with the field data, as

well as the 2D and 3D models, the 1D model yields considerably higher bed shear stresses.

A hypothetical unsteady reservoir release scenario Case C4 was simulated using the 3D model, and was compared with the 3D simulation results of the observed reservoir release Case C3. Unlike Case C3 in which two turbines worked simultaneously from the beginning, only one turbine was used to release flow during the first half hour in Case C4. Consequently, the peak flow in Case C4 was reached after nearly one-hour instead of the twenty-minute period in Case C3. Results indicate Case C4 has advantage of reducing the potential erosion area by seven times, and maintaining longer refugia availability for juvenile brown trout, as compared to those under Case C3. Results from both cases indicated that higher potential erosion area occurred at smaller discharges than the peak flow.

An unsteadiness parameter β is proposed in this study. This parameter may be used to assess the validity of the Manning formula (or other similar shear stress formula without considering the unsteady contribution in its friction slope term) for calculating unsteady shear stress, and to determine whether an unsteady flow hydrograph should be modeled using the truly unsteady dynamic flow approach or can be approximated using the quasi-steady flow strategy. It suggests that the discrepancies of predicted depths, depth-averaged velocities and bed shear stresses between these two approaches can be less then 10% if $|\beta| < 0.04$. However, for hydrographs with high degree of unsteadiness, the traditional quasi-steady flow approach could significantly underestimate the impact of flow events on stream habitat. In this case, a truly unsteady dynamic flow approach using complete unsteady shear stress formulae is recommended.

ACKNOWLEDGMENT

We thank Colin Krause (now with US Forest Service) for assistance with flood data collection in the Smith River. The support of the Virginia Department of Game and Inland Fisheries and the US Army Corps of Engineers for this study is gratefully acknowledged.

REFERENCES

Babaeyan-Koopaei, K., Ervine, D.A. Carling, P.A. and Cao, Z. 2002. Velocity and Turbulence Measurements for Two Overbank Flow Events in River Severn. *J. Hydraul. Eng., ASCE,* 128(10): 891-900.

Bares, V., Jirak, J. and Pollert, J. 2006. Bottom shear stress in unsteady sewer flow. Water Science&Technology Vol.54 No6-7 PP.93-100.

Booker, D.J. 2003. Hydraulic modeling of fish habitat in urban rivers during high flows. *Hydrol. Process.* 17, 577-599.

Booker, D.J. and Dunbar, M.J. 2004. Application of Physical Habitat Simulation (PHABSIM) Modelling to Modified Urban River Channels. *River Res. Applic.* 20: 167-183.

Bovee K.D. (1982) A guide to stream habitat analysis using the instream flow incremental methodology. *Instream Flow Information Paper no. 12*. FWS/OBSERVATION 82/86. Washington D.C., USA.

Brunner, G.W. 2008. HEC-RAS, River Analysis System User's Manual. US Army Corps of Engineers, Hydrologic Engineering Center, Davis, CA 95616.

Bunt C.M., Cooke S.J., Katopodis C., and Mckinley R.S. 1999. Movement and summer habitat of brown trout (*Salmo trutta*) below a pulsed discharge hydroelectric generating station. *Regulated Rivers: Research & Management.* 15(5): 395-403

Carney, S.K., Bledsoe, B.P. and Gessler, D. 2006. Representing the bed roughness of coarse-grained streams in computational fluid dynamics. *Earth Surf. Process. Landforms* 31: 736-749.

CFX-5 Solver Theory, 2003. CFX Ltd. Didcot Oxfordshire, UK.

Chang H.H. 1998. Fluvial Processes in River Engineering. Krieger Publ. Co., Malabar, FL., 432p.

Clough SC and Turnpenny AWH. 2001. Swimming Speeds in Fish: Phase 1. R&D Technical Report W2-026/TR1. Fawley Aquatic Research Laboratories Ltd. Environment Agency. UK.

Crowder DW and Diplas P. 2000. Using two-dimensional hydrodynamic models at scales of ecological importance. *Journal of Hydrology* 230: 172-191.

Crowder, D.W. and Diplas, P., 2006. Applying spatial hydraulic principles to quantify stream habitat.*River Res. Appl.* 22(1), 79-89.

De Sutter, R., Verhoeven, R., and Krein, A. (2001). Simulation of sediment transport during flood events: laboratory work and field experiments. *Hydrol. Sci. J*. 46(4): 599-610.

Donnell, Barbara P., Letter, Joseph V., McAnally, W.H. User's Guide for RMA2 Version 4.5. 2001. US Army Corps of Engineers, Coastal and Hydraulics Laboratory.

Eichinger, P., and Lein, G. (1992). "The influence of friction on unsteady pipe flow." International Conference on Unsteady Flow and Fluid Transients, H. Wallingford, ed.,Durham UK, 41–50.

[FOEN] Federal Office for Environment, 2008 http://www.bafu.admin.ch/gewaesserschutz/04851/index.html?lang=en. Accessed in 11/2008

Ge, L., Lee, S.O., Sotiropoulos, F. and Sturm, T. 2005. 3D Unsteady RANS Modeling of Complex Hydraulic Engineering Flows. II: Model Validation and Flow Physics. *J. Hydraul. Eng.,* ASCE, 131: 809-820.

Gordon, N.D., McMahon, T.A., Finlayson, B.L., Gippel, C.J. and Nathan, R. J. 2004. Stream Hydrology: An Introduction for Ecologists. John Wiley & Sons Ltd. 429 p.

Graf, W.H. and Qu, Z. 2004. Flood hydrographs in open channels. *Proceedings of the Institution of Civil Engineers- Water Management*, 157: 45-52.

Guensch, G.R., Hardy, T.B., Addley, R.C. 2001. Examining feeding strategies and position choice of drift-feeding salmonids using an individual-based, mechanistic foraging model. *Can. J. Fisheries Aquat. Sci.* 58, 446-457.

Henderson, F. M. 1966. *Open Channel Flow*, Macmillan, New York. 544p.

Hey RD. 1979. Flow resistance in gravel-bed rivers. *J. of the Hydr. Div.*, ASCE, 105:365-379.

Hicks, F. E., Steffler, P. M., and Gerard, R. 1991. "Finite element modeling of surge propagation and an application to the Hay River." *Canadian Journal of Civil Engineering*, 19(3), 454-462.

Hirt, C., Nichols, B., 1981. Volume of fluid methods for the dynamics of free boundaries. *J. Comput. Phys.* 39, 201-225.

Hunter M.A. 1992. Hydropower Flow Fluctuations and Salmonids: A Review of the Biological Effects, Mechanical Causes, and Options for Mitigation. Technical Report No.119. State of Washington Department of Fisheries. 46p.

Ingram GR; Chu VH (1987). Flow around islands in rupert bay: an investigation of the bottom friction effect. *J Geophys Res* 92(C13):14.521-14.533

Launder, B.E. and Spalding, D.B. 1974. The numerical computation of turbulent flows. *Comp Meth Appl Mech Eng,* 3:269-289.

Liebig,H., Cereghino, R., Lim, P., Belaud, A., Lek, S., 1999. Impact of hydropeaking on the abundance of juvenile brown trout in a Pyrenean stream. *Arch. Hydrobiol.* 144, 439-454.

Munson, B.R., Young, D.F., Okiishi, T.H., 1990. Fundamentals of Fluid Mechanics, 2nd ed. John Wiley and Sons, Inc., New York.

Montgomery, D.R., Buffington, J.M., Peterson, N.P., Schuett-Hames, D. and Quinn, T.P. 1996. Streambed scour, egg burial depths and the influence of salmonid spawning on bed surface mobility and embryo survival. *Can. J. Fish. Aquat. Sci*. 53:1061-1070.

Morvan H, Knight D.W, Wright N, Tang X & Crossley A.(2008), "The Concept of Roughness in Fluvial Hydraulics and its Formulation in 1-D, 2-D & 3-D Numerical Simulation Models", *Journal of Hydraulic Research, IAHR*, 26(2): 191-208.

Nezu, I., Nakagawa, H., Ishida, Y., and Kadota, A. 1993. Bed shear stress in unsteady open-channel flows. Proc., 1993 Hydraulic Conference, ASCE, New York, N.Y., 1458-1463.

Nezu, I., Kadota, A. and Nakagawa, H. 1997. Turbulent Structure in Unsteady Depth-Varying Open-Channel Flows. *J. Hydr. Engrg.,* ASCE,123 (9): 752-763.

Nezu, I., and Sanjou, M. 2006. Numerical Calculation of Turbulence Structure in Depth-Varying Unsteady Open-Channel Flows. *J. Hydr. Engrg.,* ASCE,132 (7): 681-695.

Nicholas, A.P. 2001. Computational Fluid Dynamics Modelling of Boundary Roughness in Gravel-bed Rivers: an Investigation of the Effects of Random Variability in Bed Elevation. *Earth Surf. Process. Landforms* 26: 345-362.

Orth, D. J., Diplas, P., Dolloff, A. and Newcomb, T. 2004. Influences of fluctuating Releases on Stream Fishes in the Smith River below Philpott Dam. Final Report (Contract No. 08220203). Richmond, VA., Federal Aid in Sport Fish Restoration Program Federal Aid Grant F-121-R-5, Virginia Department of Game and Inland Fisheries. 284p.

Parker, G., Klingeman, P.C. and McLean, D.B. 1982. Bedload size distribution in paved gravel-bed streams. *J. Hydr. Div., ASCE,*. 108(4): 544-571.

Pasternack, G.B., Wang, C.L. and Merz, J.E. 2004. Application of a 2D hydrodynamic model to design of reach-scale spawning gravel replenishment on the mokelumne river, California. *River Research and Applications* 20: 205-225.

Press, W.H., Teukolsky, S.A., Vetterling, W.T. and Flannery, B.P. 1992. Numerical Recipes in FORTRAN, 2nd ed. Cambridge University Press, Cambridge.

Qu,Z. (2002) Unsteady open-channel flow over a mobile bed. Ph.D. Dissertation. No. 2688. Ecole Polytechnique Federale de Lausanne, Switzerland.

Rowinski, P.M., Czernuszenko, W. and Pretre, J.M. 2000. Time-dependent shear velocities in channel routing. *Hydrol. Sci. J.,* 45(6):881-895.

Shen, Y. and Diplas, P. 2008. Application of two- and three-dimensional computational fluid dynamics models to complex ecological stream flows. *J. Hydro*. 348(1-2): 195-214.

Shuy, E.B. 1996. Wall shear stress in accelerating and decelerating turbulent pipe flows. *J. Hydraulic Res*. 34(2):173-183.

Sime, L.C., R.I. Ferguson, and M. Church. 2007. Estimating shear stress from moving boat acoustic Doppler velocity measurements in a large gravel bed river, *Water Resour. Res.* 43, W03418,doi:10.1029/2006WR005069.

Song, T. and Graf, W.H. 1996. Velocity and Turbulence Distribution in Unsteady Open-Channel Flows. *J. Hydr. Engrg.,* ASCE. 122 (3): 141-154.

Tu H. and Graf, W.H. 1992. Velocity distribution in unsteady open-channel flow over gravel beds. *Journal of Hydroscience and Hydraulic Engineering*, 10, No.1: 11-25.

Chapter V: CONCLUSION

SUMMARY OF MAJOR FINDINGS

It is challenging to choose appropriate tools to run physical habitat simulations in addressing as many types of channel geometries (from boulder to pool and riffle) as possible under a full range of flows (from base to peak flow). To model general flow characteristics of a river reach that is tens or hundreds of miles long, the use of 1-D models remains the most appropriate methodology to follow. A 2-D model should be employed to better characterize the lateral velocities and flow exchange between the riparian area and the main channel. Complex meso-scale flow patterns surrounding partially submerged flow obstructions could also be resolved by a 2-D model. However, the near-bed velocities surrounding deeply submerged obstructions should be computed using a 3-D model.

Complex three-dimensional flow structures and turbulence features obtained from 3-D models can be of great benefit for physical aquatic habitat assessment. Habitat Suitability Criteria (HSC) used in physical habitat studies that only consider standard metrics (e.g. velocity and depth) would be improved by encompassing measures of spatial variation of local 3-D flow patterns (e.g. vorticity and circulations).

It is found that vorticity and circulation patterns vary for different flows. For flows that are sufficiently deep to submerge various obstructions, the location and intensity of vorticity and the magnitude of the circulation metric depend on the distance of the horizontal plane to the streambed compared to the height of the obstructions. The 3-D simulations demonstrated that for a horizontal plane intersecting the obstruction, the circulation metric values are high. In this case they came out to be even higher than the corresponding values calculated at the same plane for base flow conditions. The increase

in the flow complexity may be attributed to the interaction of the horseshoe vortices, developed around the boulder base, with the strong arch-type vortices shed from the top of the submerged boulder. However, for deep flows, when the plane of interest is located at modest distance above the boulder (no intersection), the flow patterns become more uniform and the corresponding circulation metric values are very small.

Traditionally, unsteady flows are modeled as quasi-steady flows, with a series of incremental steady flows. This neglects the fact that both hydraulic characteristics and the behaviors of aquatic species may change significantly between steady flows and unsteady flows. In this thesis, unsteady numerical simulations of a measured flood released by the Philpott Reservoir using 1-D, 2-D and 3-D hydraulic models were conducted to assess their ability to reproduce time-dependent depths, velocities and shear stresses in the Smith River. For flows with moderate unsteadiness, it is acceptable to use the modified log-law in the 3-D model for estimating the unsteady shear stress. The same unsteady shear stress may be overestimated using the quasi-steady state shear stress equation based on the Manning formula in the 1-D and 2-D models. On the other side, accurate prediction of water surface elevation can be obtained regardless of the use of different roughness k_s values or which models. However, it is found that the use of smaller k_s values in the 3-D model may result in bigger wake sizes behind river obstructions.

Both observed and hypothetical unsteady reservoir release scenarios were simulated using the 3-D model. The hypothetical scenario uses only one turbine instead of two turbines to release flow during the first half hour, so that the peak flow is reached after nearly one hour in the hypothetical case rather than twenty minutes in the observed case. Results indicate that when compared with the observed case, adoption of the hypothetical scenario can reduce the potential erosion area by seven times, while maintaining refugia availability for juvenile brown trout for longer period. It is also

demonstrated that higher potential erosion area occurred at smaller discharges than the peak flow in both cases.

Validity of the Manning formula (or other similar shear stress formula that does not include the unsteady contribution in its friction slope term) for calculating unsteady shear stress may be tested using a new proposed unsteadiness parameter β. It is suggested that when $| \beta | \geq 0.04$, an unsteady flow hydrograph should be modeled using the truly unsteady dynamic flow approach instead of the traditional quasi-steady flow strategy, because the latter method could significantly underestimate the impact of flow events on stream habitat for hydrographs having high degree of unsteadiness.

DISCUSSION/FUTURE WORK

This dissertation has focused on using steady and unsteady 2-D and 3-D hydraulic models to better reproduce and quantify complex flow patterns and their impacts on physical fish habitat. The implementation of these hydraulic models and their associated turbulence closures is not straightforward, and many issues still exist and are suggested here as the subject of future work. These include (but are not limited to): researching better turbulence models to quantify the complex local flow patterns and developing spatial hydraulic metrics that can be better linked to fish habitat.

The first major challenge in reproducing complex flow patterns is to explore a better way to approximate local turbulence structures. Although the k-ε model implemented in Chapter IV can provide good predictions for many flows of engineering and biological interests, this model may not be suitable for applications such as flows with boundary layer separation and rotating fluids. The Reynolds Stress model (RSM) studied in Chapter III is theoretically better suited to complex flows including secondary flow and swirling fluids. However, increased number of transport equations in the RSM

will require much more computational effort and often result in reduced numerical robustness. This problem may hinder the modeling of large complex flow fields for natural channels. In addition, accurate prediction of flow separation is still problematic when the underlying ε-equation in the RSM is used. Currently, the most prominent two-equation models for prediction of flow separation are the k-ω based models. These kinds of models are designed to give highly accurate predictions of the onset and the amount of flow separation under the adverse pressure gradients behind the boulders. Another advantage of k-ω model lies in its near-wall treatment for low-Reynolds number computations, which is useful for smooth and low rough walls where the viscous sublayer may still exist. The model does not involve the complex non-linear damping functions required for the k-ε model and is therefore more robust. However, for walls with pronounced roughness, the logarithmic layer formulation is still used by the k-ω model since the viscous sublayer is destroyed. Further studies on the applicability of alternate modeling techniques such as the k-ω two-equation model are warranted.

The vertical vorticity studied in Chapter III can identify locations within a stream containing general nonuniform flows in a 2-D flow field. However, the vorticity can not distinguish between vortex cores and shearing motion present in the flow. Consequently, additional spatial hydraulic metrics are needed to characterize various types of complex, nonuniform flow patterns. For example, the swirling strength, which is based on the imaginary part of the complex eigenvalue of the velocity gradient tensor, is a useful metric in detecting eddies or vortices in a 3-D flow field. This metric will reveal only those vertical regions of the flow that swirl, while discriminating against the regions of strong shear. Care must be taken to minimize the numerical noise associated with grid density and velocity interpolation when calculating this metric based on the computational results. Another spatial hydraulic metric worth exploring is helicity, which

is the extent to which corkscrew-like motion occurs (i.e. helical flow). It is well known that helical flow (or secondary flow) is responsible for the creation and maintenance of river meandering pattern. In the Smith River, helical flow created between boulders could also affect the erosion and entrainment of sand particles around the brown trout redds. Detailed investigations into how to quantify the helical flows and their impacts on the fish spawning sites are needed in future research.

NOTATION

NOTATION FROM CHAPTER II

b,c = fitting constants for drift-feeding fish equation

P = prey capture success

V = total depth-averaged velocity

NOTATION FROM CHAPTER III

$\boldsymbol{B}$ = body force vector

C = log-layer constant depending on wall roughness

k = local turbulent kinetic energy

$\boldsymbol{p}$ = the total pressure

r_{water} = volume fraction of water

u, v = velocity components in the x and y directions

$\boldsymbol{U}$ = mean velocity vector

y = the normal distance to the wall

μ = molecular viscosity

$\boldsymbol{u}$= fluctuating velocity vector

$\rho\overline{\boldsymbol{u}\otimes\boldsymbol{u}}$ = Reynolds stresses

U_t = known velocity parallel to the wall at a normal distance y from it

u^* = friction velocity

κ = von Karman constant

c_μ = empirical coefficient 0.09

v = kinematic viscosity of the fluid

k_s = equivalent grain roughness height

$\hat{k}$ = a unit vector in the z direction

$|\xi|$ = absolute values of vorticity

$|\Gamma|$ = the absolute circulation

ρ = fluid density

NOTATION FROM CHAPTER IV

B = body force vector.

C = log-layer constant depending on wall roughness

c_μ = 0.09 (empirical coefficient)

d_{50} = median grain size

d_{84} = grain size for which 84% by weight of the sediment is finer

e ≈ 2.718 (an irrational constant)

f_s = quasi-steady friction factor

g = gravity acceleration

h = local instantaneous water depth

k = local turbulent kinetic energy

k_s = equivalent grain roughness height

n = the time-dependent Manning's roughness coefficient.

p = the total pressure

Re = Reynolds number

S_0 = longitudinal channel slope

S_f = local instantaneous friction slope

t = time

U_t = known instantaneous velocity parallel to the wall at a normal distance y from it

u^* = shear velocity

$\mathbf{V}$ = 3D mean velocity vector

$\mathbf{v}$ = 3D fluctuating velocity vector

V = local instantaneous total depth-averaged velocity

x = the streamwise distance along the channel

z_0 = roughness length, a small height above the bed where local near-bed velocity is zero

α = unsteadiness parameter proposed by Nezu et al. (1997)

β = unsteadiness parameter proposed in this study

Φ = unsteadiness parameter proposed by Shuy (1996)

ρ = fluid density

κ = 0.41 (von Karman constant)

τ = local instantaneous bottom shear stress

τ^* = dimensionless bed shear stress

τ^*_c = dimensionless critical stress

μ = dynamic viscosity

ν = kinematic viscosity of the fluid

σ_g = geometric standard deviation of the sediment sample size